Neurochirurgische Klinik und Poliklinik

Klinik der Ludwig-Maximilians-Universität München

Direktor: Prof. Dr. med. Jörg-Christian Tonn

The role of a previously unrecognized pericytes progenitor-like cell in glioma expansion and progression

Dissertation

zum Erwerb des Doktorgrades der Medizin

an der Medizinischen Fakultät der

Ludwig-Maximilians-Universität zu München

vorgelegt von

Yuping_Li

aus

Gansu, China

2018

Mit Genehmigung der Medizinischen Fakultät

der Universität München

Berichterstatter:	Prof. Dr. rer. nat. Rainer Glaß
Mitberichterstatter/in:	Prof. Dr. med. Jochen Herms
	PD Dr. rer. nat. Gurumoorthy Krishnamoorthy
Mitbetreuung durch den promovierten Mitarbeiter:	Dr. sc. nat. Roland Kälin
Dekan:	Prof. Dr. med. dent. Reinhard Hickel
Tag der mündlichen Prüfung:	22. 02. 2018

Eidesstattliche Versicherung

Li, Yuping

Ich erkläre hiermit an Eides statt,

dass ich die vorliegende Dissertation mit dem Thema

The role of a previously unrecognized pericytes progenitor-like cell in glioma expansion

and progression

selbständig verfasst, mich außer der angegebenen keiner weiteren Hilfsmittel bedient und alle Erkenntnisse, die aus dem Schrifttum ganz oder annähernd übernommen sind, als solche kenntlich gemacht und nach ihrer Herkunft unter Bezeichnung der Fundstelle einzeln nachgewiesen habe.

Ich erkläre des Weiteren, dass die hier vorgelegte Dissertation nicht in gleicher oder in ähnlicher Form bei einer anderen Stelle zur Erlangung eines akademischen Grades eingereicht wurde.

Munich Germany, 22. 02. 2018

Ort, Datum

Yuping Li

Unterschrift Doktorandin/Doktorand

TABLE OF CONTENTS

CONTENTS

1 INTRODUCTION

1.1 Glioma

Gliomas are the most common primary brain tumors diagnosed in adults (Stupp et al., 2005), and account for approximately 77% of the more than 250,000 new cases of primary malignant brain tumors identified each year worldwide (Louis et al., 2016). In the past, gliomas were categorized based on histological features and graded according to histopathological criteria defined by the World Health Organization (WHO) (Fuller, 2008). These histologic standards were widely applied to predict prognosis and therapeutic benefits for glioma patients. Due to increased research that has focused on molecular biomarkers and genetic profiles, the updated 2016 WHO classification of tumors of the central nervous system (CNS) now incorporates histologic features together with molecular marker information, as shown in Table 1.1 (Louis et al., 2016; Cancer Genome Atlas Research et al., 2015; Rice et al., 2016; Louis, 2016).

Currently, several molecular markers are recognized as relevant for prognosis and decision-making for glioma patients, including the isocitrate dehydrogenase (IDH) mutation, 1p/19q co-deletion, H3-K27M mutation, and O^6-methylguanin-DNA -methyltransferase (MGMT) methylation (Eckel-Passow et al., 2015; Weller et al., 2015). The new WHO classification system is based on IDH mutation, 1p/19q co-deletion, and H3-K27M mutation; whereas MGMT methylation contributes to the selection of proper chemotherapy (Olar et al., 2015; Reuss et al., 2015).

Table 1.1 Grading of selected CNS tumors according to the 2016 CNS WHO

WHO grades of select CNS tumours		
Diffuse astrocytic and oligodendroglial tumours		
Diffuse astrocytoma, IDH-mutant		II
Anaplastic astrocytoma, IDH-mutant		III
Glioblastoma, IDH-wildtype		IV
Glioblastoma, IDH-mutant		IV
Diffuse midline glioma, H3 K27M–mutant		IV
Oligodendroglioma, IDH-mutant and 1p/19q-codeleted		II
Anaplastic oligodendroglioma, IDH-mutant and 1p/19q-codeleted		III
Other astrocytic tumours		
Pilocytic astrocytoma		I
Subependymal giant cell astrocytoma		I
Pleomorphic xanthoastrocytoma		II
Anaplastic pleomorphic xanthoastrocytoma		III
Ependymal tumours		
Subependymoma		I
Myxopapillary ependymoma		I
Ependymoma		II
Ependymoma, *RELA* fusion–positive		II or III
Anaplastic ependymoma		III
Other gliomas		
Angiocentric glioma		I
Chordoid glioma of third ventricle		II
Choroid plexus tumours		
Choroid plexus papilloma		I
Atypical choroid plexus papilloma		II
Choroid plexus carcinoma		III
Neuronal and mixed neuronal-glial tumours		
Dysembryoplastic neuroepithelial tumour		I
Gangliocytoma		I
Ganglioglioma		I
Anaplastic ganglioglioma		III
Dysplastic gangliocytoma of cerebellum (Lhermitte–Duclos)		I
Desmoplastic infantile astrocytoma and ganglioglioma		I
Papillary glioneuronal tumour		I
Rosette-forming glioneuronal tumour		I
Central neurocytoma		II
Extraventricular neurocytoma		II
Cerebellar liponeurocytoma		II
Tumours of the pineal region		
Pineocytoma		I
Pineal parenchymal tumour of intermediate differentiation		II or III
Pineoblastoma		IV
Papillary tumour of the pineal region		II or III
Embryonal tumours		
Medulloblastoma (all subtypes)		IV
Embryonal tumour with multilayered rosettes, C19MC-altered		IV
Medulloepithelioma		IV
CNS embryonal tumour, NOS		IV
Atypical teratoid/rhabdoid tumour		IV
CNS embryonal tumour with rhabdoid features		IV
Tumours of the cranial and paraspinal nerves		
Schwannoma		I
Neurofibroma		I
Perineurioma		I
Malignant peripheral nerve sheath tumour (MPNST)		II, III or IV
Meningiomas		
Meningioma		I
Atypical meningioma		II
Anaplastic (malignant) meningioma		III
Mesenchymal, non-meningothelial tumours		
Solitary fibrous tumour / haemangiopericytoma		I, II or III
Haemangioblastoma		I
Tumours of the sellar region		
Craniopharyngioma		I
Granular cell tumour		I
Pituicytoma		I
Spindle cell oncocytoma		I

Reprinted from (Louis DN, 2016), with permission from the WHO

The glioblastoma multiforme (GBM), the most common type of malignant glioma, has a dismal prognosis, with a median survival of 14 to 16 months (Norden et al., 2008). Current standard therapies for GBMs include surgical resection followed by radiation and chemotherapy with temozolomide (TMZ) (Stupp et al., 2005). Even with multimodal therapy, the median overall average survival is only 3 to 9 months upon GBM recurrence (Stupp et al., 2009; Yung et al., 2000). A wide range of alternative strategies have been investigated or are under evaluation, including immunotherapy and gene therapy (Ahluwalia et al., 2011).

GBMs are highly vascularized brain tumors (Jain et al., 2007). The structures and functions of tumor vessels are significantly different from vessels in the normal brain (Keunen et al., 2011). Tumor vessels often exhibit a serpentine course, branch

irregularly and form arterio-venous shunts (Nagy et al., 2009). Blood flow through tumors does not follow a constant, unidirectional path, and vascular density decreases during tumor development, leading to ischemia and ultimately necrosis as tumors outgrow their blood supply (Gilkes et al., 2014). Previously, anti-angiogenic strategies for the treatment of GBMs have been investigated in large clinical studies, but treatment of GBMs with bevacizumab (a monoclonal antibody targeting vascular endothelial growth factor) has clinically failed (Chinot et al., 2014; Fine, 2014, Gilbert et al., 2014).

1.2 The Function of Pericyte

Charles Rouget (1873) first described pericytes as "adventitial cells" in the 19th century. Zimmermann et al. (1923) later called these cells 'pericytes', due to their close proximity to endothelial cells (ECs). Pericytes are perivascular cells located in the microvessel walls, within the basement membrane (BM) and closely opposed to the endothelium (Bergers and Song, 2005). Microscopically, mature pericytes are characterized as highly elongated, slender, and branched cells with projections that wrap around the vessel wall (Sims, 1986). Pericytes are also characterized by the expression of Desmin (Bergers and Song, 2005), platelet-derived growth factor receptor β (PDGFR-β) (Winkler et al., 2010), α-smooth muscle actin (αSMA; only in large vessels) (Hughes and Chan-Ling, 2004), CD146 (Park et al., 2016), and nerve/glial antigen 2 proteoglycan (NG2) (Diaz-Flores et al., 2009; Armulik et al., 2005). However, these markers are not restricted to pericytes. They are also not

always co-expressed, which was previously interpreted to represent varying differentiation stages, tissues-specific characteristics, and distinct pathological conditions (Schlingemann et al., 1991).

The number of pericytes and the pericyte coverage of capillaries is much higher in the CNS than in the peripheral organs (Armulik et al., 2011). In addition, endothelial cells, glial cells, pericytes, and astrocyte end-feet completely cover brain vessels, working together to form the "neurovascular unit" (NVU) (El Ali et al., 2014). Pericytes have been demonstrated to be an essential component of the NVU, and play an important role in both physiological and pathological conditions, as shown in Figure 1.1. (Enge et al., 2002; Xian et al., 2006; Nishimura et al., 2016; Paez-Ribes et al., 2009; Paquet-Fifield et al., 2009; Sweeney et al., 2016).
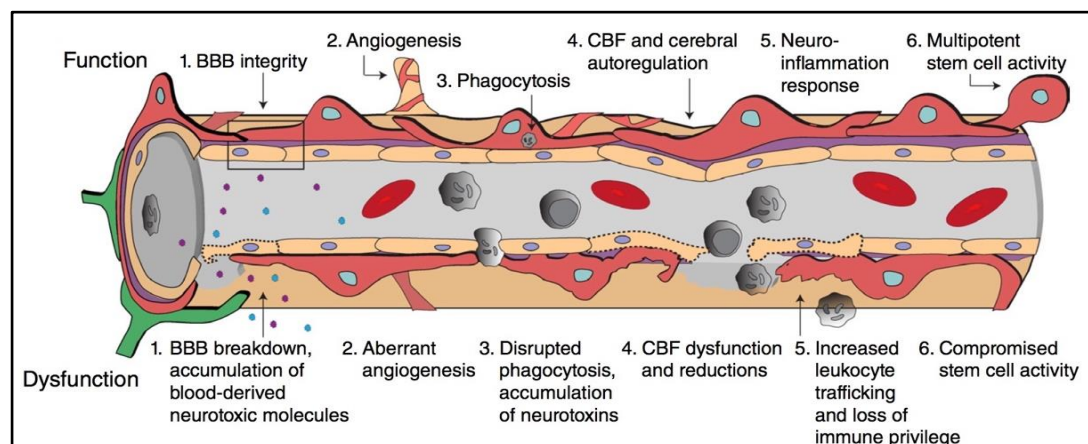
Figure 1.1 The function of pericyte in physiological and pathological condition. Under physiological conditions (top row), pericytes regulate (1) BBB integrity, i.e., tight or adherens junctions and transcytosis across the BBB; (2) angiogenesis, i.e., microvascular remodeling, stability and architecture; (3) phagocytosis, i.e., clearance of toxic metabolites from the CNS; (4) CBF and capillary diameter; (5) neuroinflammation, i.e., leukocyte trafficking into the brain; and (6) multipotent stem cell activity. Pericyte dysfunction (bottom row) is characterized by (1) BBB breakdown causing leakage of neurotoxic blood-derived molecules into the brain (for example, fibrinogen, thrombin, plasminogen, erythrocyte-derived free iron and anti-brain antibodies); (2) aberrant angiogenesis; (3) impaired phagocytosis causing CNS accumulation of neurotoxins; (4) CBF dysfunction and ischemic capillary obstruction; (5) increased leukocyte trafficking promoting neuroinflammation; and (6)

impaired stem cell-like ability to differentiate into neuronal and hematopoietic cells. Pericyte dysfunction is present in numerous neurological conditions and can contribute to disease pathogenesis.

Modified from (Sweeney et al., 2016); Re-print permission from Nature Publishing Group

Previous studies have shown that pericytes support vessel stability and permeability either through direct cell-cell contact, paracrine factors, or through a newly described chemo-mechanical signaling pathway (Bexell et al., 2009). Increased expression of genes associated with increased vascular permeability (e.g. angiopoietin-2) was observed in pericyte-deficient mice (Daneman et al., 2010). Studies have also observed decreased pericyte coverage in mice deficient in PDGFR-β or platelet-derived growth factor subunit B (PDGF-B), which resulted in increased microvascular leakage (Armulik et al., 2005, Leveen et al., 1994, Soriano, 1994). Other signaling pathways may also be involved in the interactions between ECs and pericytes, including the angiopoietin-1/2 and Tie-2 (Ang/Tie2) and transforming growth factor-β (TGF-β) pathways, which are primarily associated with EC viability and mural cell differentiation (Birnbaum et al., 2011).

In addition, pericytes are also involved in controlling the function of the blood brain barrier (BBB) by regulating cerebral blood flow and eliminating toxic cellular byproducts (Winkler et al., 2009). A study using a viable pericyte-deficient mouse model demonstrated that increased permeability occurs through endothelial transcytosis (Armulik et al., 2010). The same study also showed that pericytes regulate BBB-specific gene expression in endothelial cells and induce polarization of the astrocyte end-feet surrounding CNS blood vessels in order to maintain the normal function of the BBB (Armulik et al., 2010).

Pericytes have been shown to support endothelial cell proliferation and promote vessel remodeling and maturation. Initial vascular tubes are formed by proliferating immature ECs, which release several signals that induce pericyte recruitment. Pericyte coverage is crucial for vessel remodeling and maturation. Recently, a study demonstrated that pericytes regulate vessel remodeling via CXCR3-induced involution of ECs (Bodnar et al., 2013). The ability of pericytes to induce cord dissociation was blocked by inhibition of CXCR3 function in microvascular ECs, and thus it is though that pericytes may regulate vascular pruning. In addition, several studies have indicated that NG2 expression in pericytes plays an important role in pericyte maturation and interactions with ECs (Huang et al., 2010; Ozerdem and Stallcup, 2004).

Some evidence has suggested pericyte as an alternative source of stem/progenitor cell within the brain, and have stem cell potential in several pathological disorders (Muramatsu and Yamashita, 2014; Diaz-Flores et al., 2009). In the health mouse brain, pericytes may originate from multipotent stem cells, mesenchymal stem cells (MSCs) in the adult brain, and neuroectoderm-derived neural crest cells in the developing brain; several recent reports also indicate that pericytes could originate from bone marrow-derived pericyte progenitor cells or glioblastoma stem cells (GSCs) in mouse brain with glioma (Ricci-Vitiani et al., 2010; Lamagna and Bergers, 2006; Song et al., 2005; Bababeygy et al., 2008; Bexell et al., 2009).

MSCs are tissue-resident stem cells that can convert to an adipocytes, chondrocytes, or osteoblasts lineage (Traktuev et al., 2008; Dellavalle et al., 2007). A range of studies have proposed a close relationship between pericytes and MSCs (da Silva Meirelles et al., 2006; Crisan et al., 2008). Cultured pericytes have been shown to differentiate into osteoblasts (Brighton et al., 1992), chondrocytes (Farrington-Rock et al., 2004), and adipocytes (Tang et al., 2008). Besides demonstrating multipotency *in vitro*, pericytes and MSCs share cellular markers. For instance, pericytes express characteristic surface markers of MSCs, including CD44, CD73, CD90, and CD105; conversely, MSCs express pericyte markers, including PDGFR-β, NG2, Sca-1, and α-SMA (Rajantie et al., 2004). In a study conducted by Birnbaum et al. (2011) glioma cells induced differentiation of MSCs into pericytes in a mouse model. However, recent studies indicate that not all pericytes display similar stem cell potential (Caplan, 2008, Blocki et al., 2013) and the contribution of pericytes to the pool of MSCs in the body was rolled out by a-tracing approach (Guimaraes-Camboa et al., 2017).

In embryonic development, pericytes of the forebrain and thymus develop from neuroectoderm-derived neural crest cells (Bergwerff et al., 1998, Etchevers et al., 2002), and TGF-β1 signaling drives the differentiation of neural crest-derived progenitors into smooth-muscle-like cells (Chen et al., 2004; Darland and D'Amore, 2001).

Several studies have shown that bone marrow derived pericyte progenitor cells are able to infiltrate brain tumors and mature into pericytes and vascular smooth muscle

cells (Du et al., 2008). Du et al. (2008) reported that PDGFR-β+ ScaI+ pericytes, which account for 2% of bone marrow-derived cells, infiltrated experimental gliomas-an action that depended on expression levels of MMP-9 in CD45+ vascular modulatory cells. However, other studies found that bone marrow-derived cells did not differentiate into pericytes in intracranial tumors (Paez-Ribes et al., 2009, De Palma et al., 2005). In the present study, I will further investigate whether pericytes are derived from the bone marrow in the glioma mouse model.

Recently, Cheng et al. (2013) reported a surprising connection between pericytes and brain CSCs in GBMs. The results demonstrated that most pericytes residing in the perivascular niche of GBMs originated from CSCs. Another study demonstrated that GBM stem cells could differentiate into ECs (Wang et al., 2010). Expression of pericyte markers (Desmin, αSMA, and NG2) found to increase upon stimulation with glioma-conditioned medium, which was closely associated with the tumor vasculature (Bexell et al., 2009). Overall, these findings have revealed that pericytes, through a close interaction with CSCs and perivascular cells, participate in tumor initiation and progression by acting as tumor promoters (Caspani et al., 2014).

1.3 The role of pericytes in brain tumor angiogenesis

Angiogenesis is a multiple-step process involving many molecules and cytokines within the tumor microenvironment. Pericytes could secrete growth factors to promote EC proliferation and migration, thereby modulating the surrounding

extracellular matrix, as shown in Figure 1.2 (Gerhardt and Betsholtz, 2003; Armulik et al., 2005; Saunders et al., 2006; Stapor et al., 2014).
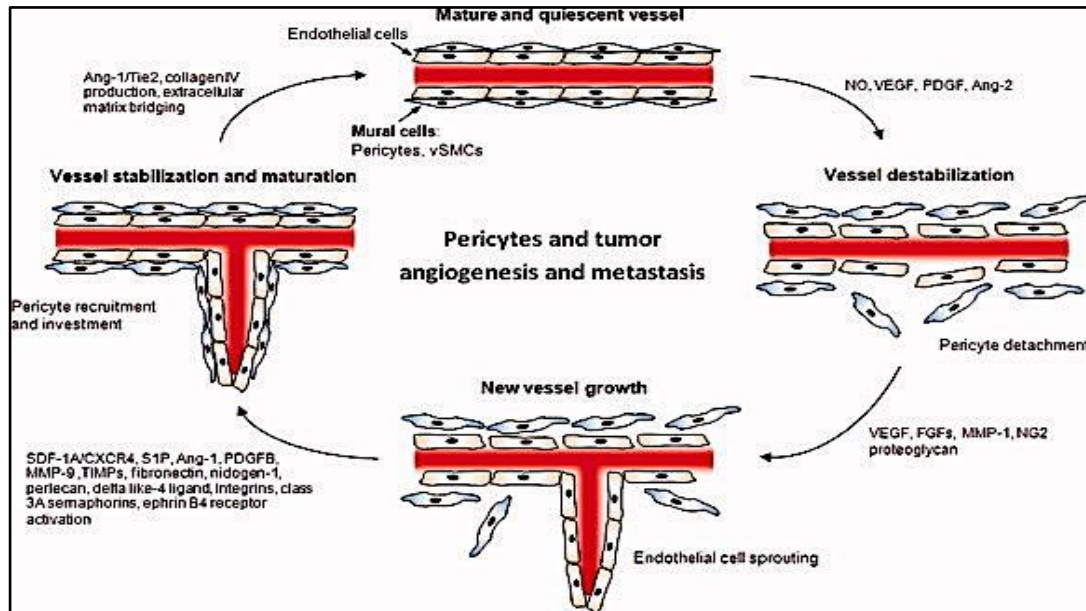

Figure 1.2. The role of pericytes in tumor angiogenesis and metastasis. In response to angiogenic stimuli, EC–pericyte contacts are disrupted, leading to activated EC and pericyte phenotypes, degradation of the basement membrane, vasodilation, and increased vessel permeability. Pericyte investment in the migrating endothelial tip is scarce. EC–pericyte crosstalk via several factors known to play critical roles in angiogenesis contribute to matrix degradation, migration, proliferation, and endothelial tube formation. Vessel maturation is characterized by pericyte recruitment, functional pericyte investment of the endothelium, and assembly of ECM components. Proper EC–pericyte association results in maintenance of vessel integrity. EC–pericyte dissociation may promote intravasation and extravasation of tumor cells across the disrupted endothelium. Ang, angiopoietin; EC, endothelial cell; ECM, extracellular matrix; FGF, fibroblast growth factor; MMPs, matrix metalloproteinases; NO, nitric oxide; PDGF, platelet-derived growth factor; S1P, sphingosin-1-phosphate; SDF-1A, stromal derived factor-1A; TIMPs, tissue inhibitors of metalloproteinases; VEGF, vascular endothelial growth factor; vSMC, vascular smooth muscle cell. **Modified from (Sweeney et al., 2016); Re-print permission from John Wiley & Sons publications**

GBMs have a complex tumor microenvironment that contains different stromal cells, including ECs, pericytes, and inflammatory cells. Extensive neoangiogenesis and tumor infiltration, including recruitment of ECs and pericytes, is considered to be one defining characteristic of GBMs (Zuniga et al., 2009). Previous studies have demonstrated that high vascularity and overexpression of vascular endothelial growth factor (VEGF) and basic fibroblasts growth factor (bFGF) in GBMs contribute

significantly to tumor growth and progression and angiogenesis (Fischer et al., 2005; Kargiotis et al., 2006; Jain et al., 2007). Several mechanisms of neovascularization have been reported for GBMs, including vessel cooption, sprouting of vessels, and vasculogenesis (Chao and Hirschi, 2010; Dome et al., 2008). Tumor vessels are irregularly shaped, excessively branched, disorganized, leaky, and tortuous (Ruoslahti, 2002). Within the tumor area, ECs and pericytes show altered functions and morphologies compared to their normal counterparts (Hashizume et al., 2000; Hellstrom et al., 2001). The BM in tumors is usually discontinuous or absent, and the endothelium may also be incomplete or multilayered (Baluk et al., 2003). Hence, pericytes in tumors often lack a physical association with ECs.

Previous studies have demonstrated that pericyte ablation leads to increased vessel permeability and poor vessel integrity. These studies have also showed that pericyte ablation suppresses tumor growth, promotes tumor invasion, and induces metastatic spread (Paez-Ribes et al., 2009; de Groot et al., 2010). Another study used NG2-deficient mice to investigate the interaction between pericytes and ECs during brain tumor growth and found that tumor volume significantly decreased in NG2-deficient mice compared with wild type mice (Huang et al., 2010). However, NG2 is not only expressed by pericytes, but also by macrophages, tumor cells, and several stromal cell types. Therefore, the NG2 deficiency is not pericyte-specific, and other NG2 expressing stromal components within tumor microenvironments may contribute to tumor progression.

1.4 Study aims

Pericytes have been shown to play an important role in regulating development and maturation of ECs and maintaining function of vessels. Previous studies indicated newly generated pericytes may derived from mature pericytes, multipotent stem or progenitor cells. In the present study, I applied a lineage-tracing system to follow the differentiation of nesting-RFP positive cells. It was discovered nestin-RFP+ cells become pericytes during the tumor progression, but initially do not carry pericyte markers. A bone marrow chimeric glioma mouse model was used to investigate the origination of RFP+ pericytes. In addition, I utilized the cell-lineage ablation glioma mouse model to investigate the role of RFP+ cells during glioma progression.

The aims of this project were:

(1) Tracing the cell lineage of nestin-RFP expressing cell in a transgenic glioma mouse model.

(2) To investigate the relationship between the RFP expressing cells and vessels;

(3) To identify the cell types of RFP expressing cells by immunofluorescence labelling experiments.

(4) Investigate if RFP expressing cells derived from the brain or from the bone marrow

(5) To study the role of RFP expressing cells during glioma progression by using the cell-lineage ablation glioma mouse model.

2 MATERIALS

2.1 Equipment and devices

Table 2.1 Equipment and devices

Equipment/ device	Name	Provider
Centrifuges	Centrifuge 5415R	Eppendorf
	Universal 30 RF	UNIVERSAL
Fridge(-80°C)	Premium	LIEBHERR
Incubator	AC-407	Heraeus
Microliter syringe	1ul micro-syringe	Hamilton
Microscopes	Axio Observer A1	Carl Zeiss
	Axioskop 2	Carl Zeiss
	Axiovert 135	Carl Zeiss
	BMS D1-223A	Carl Zeiss
Confocal microscope	Broadband TCS SP5	Leica
Microscope camera	AVT HORN	SONY
	AxioCam MRm	ZEISS
Microtome	Slide 2003	PFM AG
Perfusion system	Dose IT P910	Integra Biosciences
pH meter	WTW Multical bench	Sigma-Aldrich
Pipette boy	Comfort	Integra Biosciences
Pipettes	(0-10, 20-200, 100-1000 µl)	Eppendorf

Shaker	Digital Vortex Mixer	VWR
	Sea Star Shaker	Biozyme
Stereotactic Frame		Stoelting
Sterile hood	HERA safe	Thermo
Sutures	Ethibond excel (5-0)	Ethicon
Water bath		Memmert

2.2 Chemicals and reagents

Table 2.2.1 Chemicals and reagents

Substance	Manufacturer	Country
4′,6-Diamidin-2-phenylindol (DAPI)	Sigma - Aldrich	St. Louis, USA
Antibody diluent serum-free with background reducing components	Dako	Hamburg, Germany
Agarose	Sigma - Aldrich	St. Louis, USA
Aqua ad iniectabilia	B. Braun	Melsungen, Germany
Bepanthen® Eye- and Nosecream	Bayer	Leverkusen, Germany
CldU	Sigma-Aldrich,	Saint Louis, USA
Cryomatrix	Thermo Fisher	Waltham, USA

	Scientific	
Donkey serum	Sigma-Aldrich	Saint Louis, USA
Entellan® mounting medium	Merck	Darmstadt, Germany
Eosin G-solution 0.5%	Carl Roth	Karlsruhe, Germany
Ethylenglycol	Sigma-Aldrich	Saint Louis, USA
EtOH 100%	SAV LP	Flintsbach, Germany
EtOH 70%	SAV LP	Flintsbach, Germany
EtOH 96%	SAV LP	Flintsbach, Germany
Glycerol	Sigma-Aldrich	Saint Louis, USA
Goat serum	Sigma-Aldrich	Saint Louis, USA
HCl	Sigma-Aldrich	Saint Louis, USA
Hoechst 3342 (1:1000)	Life Technologies	Darmstadt, Germany
IB4 biotinylated (1:100)	Vector Laboratories	Burlingame, USA
IB4 FITC (1:200)	Sigma-Aldrich	Saint Louis, USA
IdU	Sigma-Aldrich	Saint Louis, USA
Ketaminhydrochlorid	Pfizer	New York, USA

(Ketavet, 100 mg/ml) injection

solution

Meyer's Hemalaun	Carl Roth GmbH	Karlsruhe, Germany
Mounting medium for fluorescence microscopy	Ibidi	Martinsried, Germany
NaCl (Sodium chloride)	Roth	
Narcoren (Pentobarbital)	Bayer	Leverkusen, Germany
Na_2HPO_4	Sigma-Aldrich	Saint Louis, USA
NaH_2PO_4	Sigma-Aldrich	Saint Louis, USA
PBS	Apotheke Klinikum der Universität München	Munich, Germany
PFA	Sigma-Aldrich	Saint Louis, USA
Protein block	Dako Germany	Hamburg, Germany
Rompun (2%) & Xylazin injection solution	Bayer	Leverkusen, Germany
Roti® Histol	Carl Roth	Karlsruhe, Germany
Sodium Tetraborate decahydrate	Sigma-Aldrich	Saint Louis, USA

Sucrose	Sigma-Aldrich	Saint Louis, USA
Tamoxifen	Sigma-Aldrich	Saint Louis, USA
Triton X-100	Roche Diagnostics	Rotkreuz, Switzerland
Tween-20	Sigma-Aldrich	Saint Louis, USA

Table 2.2.2 Commercial kits

Kit	Provider	Country
MaxFluor™ Mouse on Mouse Fluorescence Detection Kit (MaxFluor 488)	Dianova	Hamburg, Germany

2.3 Cell lines

Table 2.3 Cell lines used in this study

Cell lines	Origin origin	Provider
GL261	Mouse	Neurosurgical Research, LMU Munich

2.4 Mouse strains

Table 2.4 mouse strain applied in this study

Strain	Provider	Country
Nes-CreER$^{T2+/+}$;Td-Tomato	Neurosurgical Research, LMU Munich	Germany
Nes-CreER$^{T2+/+}$;Td-Tomato-iDTA	Neurosurgical Research, LMU Munich	Germany
PU1-GFP	Neurosurgical Research, LMU Munich	Germany

2.5 Buffers and solutions

Table 2.5 Buffers for immunolabeling

Buffer	Containing
Fixation reagent	4 % Paraformaldehyde in 0.1M PB
Nuclear localization reagent	100mM Tris, 0.9% NaCl, 0.05% Tween 20 3% Donkey Serum In 100ml PBS

Washing buffer (TBS)	100 mM Tris 150 mM NaCl, pH 7.4 in ddH2O
30 % Sucrose	Sucrose (300 g/l) in 0.05 M phosphate buffer
PBT	
Triton-PBS	

2.6. Primary antibodies

Table 2.6 Primary antibodies

Antibody	Origin	Dilution	Provider	Country
CD146	Rabbit	1:1000	Abcam	Cambridge, UK
CD31	Rat	1:25	Becton Dickinson	Heidelberg, Germany
BrdU (CldU)	Rat	1:250	Abd Serotec	Kidlington, UK
Desmin	Rabbit	1:200	Abcam	Cambridge, UK
Iba1	Rabbit	1:500	Wako Pure	Neuss, Germany
Iba1	Goat	1:500	Abcam	Cambridge, UK
BrdU (IdU)	Mouse	1:750	Becton Dickinson	Lakes, USA
GFP (ChIP grade)	Rabbit	1:250	Abcam	Cambridge, UK

Nestin	Rabbit	1:100	Millipore	Darmstadt, Germany
NG2	Rabbit	1:200	Abcam	Cambridge, UK
PDGFR-β	Goat	1:50	R+D Systems	Minneapolis, USA
RFP	Rabbit	1:200	Abcam	Cambridge, UK
SOX 2	Rabbit	1:200	Abcam	Cambridge, UK
vWF	Rabbit	1:400	Dako	Hamburg, Germany

2.7. Secondary antibodies

Table 2.7 Secondary antibodies

Antibody	Origin	Dilution	Provider	Country
Alexa Fluor 488	Goat	1:250	Dianova	Hamburg, Germany
Alexa Fluor 488	Rabbit	1:500	Life Technologies	Carlsbad, CA, USA
Alexa Fluor 594	Rabbit	1:500	Jackson Immuno-Research	West Grove, PA, USA
Cy™2	Mouse	1:250	Jackson Immuno-Research	West Grove, PA, USA
Cy™2	Rat	1:250	Jackson Immuno-Research	West Grove, PA, USA
Cy™3	Rabbit	1:250	Jackson Immuno-Research	West Grove, PA, USA

Cy™5	Mouse	1:250	Jackson Immuno-Research	West Grove, PA, USA
Cy™5	Rat	1:250	Jackson Immuno-Research	West Grove, PA, USA
Biotinylated	Rabbit	1:250	Jackson Immuno-Research	West Grove, PA, USA
Biotinylated	Mouse	1:250	Jackson Immuno-Research	West Grove, PA, USA
Biotinylated	Goat	1:250	Jackson Immuno-Research	West Grove, PA, USA
Biotinylated	Rat	1:250	Jackson Immuno-Research	West Grove, PA, USA
Alexa Fluor 488 streptavidin	-	1:500	Jackson Immuno-Research	West Grove, PA, USA
Alexa Fluor 594 streptavidin	-	1:500	Jackson Immuno-Research	West Grove, PA, USA

2.8 Software

Table 2.8 Software products

Product	Supplier
Image J	NIH, Bethesda, MD, USA
SPSS	IBM
Adobe	Microsoft
GraphPad PRISM 5	GraphPad Software Inc.
Microsoft office 2011 for mac	Microsoft
Mac OS X	Mac

3 METHODS

3.1 Mouse models

3.1.1 Animal maintenance

All *in vivo* experiments were conducted and housed in standardized cages in the Walter Brendel Centre for Experimental Medicine, Department of Neurosurgical Research, LMU Munich. We performed the animal experiments according to the German animal protection act guidelines and were approved by the government of Upper Bavaria. The standard water and food were provided available ad libitum. A circadian day and night light rhythm of 12 h was maintained.

3.1.2 Tumor inoculation

In our brain tumor model, 100.000 GL261 mouse glioma cells per mouse were inoculated to the mouse brain and this was defined as day 0 of the experiment. For tumor inoculation, mice were anesthetized depending on their individual body weight (7uL/g) with anesthetic (0.36 mL 2% Rompun, 1.02 mL 10% Ketavet and 4.86 mL 0.9% NaCl). After disinfection with 10% potassium iodide solution, the skin of the skull was cut with a scalpel blade. Next, we placed the mouse head in the stereotactic frame and carefully fixed it in the flat-skull position. Corneas were kept moisturized with Bepanthen® eye and nose ointment. A burr hole was made 1.5 mm anterior and 1.5 mm right of the bregma by drilling with a 23-gauge needle tip. A syringe containing 1um of 100,000 GL261 tumor cells was inserted 4 mm deep into the mouse brain through the bone hole, and then the needle was retracted to a position of 3 mm into the brain. The injection was then performed at a rate of 50,000 cells/min. After the tumor inoculation, the syringe was carefully taken out over a entire-course

of 5 minutes. Finally, the wound was sutured and the animal was returned to its habitat.

3.1.3 Nes-CreER$^{T2+/+}$;Td-Tomato reporter mouse model

The Nes-CreER$^{T2+/+}$;Td-Tomato reporter mouse was applied *in vivo* studies. Based on the Cre (cyclization recombination)/loxP (locus of X over P1) system, a site-specific recombinase technology, the selected DNA sequences can be deleted, inserted, or inversed. Generally, loxP sites on bacteriophage P1 contain 34 bp DNA sequences, including an 8 bp non-palindromic core region and two sets of 13 bp palindromic core region (Albanese et al., 2002). Cre recombinase can specifically recombine the loxP sites (Lakso et al., 1992), and delete or recombine a DNA sequence of interest, (Missirlis et al., 2006).

In this study, Nes-CreER$^{T2+/+}$;Td-Tomato mice carrying the Cre transgene under the control of the nestin promoter and enhancer located in the second intron of the nestin gene were used. Hence, all nestin positive cells also express Cre recombinase (Mignone et al., 2004). Nonetheless, in these transgenic mice, Cre recombinase can only gain access to the nucleus after Tamoxifen-binding to the ligand binding domain of the mutated estrogen receptor α, which is linked to the recombinase. Consequently, tamoxifen injection determines the time point of genetic recombination (Feil et al., 1997).

In Rosa26-tdTomato mice, a lox-P-site flanked the stop cassette precedes an open reading frame encoding red fluorescent protein (RFP) (Soriano, 1999). Thus, if NesCreER^{T2} and Rosa26-tdTomato mice are crossbred generating Nes-CreER$^{T2+/+}$;Td-Tomato mice, Cre recombinase excises the floxed stop cassette of the RFP gene after tamoxifen administration (Soriano, 1999). In these mice, all cells

that carry the Cre gene sequence will express an RFP signal (i.e., all cells that are Nestin positive at the time of tamoxifen administration). As a result, Nes-CreER$^{T2+/+}$;Td-Tomato mice can be used as a fate-mapping model for Nestin-positive cells with RFP as the reporter molecule.

3.1.4 Generation of bone marrow chimeric mice and ip. TAM application

The bone marrow chimeric mouse model was applied to investigate the origin of RFP+ pericyte progenitor cells (Holl, 2013). In this study, two transgenic reporter mice models were used as the donor mice, including Nes-CreER$^{T2+/+}$;Td-Tomato and PU1-GFP donor mice. PU1 is a transcriptional activator that is expressed by mature myeloid and lymphoid lineage cells (DeKoter and Singh, 2000, Chen et al., 1995). PU1-GFP mice are suitable to observe cells of myeloid lineage as described previously (Back et al., 2004). Bone marrow-derived cells were harvested from tibiae and femurs of 6 ~ 8-week donor mice. The BM cells (5 x 10^6), including PU1-GFP and Nes-Cre-RFP cells, were transferred to lethally irradiated (split dose: 600 rad at day -1) recipient WT_ C57BL/6 and Nes-CreER$^{T2+/+}$;Td-Tomato mice by intravenous (IV) injection. After BM transfer, the mice received an antibiotic treatment for one month (tetracycline 0.1g/L, drinking water). Successful reconstitution was defined as > 94% engraftment of blood GFP+/RFP+ cells by FACS analysis. The TAM injection was performed at days 4 to 6 after the tumor inoculation.

3.1.5 Nes-CreER$^{T2+/+}$;Td-Tomato with loxP-conditional diphtheria toxin A (iDTA) mouse model

The genetic cell lineage ablation mouse model of Nes-CreER$^{T2+/+}$;Td-Tomato-iDTA (tamoxifen-inducible diphtheria toxin expression) was generated by crossing Nes-CreER$^{T2+/+}$;Td-Tomato mice with ROSA-iDTA transgenetic mice

(Brockschnieder et al., 2006). When we injected TAM, the ROSA-26Sor promoter could induce the expression of diphtheria toxin (DT) in the Nes-cre-expressing cells (RFP+ cells). This mouse model allows ablation of Cre recombined RFP+ cells, namely the Nes-iDTA group. Nes-CreER$^{T2+/+}$;Td-Tomato mice were crossed with ROSA-iDTA wild type mice were applied as the control group, namely the Nes-RFP group.

3.2 Group design of different mouse models and treatment procedure

In cell lineage-tracing experiments, male and female Nes-CreER$^{T2+/+}$;Td-Tomato transgenic mice were divided into three groups, including the Nes-7 days, the Nes-14 days, and the Nes-21 days group. The GL261 tumor cells were inoculated on day 0 followed by the TAM administration on day 1 to day 3 in the Nes-7 days group, on day 4 to day 6 in the Nes-14 days group and the Nes-21 days group. Mice were sacrifice at 7, 14, 21 days after tumor inoculation in the Nes-7, the Nes-14, and the Nes-21 days groups, respectively (Figure 3.1-A). As controls, three further groups were included in this experiment, as shown in Figure 3.1-B. They were genetically modified and treated in the same manner as the experimental groups with the following modificatious conditions: mice of the Control 1 group did not carry the NesCreER^{T2} transgene; the Control 2 group did not receive tamoxifen treatment; the Control 3 group was not inoculated with GL261 tumor cells but stabbed with the injection needle (stab-wound control). Table 1 shows the detail for all experimental mice.

A: Experimental groups
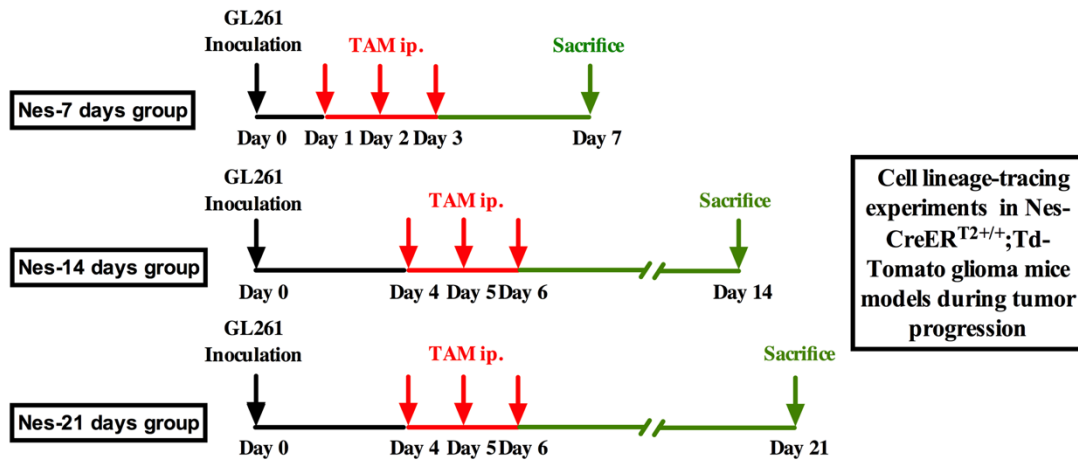
B: Control groups
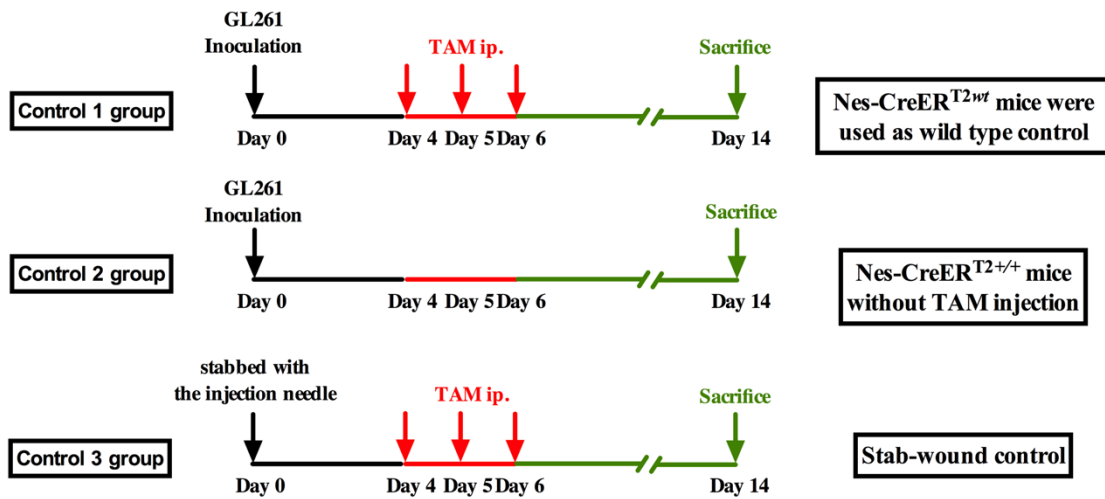
Figure 3.1 Treatment scheme for Cell lineage-tracing experiments

Table 3.1 Characteristics of different groups in this study

Group name	Mouse model	Number	Sacrifice date after tumor inoculation
Nes-7 days	Nes-CreER$^{T2+/+}$;Td-Tomato	6	7
Nes-14 days	Nes-CreER$^{T2+/+}$;Td-Tomato	8	14
Nes-21 days	Nes-CreER$^{T2+/+}$;Td-Tomato	8	21
Nes-18 days	Nes-CreER$^{T2+/+}$;Td-Tomato	3	18
Nes-P90	Nes-CreER$^{T2+/+}$;Td-Tomato	4	14

Nes-P360	Nes-CreER$^{T2+/+}$;Td-Tomato	4	14
Control 1	Nes-CreER^{T2wt};Td-Tomato	3	14
Control 2	Nes-CreER$^{T2+/+}$;Td-Tomato	3	14
Control 3	Nes-CreER$^{T2+/+}$;Td-Tomato	3	14
BM/Nes-Td-Tomato	Recipient: C57BL/6 Donor: Nes-CreER$^{T2+/+}$;Td-Tomato	2	14
BM/PU1-GFP	Recipient: Nes-CreER$^{T2+/+}$;Td-Tomato Donor: PU1-GFP	4	14
Nes-iDTA	Nes-CreER$^{T2+/+}$;Td-Tomato -iDTA	6	14
Nes-RFP	Nes-CreER$^{T2+/+}$;Td-Tomato -iDTA^{wt}	5	14

To investigate if recombined cells would only be generated in the early stage of tumor growth or also later in tumor progression, we designed another experimental group in which Cre recombinase was activated by TAM treatment on 12 to 14 days after tumor cells injection, namely Nes-18 days group. In this experiment, we compared recombined cells between the Nes-7 days group and the Nes-18 days group. (Figure 3.2).
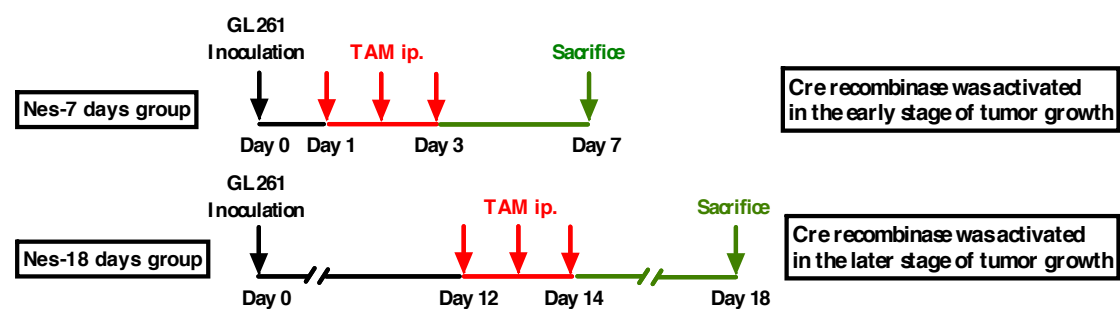
Figure 3.2 Treatment scheme and procedures for the experiment to investigate recombined cells between the early- and the later-stage during tumor progression

To investigate whether age influenced the number of RFP expression cells during tumor progression. Nes-CreER$^{T2+/+}$;Td-Tomato mice, in which received tumor inoculation at postnatal day 90, were used as the Nes-P90 group to investigate the

RFP expression in young mouse brain. For aging mice, Nes-CreER$^{T2+/+}$;Td-Tomato mice were inoculated with tumor cells at postnatal day 360, namely the Nes-P360 group. Then, the treatment scheme was same as the procedure for the Nes-14 days group (Figure 3.3)
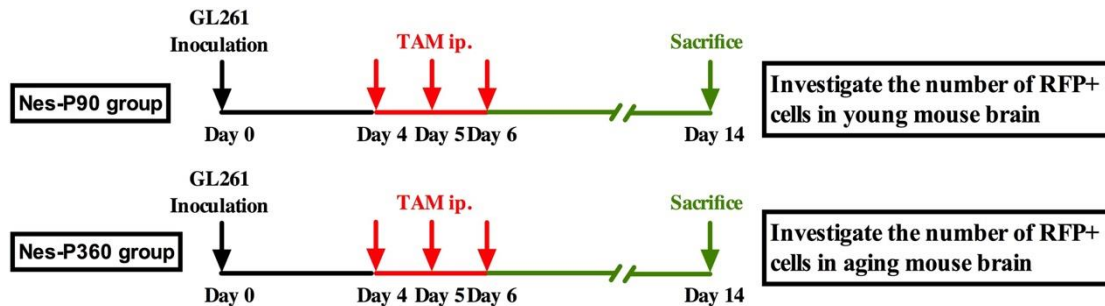
Figure 3.3 Treatment scheme and procedures for the experiment to investigate the number of RFP expression cells recombined cells between the young and the aging mouse brain during tumor progression

In the bone marrow chimeric experiments, C57B1/6 wild type mice were transplanted with the Nes-Cre-RFP donor cells from Nes-CreER$^{T2+/+}$;Td-Tomato transgenic mice after lethal irradiation, namely the BM/Nes-Td-Tomato group. For the positive control group, Nes-CreER$^{T2+/+}$;Td-Tomato transgenic mice were transplanted with PU1-GFP donor cells after lethal irradiation, namely the BM/PU1-GFP group (Fig. 3.4). After one month of antibiosis, I orthotopically inoculated the Gl261 cells and then animals were treated as outline for Nes-14 days group (Fig. 3.1-A).

The BM/PU1-GFP group   The BM/Nes-Td-Tomato group

| Recipient: Nes-CreER$^{T2+/+}$;Td-Tomato mice | Recipient: C57B1/6 mice |

Recieve Lethal Irradiation 1 x 10 Gy

**Transplanted with PU1-GFP cells
From PU1-GFP donor mice
(5,000,000 cells)**

**Transplanted with Nes-Cre-RFP cells
From Nes-CreER$^{T2+/+}$;Td-Tomato donor mice
(5,000,000 cells)**

Recieve Antibiotics Treatment for One Month (Tetracycline 0.1g/L)

Tumor Inoculation (GL261, 100,000 cells)

TAM Injection at Day 4 - Day 6 After the tumor inoculation

Sacrifice at Day 14 After the tumor inoculation

Figure 3.4 Treatment scheme and pocedures for bone marrow chimeric experiments.

For cell lineage depletion experiment, two groups were designed including the Nes-iDTA group (with cell-lineage ablation) and the Nes-RFP control group (without cell-lineage ablation). GL261 tumor cells were inoculated on day 0 followed by the TAM administration on day 4 to day 6. Mice were sacrificed at 14 days after tumor inoculation, as shown in Figure 3.5.

Nes-iDTA group — GL 261 Inoculation — Day 0 — TAM ip. — Day 4 Day 5 Day 6 — Sacrifice — Day 14 — Nes-CreER^{T2};Td-Tomato with cell-lineage ablation

Nes-RFP group — GL 261 Inoculation — Day 0 — TAM ip. — Day 4 Day 5 Day 6 — Sacrifice — Day 14 — Nes-CreER^{T2};Td-Tomato without cell-lineage ablation

Figure 3.5 Treatment scheme and procedures for cell lineage depletion experiment.

3.3 Induction of Cre recombinase by tamoxifen injection

Based on the treatment protocol, 75 mg tamoxifen/kg body weight of the animal (dissolved in corn oil) was administered. The injections were performed intraperitoneally once in 3 continuous days. Mice of control 2 group only received a corn oil injection.

3.4 Histology

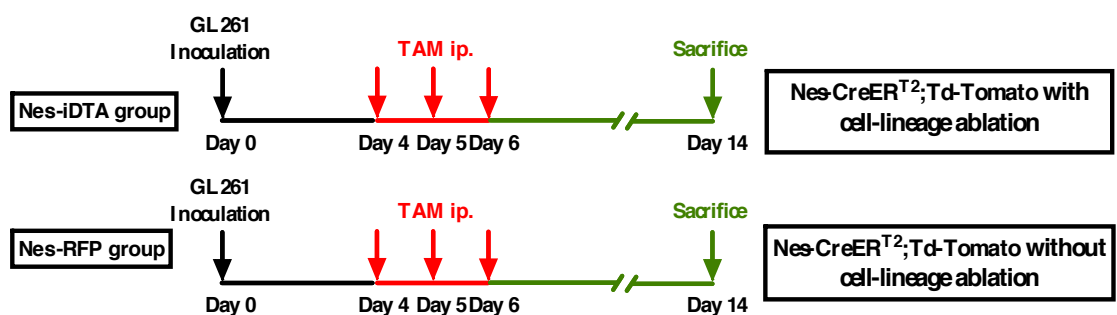**3.4.1 Perfusion and tissue preparation**

Mice were killed at 7, 14, 18, and 21 days after glioma cells inoculation and perfused with phosphate buffered saline (PBS) followed by 4% paraformaldehyde (PFA) (Gage et al., 2012). After successful perfusion, the brain parenchyma was dissected and kept in a 4% PFA solution for 2 days at 4°C in order to postfix the tissue. Afterwards, the specimens were dehydrated in a 30% sucrose solution diluted in PBS. Then, brains were frozen in Cryomatrix for at least 1 day at −20°C. As the tissue was then prepared for cutting, 40-μm horizontal sections were made and preserved as free-floating sections in a 24-well-plate filled with cryoprotectant (ethylenglycol, glycerol and 0.1 M PO_4 buffer in a 1:1:2 solution at pH 7.4), which protects the tissue from freezing. The whole well plate was kept at −20°C protected from light by aluminium foil.

3.4.2 H&E staining

Hematoxylin-eosin staining (H&E staining) includes the application of the basic dye hematoxylin, which colors acid structures blue, and an alcohol-based acidic Eosin, which colors base structures bright pink (Feldman and Wolfe, 2014). This staining

was conducted as follows in order to estimate the individual tumor volume of the mice in the various groups:

a) Mounting of the sections

b) Dehydration in 100% Ethanol for 30 sec

c) Staining in Meyer's Hemalaun solution for 5 min

d) Rinsing in running tap water for 5 min

e) Counter staining with 0.5% Eosin G-solution for 10 sec

f) Dipping very shortly in a. dest. (Caution: Eosin is water soluble)

g) Dehydration through ascending alcohol series starting with 70% EtOH for 20 sec

h) Continued by 96% EtOH for 1 min

i) Continued by 100% EtOH for 1 min

j) Continued by Roti®-Histol for 1 min

k) Repetition of the last step with fresh Roti®-Histol

l) Covering with mounting medium

3.5 Immunohistochemistry

Immunohistochemistry was performed by the direct, indirect, or labeled streptavidin-biotin (LSAB method) using fluorescence techniques (Chen et al., 2010, Furukawa et al., 2017, Ramos-Vara, 2005). However, all of them rely on the same principle of an antibody specifically detecting its respective antigen in the mouse tissue. All stains were performed as free-floating sections, which lead to improved antibody penetration. Sections were washed in PBST (PBS with 0.1% Tween-20) 3 × 5 min at room temperature and then incubated with blocking solution (5% normal donkey serum in PBS, with 0.3% Triton-X100) for 1 h at room temperature (RT). The free-floating sections were incubated at 4°C or RT overnight with primary antibodies

diluted in 3% normal donkey serum. After washing by PBT, antibody staining was revealed using species-specific fluorophore-conjugated (Cy3, Cy5, Cy2 from Jackson, Alexa 488, Alexa 594 from molecular probes) or biotin-conjugated secondary antibodies (Invitrogen), which then react with fluorescent-dye labeled Streptavidin (Alexa 488, Alexa 594 with con-streptavidin, Cy5 with con-streptavidin). DAPI (1 μg/mL, Sigma) was used for counterstaining. The sections of control were stained with secondary antibody alone. The Immunohistochemistry was used for vWF, Desmin, PDGFR-β, SOX2, NG2 and CD146 stains.

3.5.1 Stain with Mouse-on-Mouse kit

Staining with anti-mouse antibody on mouse tissue can present a challenge. As secondary antibodies may also detect endogenous mouse IgG in inflamed tissue in tumors. As the blood-brain-barrier is opened, due to tumor progression in glioma mouse models, the immunoglobulin can directly penetrate to the tumor and is then detected by the secondary antibody. In order to reduce this background staining, a Dianova MaxFluor™ Mouse-on-Mouse Fluorescence Detection Kit was utilized (Goodpaster and Randolph-Habecker, 2014). The procedure was conducted as follows:

a)   Washing in PBST (PBS, 0.1% Tween-20) 2 x 5 min at room temperature

b)   Washing in H_2O 2 x 5 min at room temperature

c)   Denaturation in 2 M HCl for 45 min at room temperature

d)   Neutralization with 0.1 M sodium tetraborate for 15 min at room temperature

e)   Washing in PBST (PBS, 0.1% Tween-20) 6 x 10 min at room temperature

f)   Mounting and circleing the sections with a Dako pen (a fat pen which ensures that the different solutions remain on the section)

g) Fixation on the microscope slide with 4% PFA for 10 min

h) Washing in PBST (PBS, 0.1% Tween-20) 3 x 2 min at room temperature

i) Blocking with Protein blocking solution (reagent 1) for 10 min at room temperature

j) Blocking with MaxMOM blocking reagent (reagent 2) for 1 h at room temperature

k) Primary antibody (see table for dilutions) diluted in PBS, 0.3% Triton X-100, 5% serum of the secondary antibody's host species over night at 4 °C

l) Washing in PBST (PBS, 0.1% Tween-20) 3 x 2 min at room temperature

m) Fluorescence signal enhancer (reagent 3) for 30 min at room temperature

n) Washing in PBST (PBS, 0.1% Tween-20) 3 x 2 min at room temperature

o) Max Fluor labeled linker (reagent 4) 1:200 and secondary antibody (see table for dilutions) diluted in Fluorescent Diluent (reagent 5) for 2 h at room temperature

p) Washing in PBST (PBS, 0.1% Tween-20) 3 x 2 min at room temperature

q) Rinsing shortly in distilled water

r) Alexa Hoechst 1:1000 for 1 min at room temperature as a nuclear stain

s) Covering with fluorescence mounting medium

3.6 Microscopy

In this study, light, fluorescence and confocal microscopies were conducted. Light microscopy was only applied for the evaluation of H&E stains using a Zeiss Axioskop 2 light microscope and a Breukoven BMS D1-223A light microscope. For quantification of fluorescent structures, fluorescence microscopy and confocal microscopy were conducted. Unlike conventional wide-field microscopes, confocal microscopy was applied to control depth of field, and reduce of background

information; also, optical sections from thick tissues can be collected. This was performed to obtain high-resolution imaging. Image series were viewed as both a maximal projection of all plains and as a single plain at a chosen z-position.

3.7 Evaluation criteria

For immunohistochemical staining, the extent of colocalization of the traced cells with a variety of markers was evaluated according to the following criteria: As the reporter molecule (RFP) is expressed in the cytoplasm, markers that are present in the same compartment (Desmin) were interpreted as colocalized if both fluorophores were clearly identifiable in the cytoplasm of the same cell. If the used marker, however, is expressed in other compartments as the nucleus (SOX2) or the cell surface (NG2, PDGFR-β, VWF), cells were interpreted as colocalized if RFP-positive cell contained a stained nucleus. Cells were interpreted as perivascular if they were located at maximum 1 μm to a vWF positive vascular structure.

For all quantifications, a 20× and a 100×magnification were used. Quantifications were conducted from four randomly selected optical fields in the tumor, the peritumoral (optical field surrounding the tumor), and the contralateral (optical field of a corresponding region in the contralateral, tumor-free hemisphere) regions per section. Four sections from corresponding brain regions were taken per animal, a total of 48 optical fields per animal were evaluated for every immunohistochemical stain. All quantifications were performed from a picture of the respective optical field. The counting was performed by hand with the support of *Image J* software.

Confocal image analyses were performed using the maximal projection and crosshair mode of Leica LAS AF imaging software. Only if pixels colocalized in the three directions (xy-, xz- and yz- plane) were the cells regarded as double/triple positive.

3.8 Statistical analysis

The acquired data were analyzed by the GraphPad Prism software (version 5.04). The unpaired Student's t-test was applied to compare quantified data between experiment and control groups; each experiment was performed at least three times. I applied 1-way analysis of variance to analyze the quantification results of the tumor area, the peritumoral area, and the contralateral side. Statistical significance is assumed if $P \leq 0.05$.

4 RESULTS

4.1 RFP expression in the Nes-CreER$^{T2+/+}$;Td-Tomato glioma mouse model

4.1.1. Localization and characterization of RFP positive cells

In order to investigate the localization of nestin-RFP+ cells in our glioma mouse model, I analyzed tumor, peritumoral, contralateral, subventricular zone (SVZ), and olfactory bulb (OB) in Nes-CreER$^{T2+/+}$;Td-Tomato mice. I found the most RFP+ cells in the tumor (Fig. 4.1.1-a), SVZ (Fig. 4.1.1-b), and OB (Fig. 4.1.1-d); while few cells were found in the peritumoral area (Fig. 4.1.1-c) and the contralateral tumor-free brain hemisphere (Fig. 4.1.1-e). Furthermore, I found that RFP+ cells present a vessel-like morphology at 21 days after tumor inoculation, as shown in Fig. 4.1.1-f. Therefore, we analyzed the RFP expression by co-staining with VWF (see Fig. 4.2)
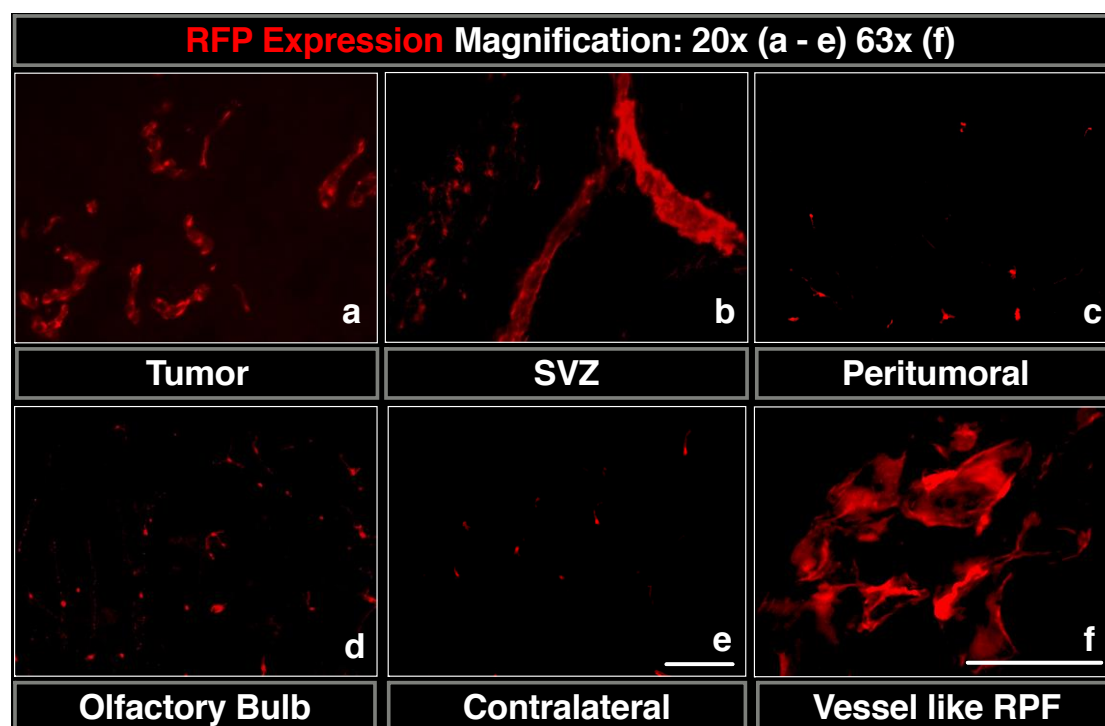

Figure 4.1.1: Localization and characterization of RFP expressing cells in the Nes-CreER$^{T2+/+}$; Td-Tomato glioma mouse model at 21 days after tumor cells inoculation. Fluorescence images show RFP expressing cells in the tumor (a), SVZ (b), peritumoral (c), OB (d), and contralateral tumor-free brain hemisphere (e) in Nes-CreER$^{T2+/+}$;Td-Tomato mice at 21 days after tumor cells inoculation (20x). In addition, f showed the morphology of RFP+ cells like vessel structures (63x). Scale bars are 200 μm in 20x pictures, and 50 μm in 63x pictures.

4.1.2. Tracing RFP+ cells in the Nes-CreER$^{T2+/+}$;Td-Tomato glioma mouse model during glioma progression

During tumor progression, the number of RFP+ cells significantly increased in the Nes-21 days group as compared with the Nes-7 days group in the tumor area, the peritumoral area, and the contralateral area (Fig. 4.1.2-A). In the tumor area, the number of RFP+ cells was 13.58 ± 2.62 in the Nes-7 days group, and the number increased to 21.55 ± 3.45 in the Nes-14 days group and 31.05 ± 3.47 in the Nes-21 days group ($p < 0.0001$, Fig. 4.1.2-B). In the peritumoral and the contralateral area, the number of RFP+ cells increased from 7.81 ± 2.9 and 4.27 ± 1.38 in the Nes-7 days group to 11.31 ± 2.54 and 6.21 ± 2.75 in the Nes-21 days group, respectively.
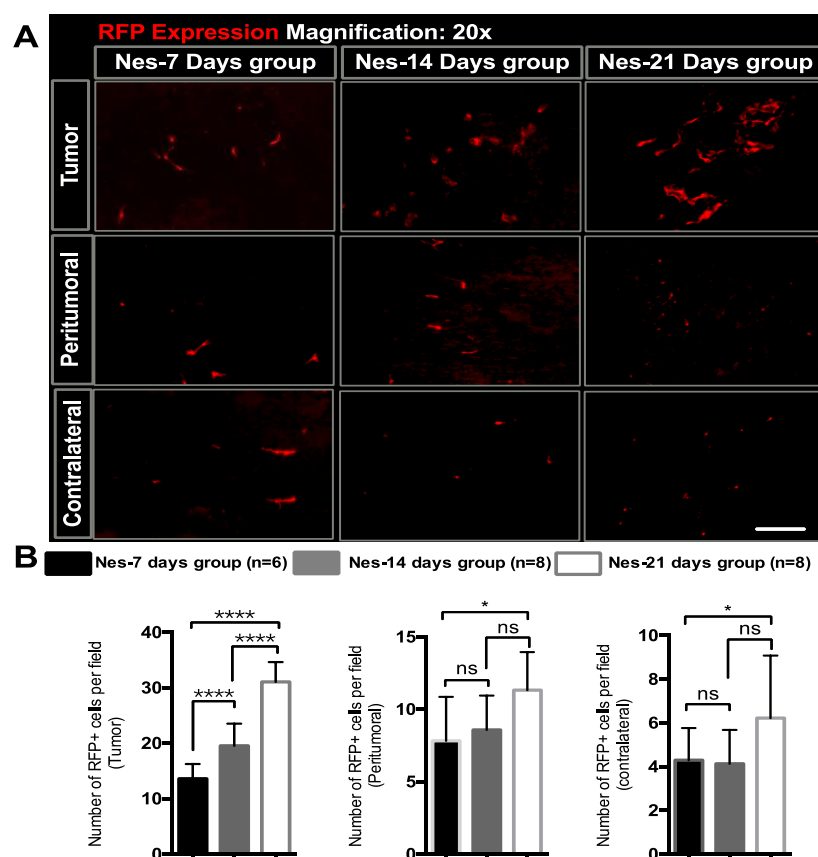

Figure 4.1.2 The number of RFP+ cells increased in Nes-CreER$^{T2+/+}$;Td-Tomato mice during glioma progression. A) The RFP+ (red) expression significantly increased from 7 days to 21 days after tumor inoculation within the tumor, the peritumoral, and contralateral tumor-free brain hemisphere. B) Quantification of the number of RFP+ cells (n = 12 random fields per mouse): the amount of RFP positive cells significantly increased from 7 to 21 days, especially in the tumor (p<0.0001) but also in the peritumoral (p < 0.05) and the contralateral area (p < 0.05). Data are represented as mean ± SEM. Scale bar is 200 μm (*p < 0.05, ****p < 0.0001, ^{ns}no significant).

4.1.3 RFP positive cells are continuously generated during tumor development

In order to investigate if recombined cells are generated in the early stage of tumor growth or are also generated later in tumor progression, I compared RFP expression between the Nes-7 days group and the Nes-18 days group (Fig. 3.2; Table 3.1). The results showed no difference in the number of RFP expressing cells between the Nes-7 days group and the Nes-18 days group in the tumor, peritumoral, and contralateral tumor-free brain hemispheres (Fig. 4.1.3). Thus, my results showed that the Cre recombined cells are continuously generated during tumor development.
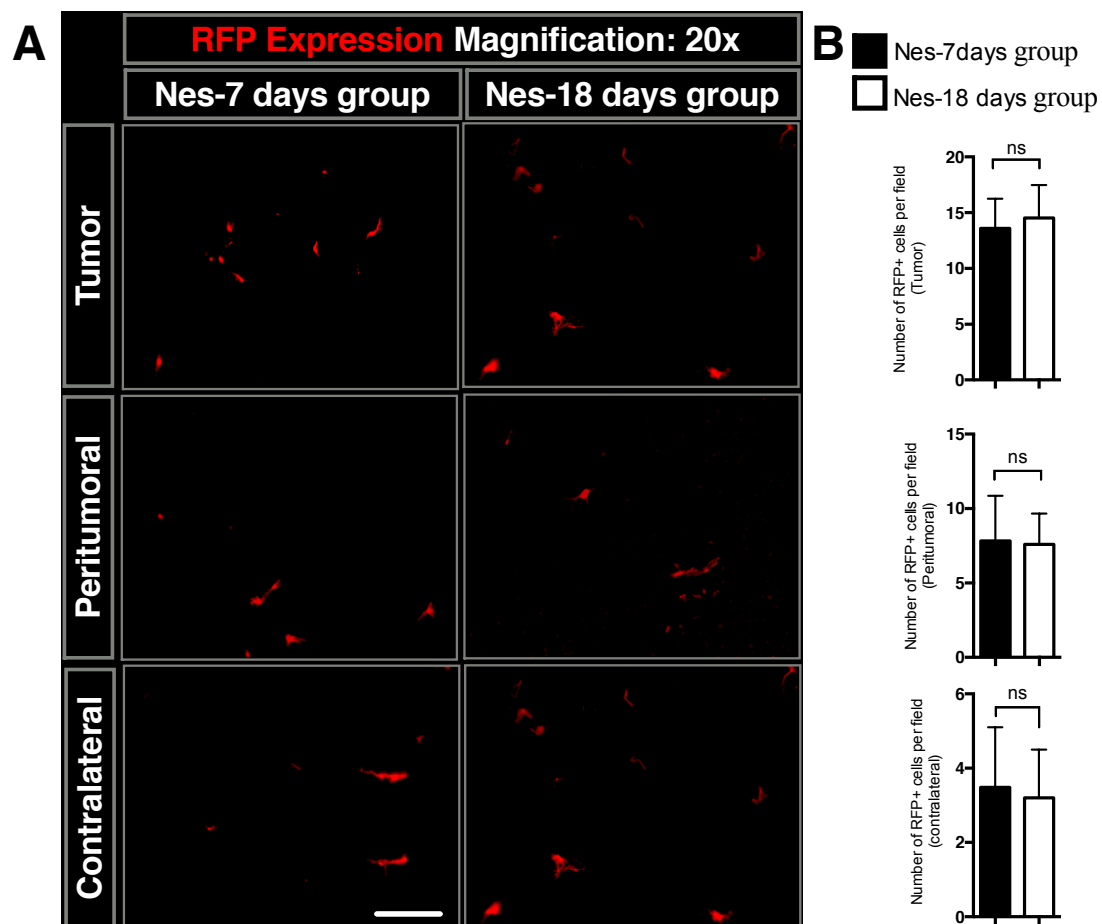
Figure 4.1.3 The number of RFP expressing cells between the Nes-7 days group and the Nes-18 days group. (A) Representative images showed the number of RFP expression was similar between two groups. (B) Quantification of the number of cre recombined RFP+ cells (n = 12 random fields per mouse) showed no significant difference between the Nes-7 days group and the Nes-18 days group in the tumor, the peritumoral, and the contralateral area. Data are represented as mean ± SEM ([ns] no significant). Scale bar is 200 μm.

4.1.4 The number of RFP expressing cells decreased in aging mouse brain as compared with young mice

Several previous studies suggested that the regeneration capacity of neural stem cells is reduced in the aging brain. To investigate whether age influences the number of RFP expression cells during tumor progression, I compared the RFP expression between the Nes-P90 group (age at operation was 90 day) and the Nes-P360 group (age at operation was 360 day) (Fig. 3.3; Table 3.1) at 14 days after tumor cells inoculation. As compared with the Nes-P360 group, the number of RFP+ cells was significantly higher in the Nes-P90 group in the tumor area (21.55 ± 3.45 young versus 17.06 ± 2.93, aged; $P = 0.0005$), the peritumoral area (8.57 ± 2.29 young versus 2.45 ± 2.10 aged; $P < 0.0001$), and the tumor-free brain hemisphere (4.12 ± 1.45 young versus 1.90 ± 1.44 aged; $P = 0.0063$), (Fig. 4.1.4). These results indicate that RFP positive cells have a somewhat reduced capacity to generate new progeny with advanced age, but the ability to generate new pericytes in the older brain is maintained. This is in state contrast to the capacity for adult neurogenesis, which declines much more in the old brain.
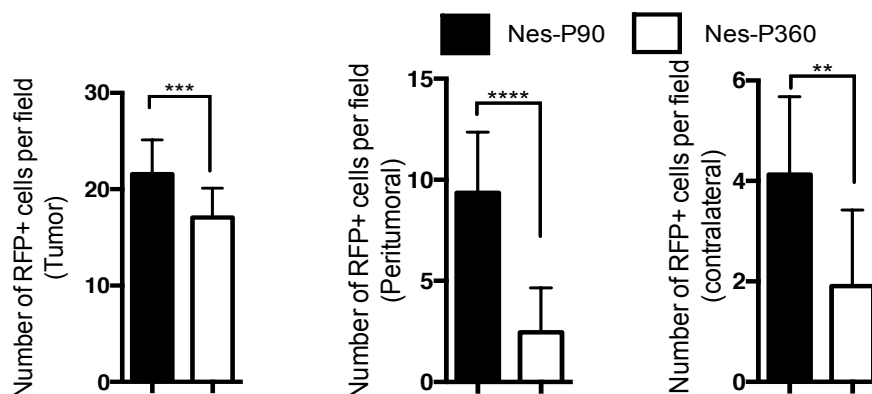
Figure 4.1.4 Quantifications of the number of RFP+ cells between the Nes-P90 group and the Nes-P360 group. There are 4 mice in the Nes-P90 group (age at operation was 90 day) and 4 mice in the Nes-P360 group (age at operation was 360 day). The number of RFP+ cells (n = 12 random fields per mouse) was decreased in the Nes-P360 group as compared with the Nes-P90 group within the tumor (p < 0.005), peritumoral (p < 0.001), and contralateral areas (p < 0.01). Data are represented as mean ± SEM (**p < 0.01, ***p < 0.005, **** p < 0.0001).

4.2 RFP+ cells form close associations with vWF+ cells

Then we assessed the relationship between RFP+ and vascular cells by immunofluorescence staining with an antibody directed against vWF. The results showed that RFP+ cells localized near vWF+ endothelial cells in the tumor area. Morphologically, RFP+ cells extended long cell processes across the surface of endothelial cells (Fig. 4.2.1.)
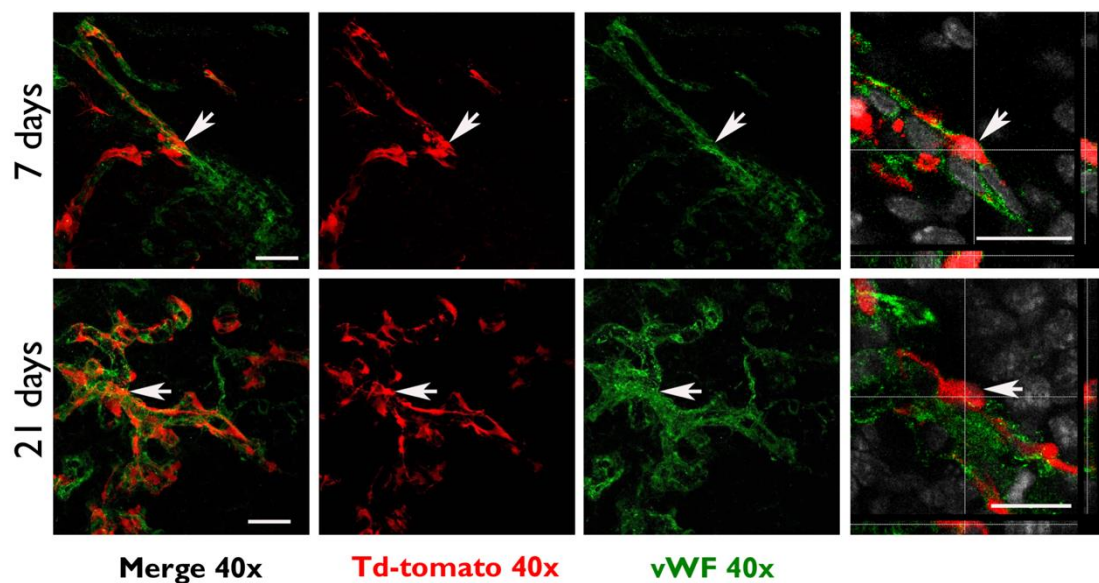

Figure 4.2.1 Confocal microscopy for intratumoral RFP+ cells and immunofluorescence labelling of von Willebrand Factor (vWF) in the Nes-7 days group and the Nes-21 days group. Confocal microscopy showing RFP+ cells in the tumor-core and immunofluorescence labeling for the endothelial cell-marker vWF in the Nes-CreER$^{T2+/+}$;Td-Tomato glioma mouse model at 7 days and 21 days after tumor inoculation; note that RFP+ cells do not colocalize with vWF, suggesting the perivascular localization of RFP+ cells. Scale bars are 50 μm in overview-pictures, and 20 μm in orthogonal view (crosshairs).

The number of RFP+ located next to vWF+ cells significantly increased with tumor progression from 4.53 ± 1.31 in the Nes-7 days group to 28.57 ± 2.37 in the Nes-21 days group (Fig. 4.2.2-A). Seven days after tumor inoculation, only a small portion of RFP+ cells localized near vWF+ cells in the tumor area (21.62%). The proportion of RFP+ cells located next to vWF+ cells accounting for all RFP+ cells was quantified as 82.86% in the Nes-14 days group and as 92.23% in the Nes-21 days group (Fig.

4.2.2-B). The percentage of RFP+ cells located next to vWF+ cells accounting for all VWF+ cells was 15.14% in the Nes-7 days group; then that increased to 48.55% in the Nes-21 days group (Fig. 4.2.2-C).
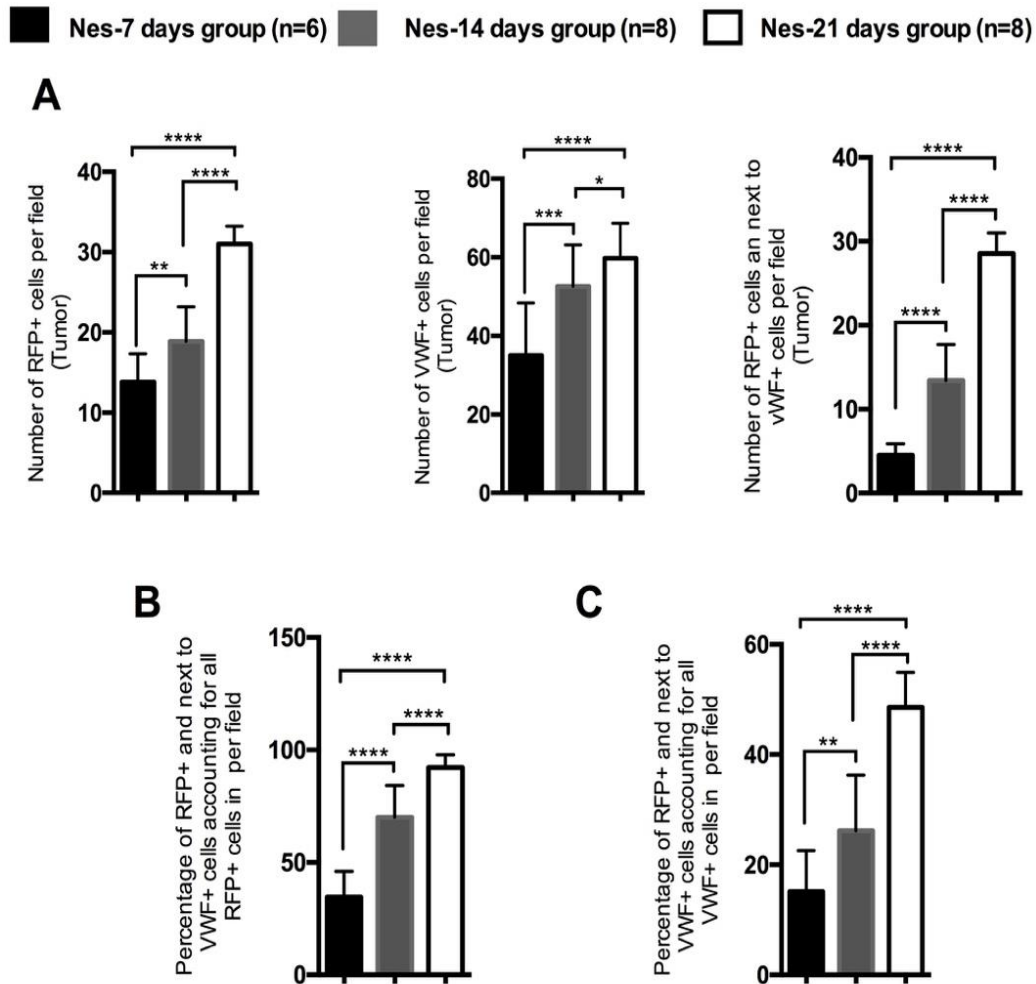
Figure 4.2.2 Quantification of intratumoral RFP and VWF expressing cells in Nes-CreER[T2+/+];Td-Tomato glioma mice at the 7 days, 14 days, and 21 days after tumor inoculation. A) Quantification of RFP+, vWF+, and RFP+ cells located next to vWF+ cells (n = 12 random fields per mouse) in the tumor area in the Nes-7 (n = 6), Nes-14 (n = 8), and Nes-21 days (n = 8) groups. The percentage of RFP+ cells located next to vWF+ cells accounting for all RFP+ cells (B) and all VWF+ cells (C) were compared between three experimental groups. Data are represented as mean ± SEM (*p < 0.05, **p < 0.01, ***p < 0.005, ****p < 0.0001).

4.3 Observing the pericyte-lineage in a glioma mouse model during tumor progression

4.3.1 RFP+ cells differentiated into pericytes expressing Desmin

After I confirmed that the RFP+ cells become perivascular cells over the course of tumor growth, we applied several pericyte markers to identify the cell-lineage relationship of these RFP+ cells. First, I performed Desmin staining to label pericytes. In the tumor area, RFP+ cells, Desmin+ cells, and RFP/Desmin double+ cells are abundantly increased during tumor progression from 7 days to 21 days after tumor inoculation. At a later stage of tumor development, RFP+ cells mostly express a marker for mature pericytes (Desmin). The highest number of RFP/Desmin double positive cells was observed in the Nes-21 days group (22.26 ± 3.05), which is significantly different from double positive cells in the Nes-7 days group (3.15 ± 0.66, $p < 0.0001$) and the Nes-14 days group (9.44 ± 2.62, $p < 0.0001$) (Fig. 4.3.1.1-A). The percentage of RFP/Desmin double positive cells among all RFP+ cells was 23.23% in the Nes-7 days group; then that increased to 71.98% in the Nes-21 days group ($p < 0.0001$, Fig. 4.3.1.1-B). The percentage of RFP+/Desmin double positive cells among all Desmin+ cells significantly increased to 33.44% in the Nes-21 days group as compared with 7.47% in the Nes-7 days group (Fig. 4.3.1.1-C).
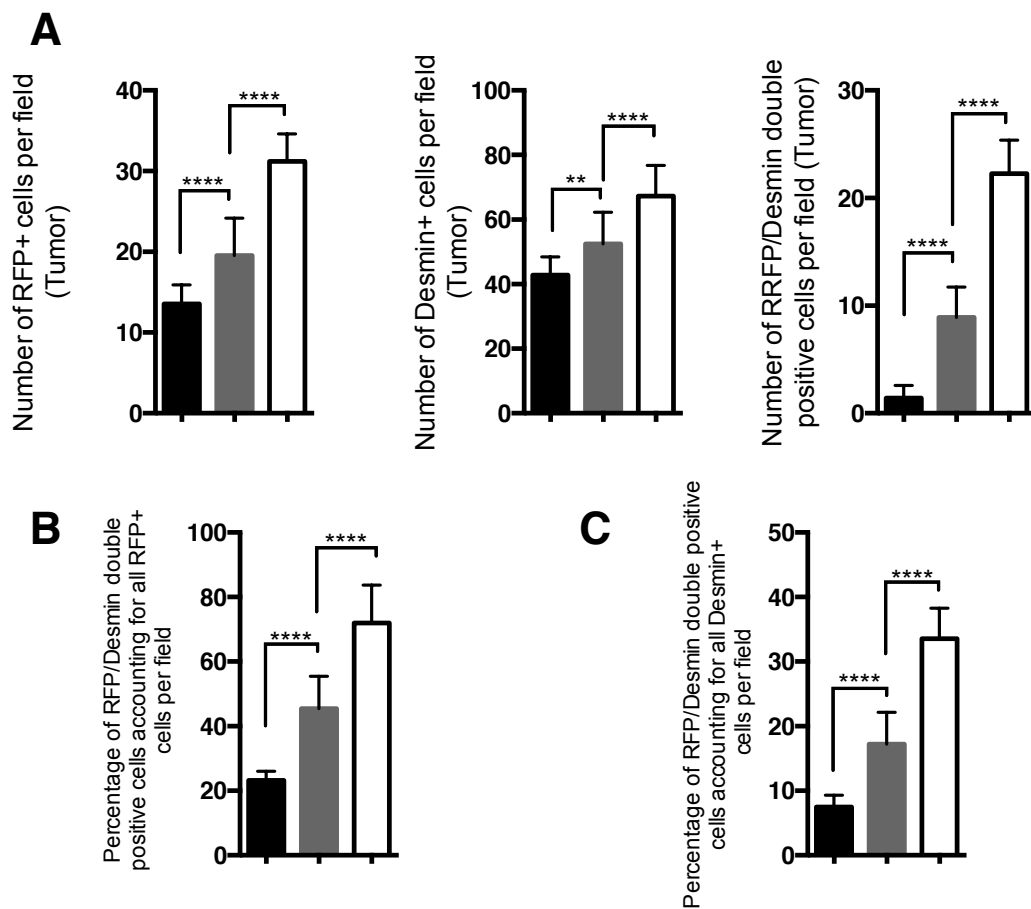
Figure 4.3.1.1 Quantification of the number of RFP+, Desmin+, and RFP/Desmin double positive cells in the tumor area of Nes-CreER$^{T2+/+}$;Td-Tomato glioma mice. A) The number of RFP+, Desmin+, and RFP/Desmin double+ cells in the Nes-7 (n = 6), Nes-14 (n = 8), and Nes-21 days groups (n = 8). The percentage of double+ cells accounting for all RFP+ cells (B) and all Desmin+ cells (C) were compared between three experimental groups. Data are represented as mean ± SEM (**p < 0.01, ****p < 0.0001).

Confocal microscopy demonstrated that RPF+ cells co-localized with immunofluorescence labeling for Desmin+ cells. Most RFP+ cells did not express Desmin in the Nes-7 days group; however, the majority of RFP+ cells co-localized with Desmin+ cells in the Nes-21 days group, indicating the RFP+ cells differentiated into mature pericytes during tumor progression. (Fig. 4.3.1.2).

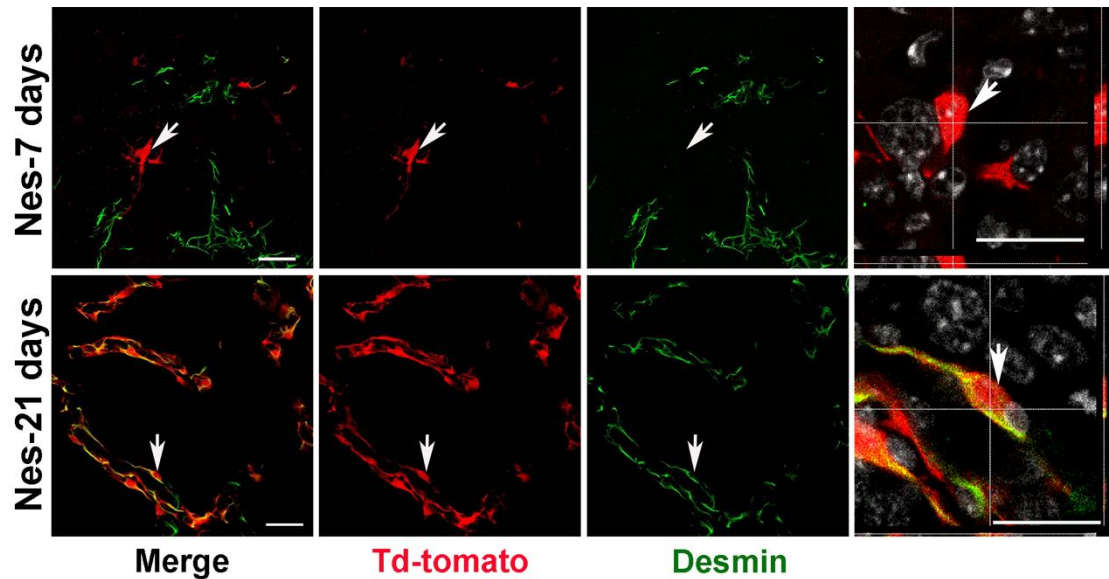**Figure 4.3.1.2 Immunofluorescence labelling for Desmin to investigate if RFP+ cells are pericytes.** Confocal fluorescence images showed the expression of RFP (red) and Desmin (green) in the tumor area between the Nes-7 days group and the Nes-21 days group. Scale bars are 50 μm in overview-pictures, and 20 μm in orthogonal view (crosshairs).

Furthermore, we observed that RFP+ cells expressing Desmin were located close to blood vessels. The number of double positive (RFP+, Desmin+) cells located close to blood vessels significantly increased from 2.38 ± 0.83 in the Nes-7 days group to 20.88 ± 3.27 in the Nes-21 days group ($p < 0.00001$, Fig. 4.3.1.2). The percentage of RFP/Desmin double+ cells located close to blood vessels accounting for all double+ cells was 66.6% in the Nes-7 days group and 93.61% in the Nes-21 days group. These results confirmed that RFP+ cells expressing Desmin are mature pericytes.
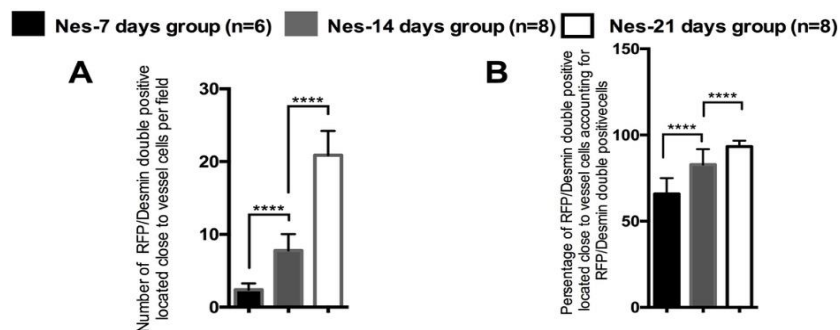

Figure 4.3.1.3 Quantification of the RFP/Desmin double positive located close to vessel cells in glioma. A) the number of RFP/Desmin double+ cells located close to vessel cells (n = 12 random fields in the tumor area); B) the proportion of RFP/Desmin double+ cells to vessel cells accounting for all double+ cells. Data are represented as mean ± SEM **** $p < 0.0001$).

In the peritumoral area, the number of single RFP+ and RFP/Desmin double positive cells only marginally increased in the Nes-21 days group as compared to those in the Nes-7 days group (Fig. 4.3.1.4-A). No difference was observed in the percentage of RFP/Desmin double+ cells accounting for all RFP+ cells (Fig. 4.3.1.4-B) or all Desmin+ cells (Fig. 4.3.1.4-C) between the Nes-7, Nes14, and Nes-21 days groups.
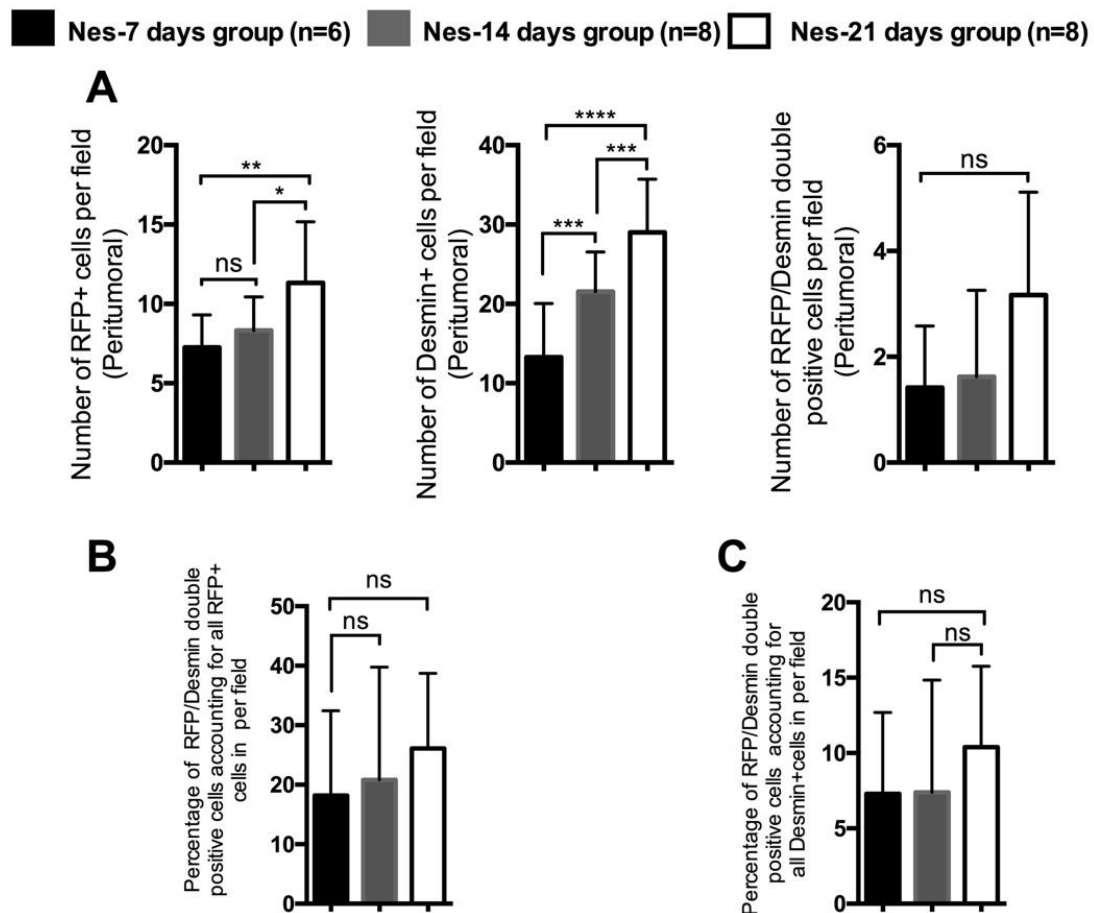
Figure 4.3.1.4 Quantification of the number of RFP+, Desmin+, and RFP/Desmin double positive cells in the peritumoral area of Nes-CreER$^{T2+/+}$;Td-Tomato glioma mice. A) The number of RFP+, Desmin+, and RFP/Desmin double+ cells in the Nes-7 (n = 6), Nes-14 (n = 8), and Nes-21 days groups (n = 8). The percentage of double+ cells accounting for all RFP+ cells (B) and all Desmin+ cells (C) between three experiment groups. Data are represented as mean ± SEM (*p < 0.05, **p < 0.01, ***p < 0.005, ****p < 0.0001, [ns] no significant).

In the contralateral hemisphere, no differences were observed in the number of RFP+, Desmin+, and RFP/Desmin double positive cells, and the percentage of RFP/Desmin double positive cells among all RFP+ or all Desmin+ cells between Nes-7, Nes-14, and Nes-21 days groups remained constant over time (Fig. 4.3.1.5).
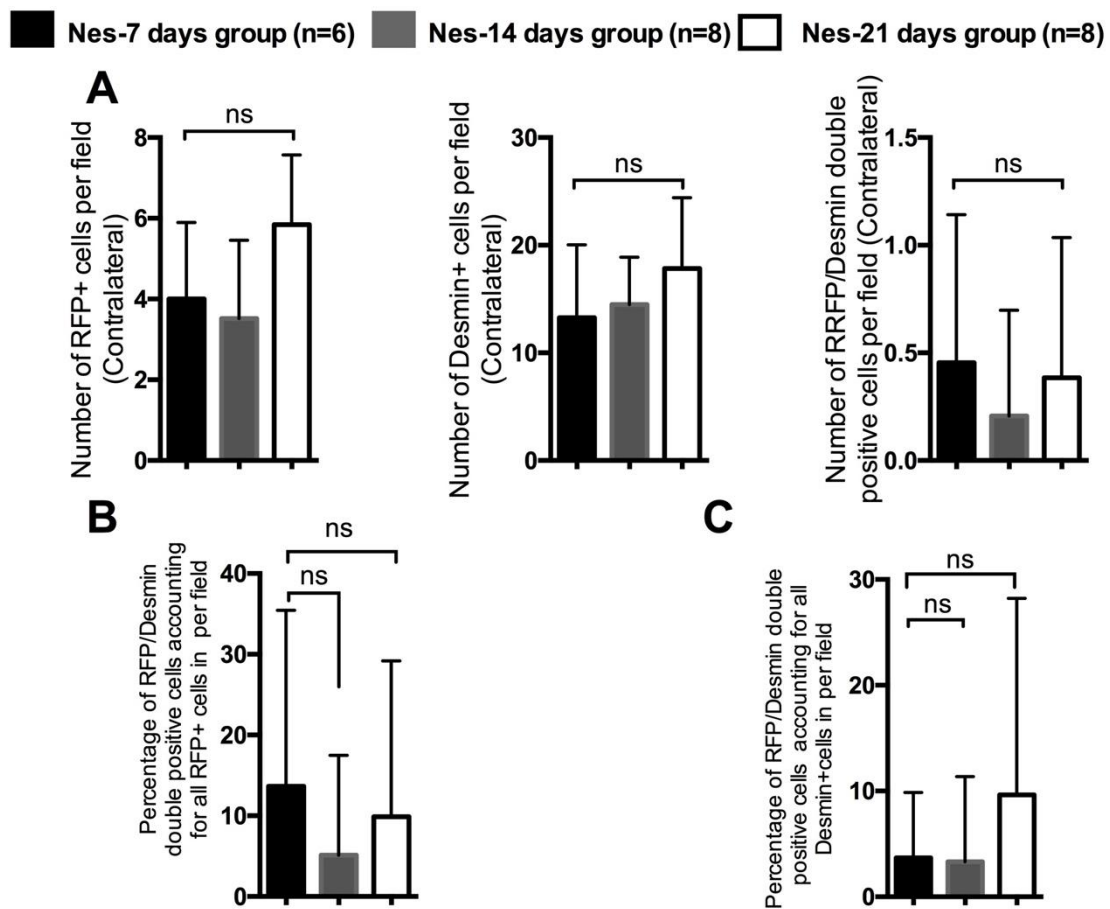
Figure 4.3.1.5 Quantification of the number of RFP+, Desmin+, and RFP/Desmin double positive cells in the contralateral tumor-free brain hemisphere of Nes-CreER$^{T2+/+}$;Td-Tomato glioma mice. A) The number of RFP+, Desmin+, and RFP/Desmin double+ cells in Nes-7 (n = 6), Nes-14 (n = 8), and Nes-21 days groups(n = 8). The percentage of double+ cells accounting for all RFP+ cells (B) and all Desmin+ cells (C) between three experimental groups. Data are represented as mean ± SEM (^{ns} no significant).

4.3.2 Differentiated RFP+ cells expressing PDGFR-β during the tumor progression

Immunostaining for PDGFR-β, another frequently used pericytes marker (Winkler et al., 2010), was applied to identify RFP+ cells throughout glioma growth. The confocal imaging showed that the RFP+ cells were negative for PDGFR-β in the Nes-7 days group. These RFP expressing cells colocalized with PDGFR-β+ cells in the Nes-21 days group, indicating the RFP+ cells differentiated to mature pericytes and expressed pericyte markers during glioma growth (Fig. 4.3.2.1).
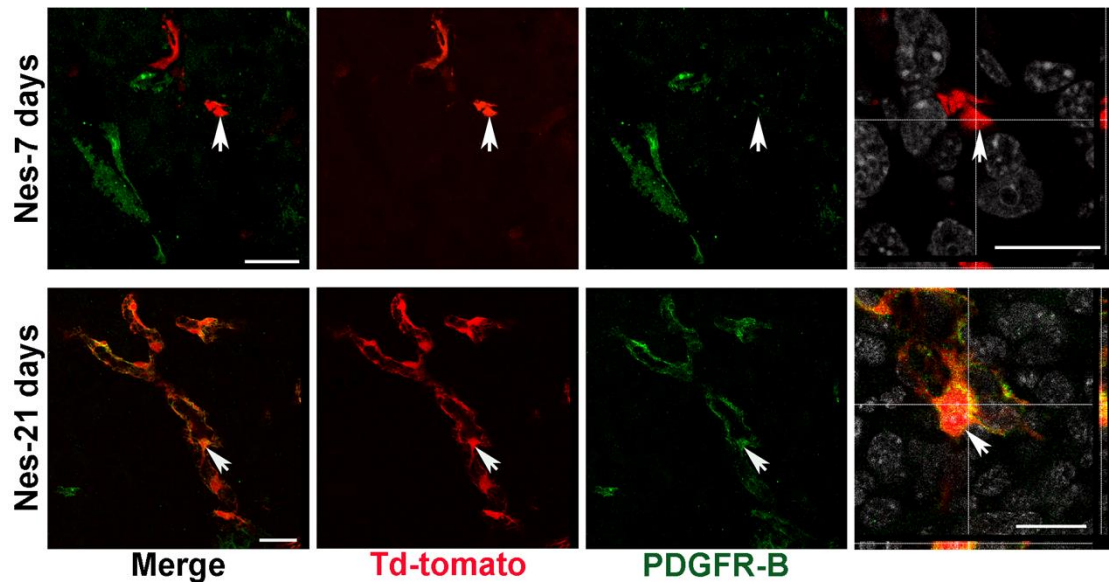
Figure 4.3.2.1 Immunofluorescence detection of RFP and PDGFR-β expression in the tumor area of animals from the Nes-7 days and the Nes-21 days group. Confocal fluorescence images showed the expression of RFP (red) and PDGFR-β (Green) in the tumor area of mice from the Nes-7 days and the Nes-21 days group. Scale bars are 50 μm in overview-pictures, and 20 μm in orthogonal view (crosshairs).

According to my analysis, the number of RFP/PDGFR-β double positive cells in the tumor area was significantly increased from 4.0 ± 0.88 in the Nes-7 days group to 9.35 ± 3.08 in the Nes-14 days group ($p < 0.0001$) and 24.28 ± 5.61 in the Nes-21 days group ($p < 0.0001$) (Fig. 4.3.2.2-A). The percentage of RFP/PDGFR-β double positive cells accounting for all RFP+ cells showed a steep increase from 7 days ($27.05\% \pm 4.31$) to 21 days ($79.14\% \pm 9.17$) after tumor cells inoculation ($p < 0.0001$, Fig. 4.3.2.2-B). The percentage of double positive cells accounting for all PDGFR-β+ cells increased from $9.49\% \pm 1.93$ in the Nes-7 days group to $31.06\% \pm 9.01$ in the Nes-21 days group ($p < 0.0001$, Fig. 4.3.2.2-C).

Figure 4.3.2.2 Quantification of the number of RFP+, PDGFR-β+, and RFP/ PDGFR-β double positive cells in the tumor area of Nes-CreER^{T2+/+};Td-Tomato glioma mice. A) The number of RFP+, PDGFR-β+ and RFP/ PDGFR-β double+ cells in Nes-7 (n = 6), Nes-14 (n = 8), and Nes-21 days (n = 8) groups. The percentage of RFP/ PDGFR-β double+ cells accounting for all RFP+ cells (B) and all PDGFR-β+ cells (C) between three experimental groups. Data are represented as mean ± SEM (****p < 0.0001).

In the peritumoral area, the number of RFP+ and RFP/PDGFR-β double+ cells increased during tumor progression. However, the number of single PDGFR-β + cells increased from 20.66 ± 4.39 in the Nes-7 days group to 38.86 ± 11.13 in the Nes-14 days group; then the number declined to 31.96 ± 7.01 in the Nes-21 days group (Fig. 4.3.2.3-A). Furthermore, the proportion of RFP+/PDGFR-β double positive cells accounting for all RFP+ cells also showed a decline in the Nes-21 days group (6.02 ± 4.91), even lower than the Nes-7 days group (7.53 ± 5.31) (Fig. 4.3.2.3-B), while no difference was observed in the proportion of RFP/PDGFR-β double+ cells accounting for all PDGFR-β+ cells (Fig. 4.3.2.3-C). In my previous results, the number of

PDGFR-β+ cells significantly increased in the tumor area during glioma progression. However, in the peritumoral area, the number of RFP+ and PDGFR-β+ cells declined with tumor growth. It is possible that PDGFR-β+ cells from the peritumoral area migrate to the tumor area to support tumor growth. This hypothesis needs to be addressed in future studies. No significant difference was observed in the percentage of RFP+/PDGFR-β+ cells accounting for all PDGFR-β+ cells in the Nes-7, Nes-14, and Nes-21 days groups.
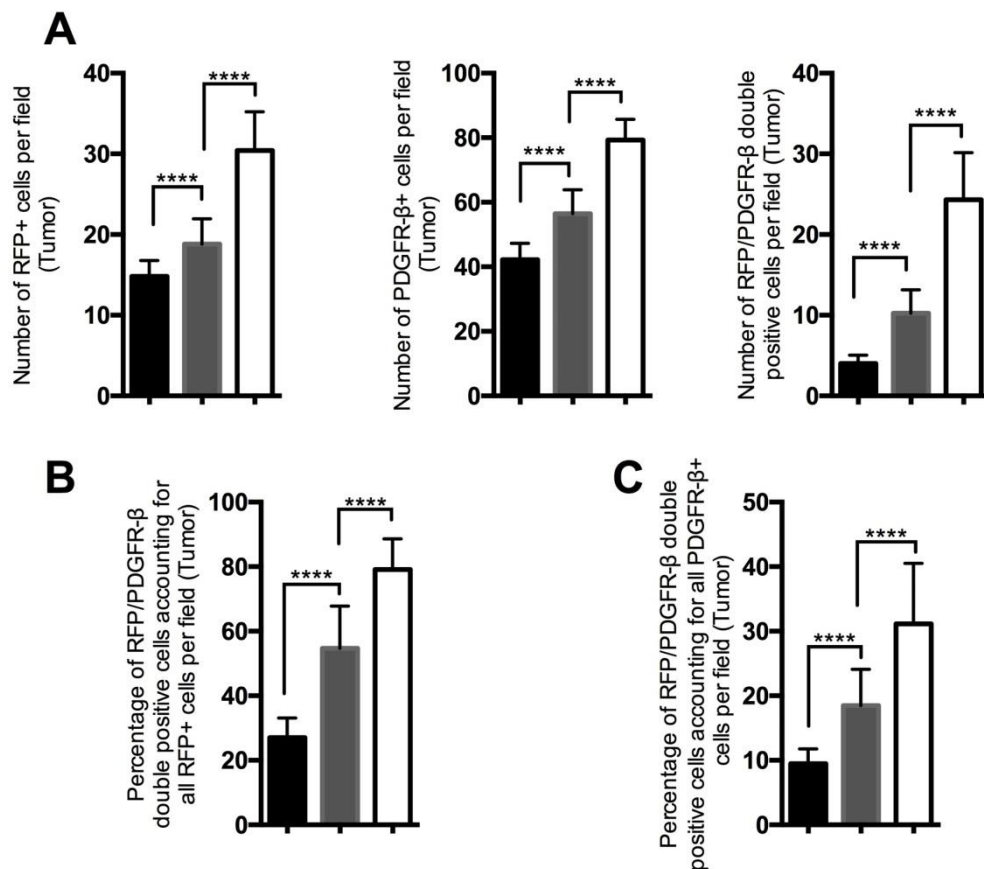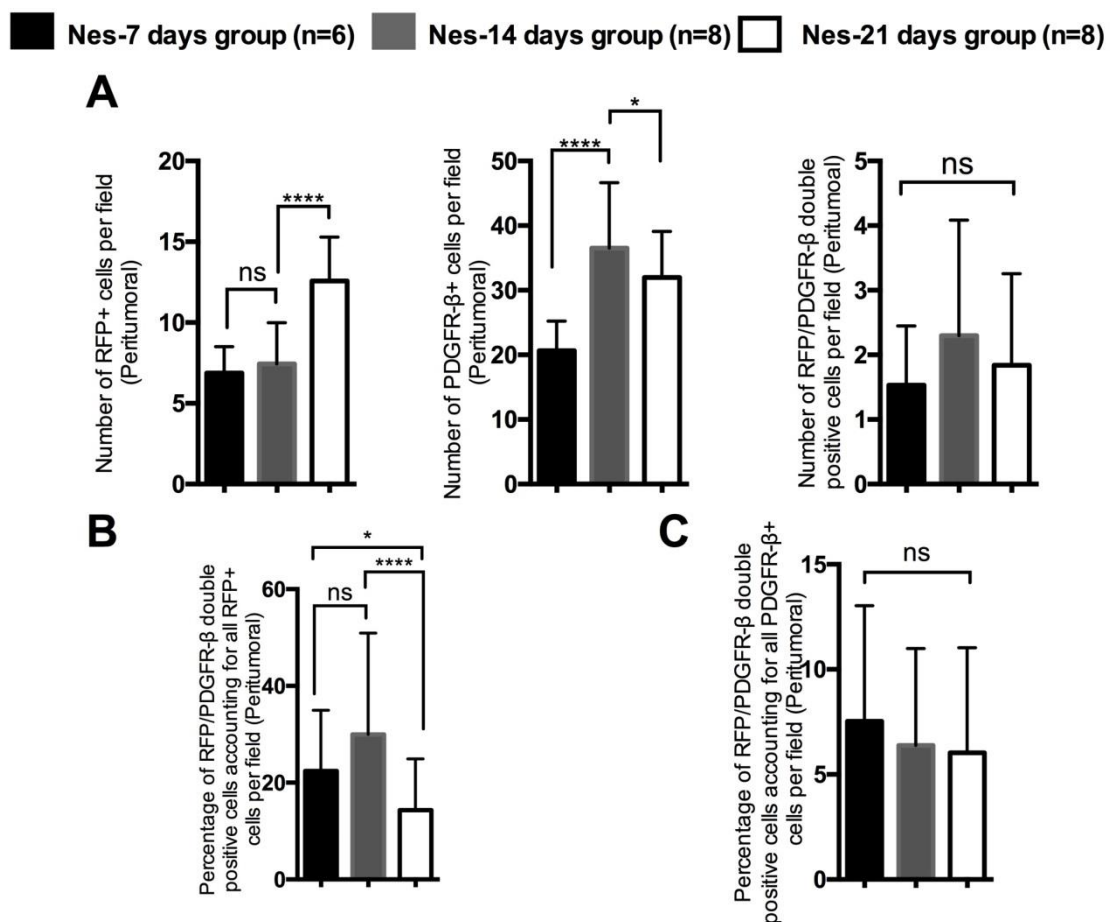

Figure 4.3.2.3 Quantification of the number of RFP+, PDGFR-β+, and RFP/ PDGFR-β double positive cells in the peritumoral area of Nes-CreER[T2+/+];Td-Tomato glioma mice. A) The number of RFP+, PDGFR-β+ and RFP/ PDGFR-β double+ cells in the Nes-7 (n = 6), Nes-14 (n = 8), and Nes-21 days groups (n = 8). The percentage of RFP/ PDGFR-β double+ cells accounting for all RFP+ cells (B) and all PDGFR-β+ cells (C) between three experimental groups. Data are represented as mean ± SEM (*p < 0.05, ****p < 0.0001, [ns] no significant).

In the contralateral hemisphere, no differences were observed in the number of positive cells or the percentages of RFP/PDGFR-β double+ cells in the Nes-7, Nes-14, and Nes-21 days groups (Fig. 4.3.2.4). This suggests that RFP+ or PDGFR-β+ cells in the contralateral tumor-free brain hemisphere were not influenced by tumor progression.
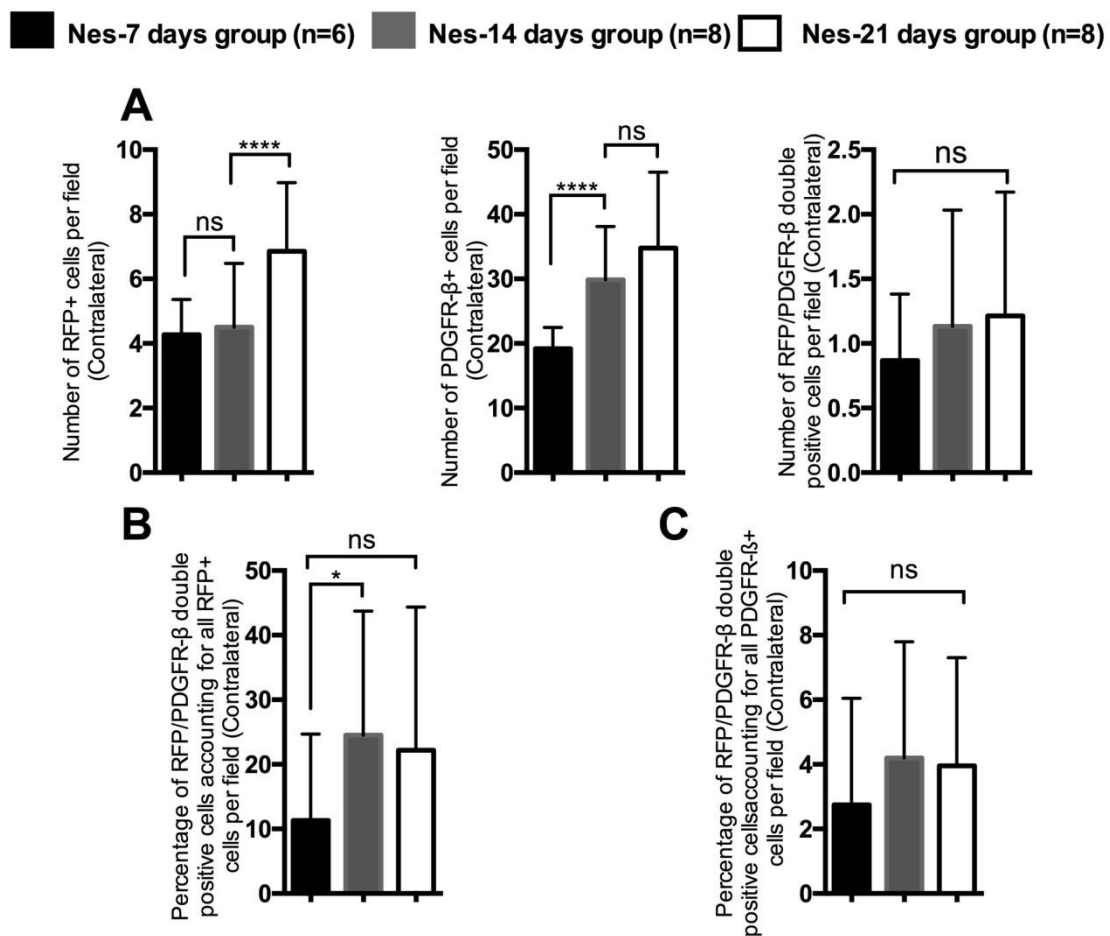
Figure 4.3.2.4 Quantification of the number of RFP+, PDGFR-β+, and RFP/ PDGFR-B double positive cells in the contralateral tumor-free brain hemisphere of Nes-CreER$^{T2+/+}$;Td-Tomato glioma mice. A) The number of RFP+, PDGFR-β+ and RFP/ PDGFR-β double+ cells in Nes-7 (n = 6), Nes-14 (n = 8), and Nes-21 days groups (n = 8). The percentage of RFP/ PDGFR-β double+ cells accounting for all RFP+ cells (B) and all PDGFR-β+ cells (C) between three experimental groups. Data are represented as mean ± SEM (*p < 0.05, ****p < 0.0001, [ns] no significant).

4.4 Lineage-tracing and cell-type identification using multiple pericyte markers

Several markers are commonly applied to identify pericytes, including Desmin, PDGFR-B, CD146, and NG2 (Armulik et al., 2011). Therefore, we performed combined staining with Desmin, PDGFR-β, CD146, and NG2 all together observed in one immunofluorescence channel to directly investigate the relationship between the cell lineage of RFP+ cells with pericytes. The confocal imaging showed that very few RFP+ cells expressed pericyte markers in the Nes-7 days group; while RFP+ cells were abundantly co-localized with pericyte marker-labelling cells in the Nes-21 days group (Fig. 4.4-A). The quantification showed that the number of RFP and Desmin-/PDGFR-β-/CD146-/NG2- positive cells significantly increased from 3.63 ± 1.49 in the Nes-7 days group to 26.18 ± 4.55 in the Nes-21 days group ($p < 0.05$). In addition, we found that the majority of RFP+ cells (75%) are negative for mature pericyte markers, including Desmin, PDGFR-β, NG2, CD146 at 7 days after the tumor inoculation, but most of RFP+ cells (88.10%) acquired mature pericyte markers becoming RFP positive, and Desmin-, PGGFR-β-, NG2-, or CD146 positive cells at 21 days after tumor injection (Fig. 4.4-B). Previous studies have shown that mature pericytes express pericyte markers (Bergers and Song, 2005, Winkler et al., 2010). The present study has shown that the newly generated RFP+ pericytes are derived from RFP+ pericyte progenitor cells (PPCs), which are RFP positive and Desmin-/PDGFR-β/NG2-/CD146-negative cells. These results suggest that these PPCs differentiate into mature pericytes during glioma progression.
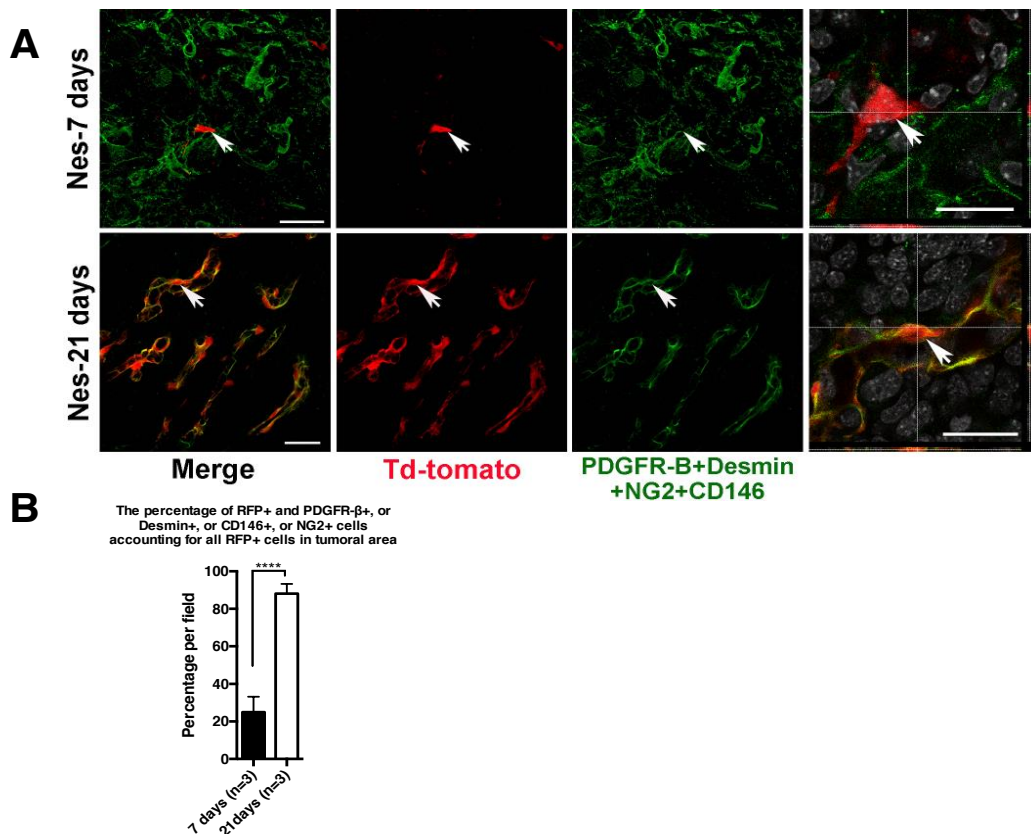
Figure 4.4. Combinatorial Immunofluorescence labelling for established pericyte markers (PDGFR-B, Desmin, NG2 and CD146; simultaneously detected in the green channel) to investigate if RFP+ cells differentiate to pericytes during tumor growth. A) RFP+ cells in the tumor-core are not pericytes in early gliomagenesis (7 days after orthotropic glioma implantation), but are pericytes in the fully established tumor (21 days; a quantification for these immunofluorescence data is shown); note that RFP+ cells represent a very large fraction of all intratumoral pericytes. B) Quantification of the percentage of RFP+ cells with positive pericyte markers accounting for all RFP+ cells. Data are represented as mean ± SEM (**** p < 0.0001). Scale bars are 50 μm in overview-pictures, and 20 μm in orthogonal view (crosshairs)

4.5 Pericyte progenitor-like cells are not derived from the bone marrow

Previous reports suggested that the bone marrow contributes pericytes to the glioma vasculature (Song et al., 2005). In the present study, lineage-tracing experiments in different bone marrow chimeric glioma models were applied to determine whether the RFP+ PPCs are derived from the bone marrow during tumor development. In the BM/Nes-Td-Tomato group, C57B1/6 wild type mice were reconstituted with bone marrow donor cells from the Nes-CreER$^{T2+/+}$;Td-Tomato transgenic strain; while, in the BM/PU1-GFP group, Nes-CreER$^{T2+/+}$;Td-Tomato transgenic mice were reconstituted with bone marrow from myeloid-reporter mice (PU.1-GFP mouse strain).

In the BM/PU1-GFP group, we found many PU1-GFP+ cells in the tumor area, indicating that bone marrow-derived myeloid cells could go through the BBB into the brain as expected (Fig.4.5.1-A) (Harrison-Brown et al., 2016). If the RFP+ cells are generated from bone marrow-derived cells, the Nes-Cre-RFP donor cells in the C57B1/6 wild type mouse model should also infiltrate to the tumor area. However, in the BM/Nes-Td-Tomato group, I did not detect RFP+ cells in the tumor area, suggesting RFP+ donor cells are not contributed by the bone morrow (Fig4.5.1-B).
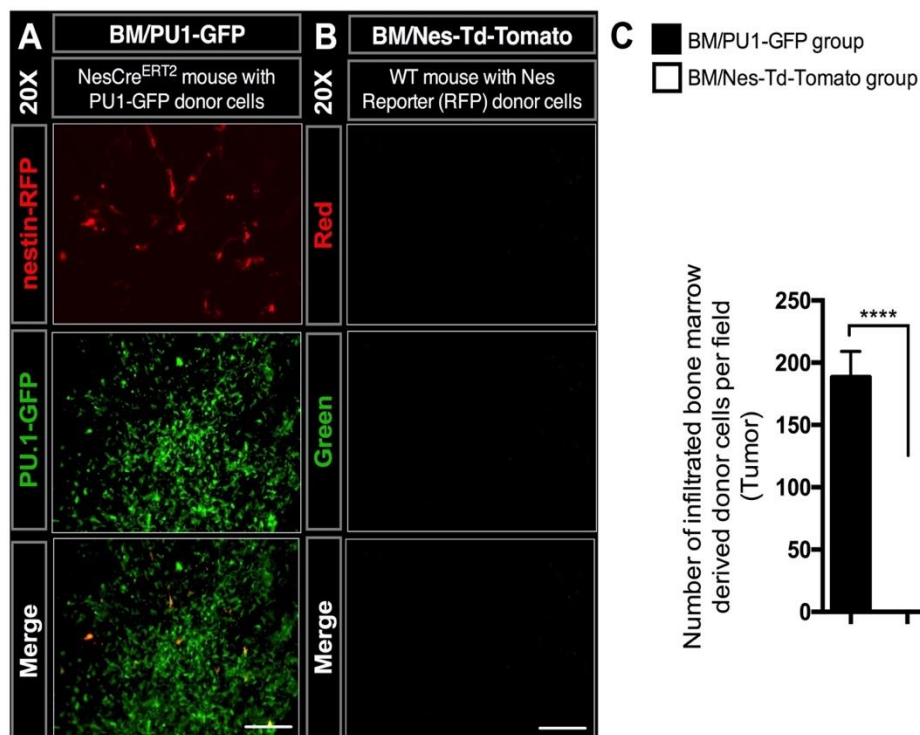
Figure 4.5.1. The bone marrow derived donor cells infiltrate to the tumor area. To investigate if RFP+ pericytes in our glioma model are bone-derived we created different bone-marrow chimera. A) We used Nes-CreERT2$^{+/+}$;Td-Tomato mice reconstituted with bone marrow from myeloid-reporter mice (PU.1-GFP mouse strain) and found that RFP+ cells still develop into pericytes (14 days after glioma-induction); the efficiency of bone-marrow-reconstitution is corroborated by the large number of GFP+ cells accumulating in experimental gliomas. B) Wild-type mice were reconstituted with bone marrow from the Nes-CreERT2$^{+/+}$;Td-Tomato transgenic strain, 14 days after orthotropic glioma-inoculation no intratumoral RFP+ are visible. C) Quantification of data from figures (A) and (B); data are represented as mean ± SEM (**** p < 0.0001). Scale bars are 200 μm.

To investigated the cell type of the tumor-infiltrating bone marrow-derived cells in the BM/PU1-GFP group, we performed immunostaining for Iba1 to label microglia or macrophages. The fluorescence images showed that most of the intratumoral

PU1-GFP+ (green) cells also express the microglia/macrophage marker (Iba1) in the BM/PU1-GFP group. These results confirm that most bone marrow-derived PU1-GFP+ cells are microglia or macrophages.

40x magnification

| iBa1 | PU1-GFP | Merge |
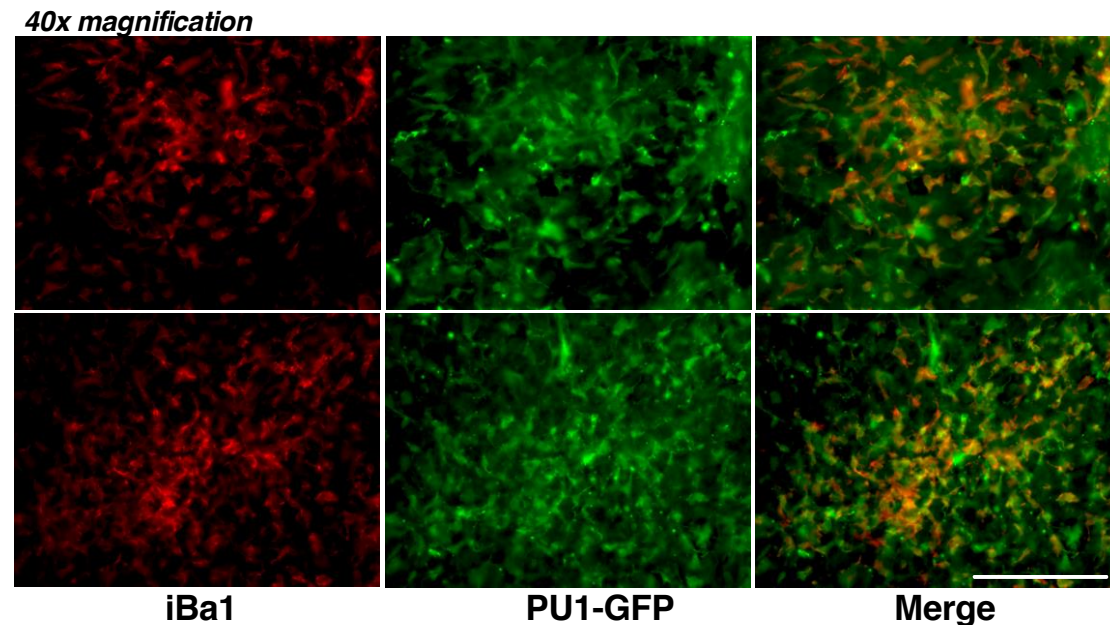
Figure 4.5.2. Immunofluorescence detection of PU1-GFP and iba1 expression in the tumor-core of the BM/PU1-GFP group at 14 days after tumor inoculation; note that RFP+ cells colocalize with iba1+ cells. Scale bars are 200 μm.

Because irradiation could influence RFP expression in Nes-CreER$^{T2+/+}$;Td-Tomato mice, we further analyzed RFP expression between the Nes-14 days group (without lethal irradiation) and the BM/PU1-GFP group (with lethal irradiation). We found that RFP expression significantly increased in the BM/PU1-GFP group as compared with the Nes-14 days group (Fig. 4.5.3-A). The number of RFP+ cells in the BM/PU1-GFP group was 27.8 ± 4.4 in the tumor area, 17.5 ± 2.62 in the peritumoral area, and 13.6 ± 2.65 in the contralateral tumor-free brain hemisphere, compared with 21.55 ± 3.45 in the tumor area, 8.57 ± 2.29 in the peritumoral area, and 4.12 ± 1.45 in the contralateral area of mice from the Nes-14 days group (Fig. 4.5.3-B). Altogether, these results indicated that the irradiation does not have a large effect on the number

of recombined cells in the tumor, but can strongly increase the number of RFP+ cells in the peritumoral area and in the tumor-free brain.
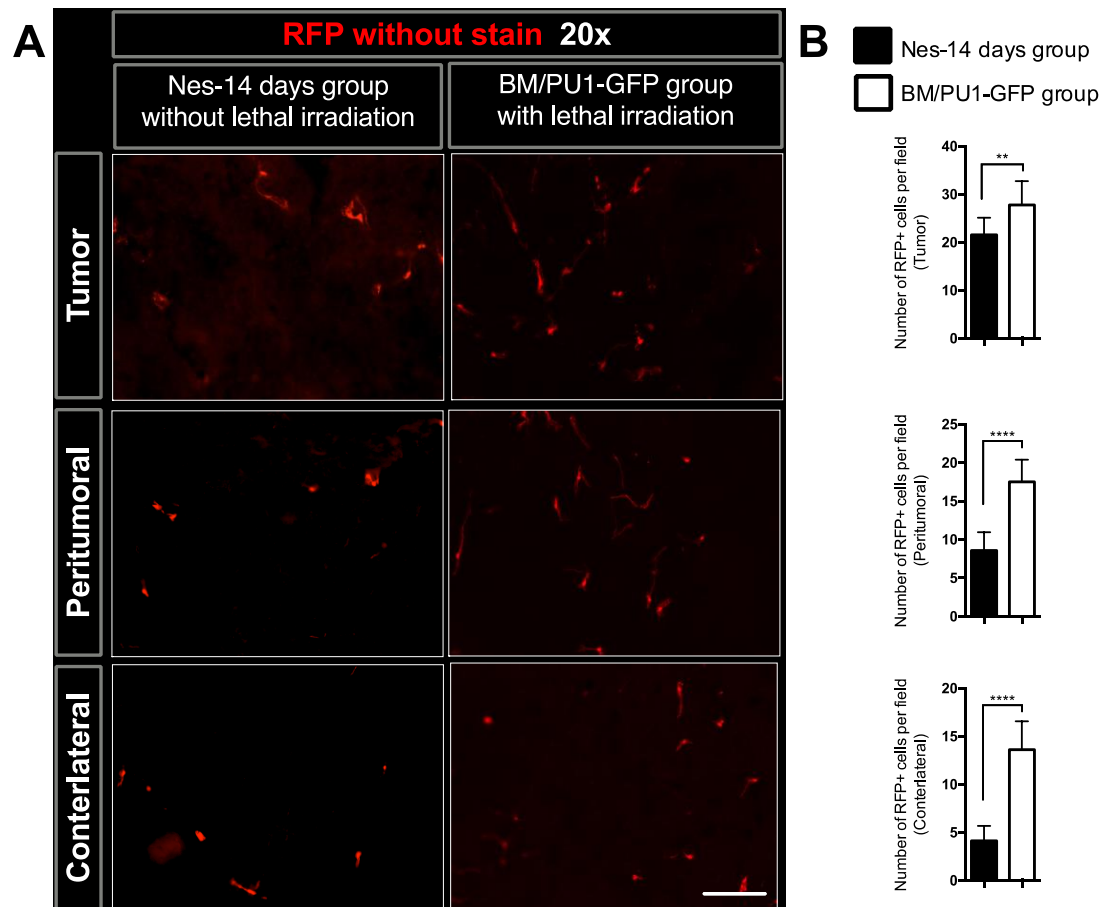
Figure 4.5.3. The number of RFP expressing cells in BM/PU1-GFP and Nes-14 days groups in the tumor, peritumoral area, and contralateral tumor-free brain hemisphere. A) Fluorescence imaging of RFP expression in the BM/PU1-GFP and the Nes-14 days group in the tumor, peritumoral, and contralateral areas (20x magnification). B) Quantification of the number of RFP+ cells in the tumor, peritumoral, contralateral areas (n = 12 random fields per mouse) in BM/PU1-GFP and Nes-14 days groups. Data are represented as mean ± SEM (**p < 0.01, **** p < 0.0001). Scale bar is 200 μm.

Moreover, we quantified the number of PDGFR-β+ cells in the Nes-14 days group and the BM/PU1-GFP group. In Fig. 4.5.4-A, it is clear that fewer cells stained for PDGFR-β in the BM/PU1-GFP group as compared with the Nes-14 days group. The number of PDGFR-β+ cells was 26.0 ± 5.51 in the BM/PU1-GFP group and 57.42 ± 7.44 in the Nes-14 days group (p < 0.00001), as shown in Fig. 4.5.4-B. These results showed that there are more RFP+ pericyte progenitors, but less pericyte differentiation in the mouse brain after irradiation.
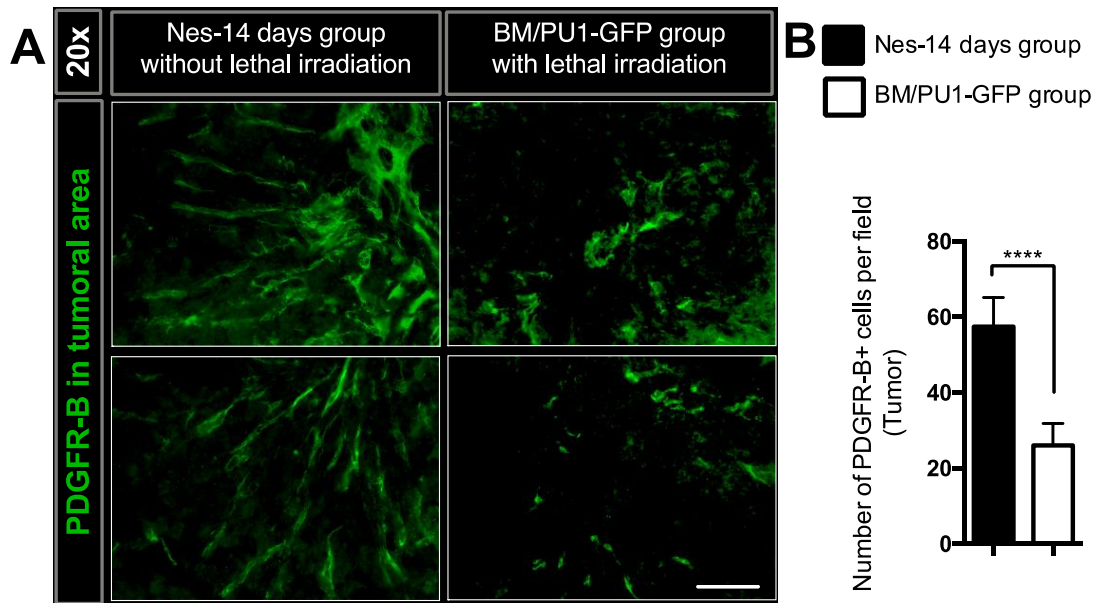
Figure 4.5.4. The PDGFR-β expression in the tumor area in BM/PU1-GFP and the Nes-14 days groups. A) fluorescence imaging of PDGFR-β expression in the BM/PU1-GFP group and the Nes-14 days group (20x magnification). B) Quantification of the number of RFP+ cells in the tumor area (n = 12 random fields per mouse) between the BM/PU1-GFP group and the Nes-14 days group. Data are represented as mean ± SEM (**** p < 0.0001). Scale bar is 200 μm.

4.6 Ablation of pericyte progenitor like cells reduces tumor size, tumor angiogenesis, and the number of pericytes

In order to investigate the role of PPCs during tumor progression, I applied a lineage ablation glioma mouse model to kill the Cre recombined RFP+ cells. Because our previous results (Figure 4.4) showed that most RFP positive cells are PPCs at the early stage of tumor development, we performed TAM injection to ablate recombined RFP+ cells at 4 days after tumor inoculation. RFP expression was compared in transgenic models with (the Nes-iDTA group) and without (the Nes-RFP group) iDTA cell-lineage ablation (Fig 4.6.1-A, groups define shown in Table 3.1). The number of RFP+ cells significantly decreased in the Nes-iDTA group (10.29 ± 4.77) as compared with the Nes-RFP group (20.61 ± 4.09, p < 0.0001) in the tumor area. After TAM administration in the Nes-iDTA group, the number of RFP+ cells was reduced by approximately 50% in the tumor area. These results indicated that we successfully established a mouse model to ablate the RFP+ PPCs.

A

B
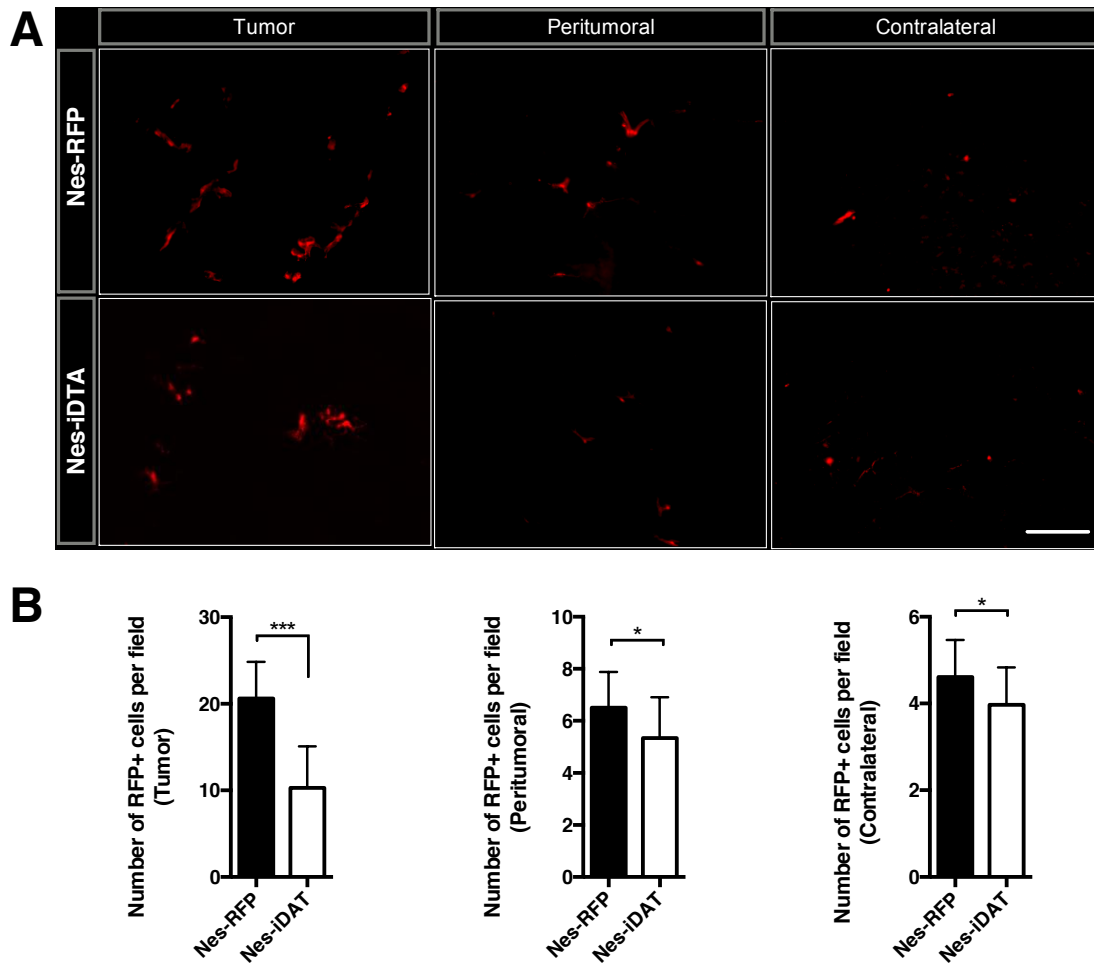
Figure 4.6.1. The number of RFP expressing cells between the Nes-iDTA group and the Nes-RFP group. A) Fluorescence imaging of the RFP expression between the Nes-iDTA group and Nes-RFP group in the tumor, peritumoral, and contralateral areas. B) Quantification of the number of RFP+ cells in the tumor, peritumoral, and contralateral areas (n = 12 random fields per mouse) in two experimental groups. Data are represented as mean ± SEM (*p < 0.05, *** p < 0.0005). Scale bar is 200 µm.

We performed a H&E staining to investigate the tumor volumes in the Nes-iDTA group and the Nes-RFP group. I found that tumor volumes were smaller in the Nes-iDTA group as compared with the Nes-RFP group, as shown in Fig 4.6.2-A. The quantification showed a significant decrease of tumor volumes in the Nes-iDTA group as compared with the Nes-RFP control group (4.75 mm^3 ± 2.25 versus 8.55 mm^3 ± 2.36; p = 0.0357; Fig. 4.6.2-B). The tumor volume was reduced by 45%, when we ablated RFP+ PPCs.
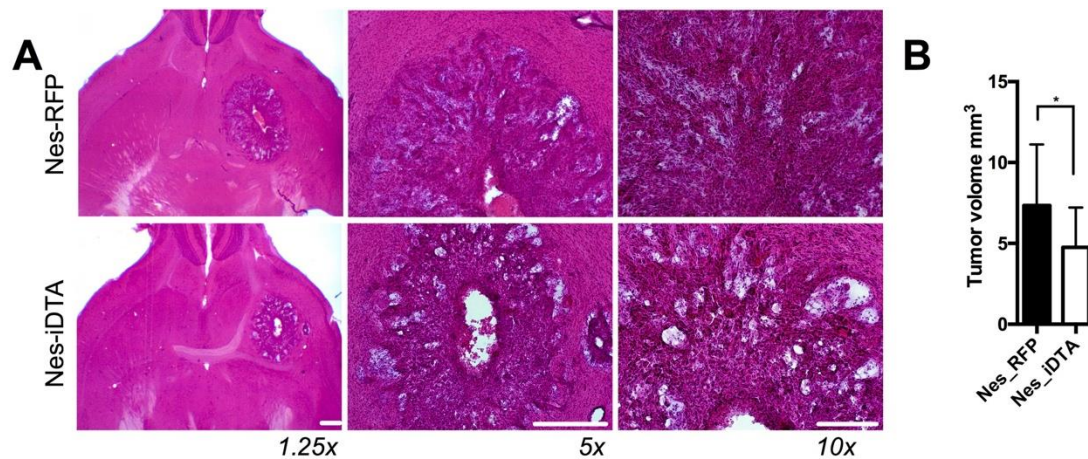
Figure 4.6.2. Tumor volumes were decreased after ablating the RFP+ PPCs. Tumor volume was compared in transgenic models with (Nes-iDTA) and without (Nes-RFP) -iDTA cell-lineage ablation. Animals were treated as the Nes-14 days group, which assures that preponderantly pericyte-progenitors are ablated in the Nes-iDTA model and that a large tumor mass is formed. A) Illustrates tumor morphology by H&E staining in both experimental groups. B) Quantification of the tumor volume (mm^3) in both groups; note that pericyte progenitor ablation largely reduces tumor volume, data are represented as mean ± SEM (*p < 0.05). Scale bars are 200 μm in 1.25x and 5x magnification; 100 μm in 10x magnification.

To investigate tumor angiogenesis in our glioma mouse model after ablation of RFP+ cells, a vWF staining was performed. The illustrated fluorescence images show the number of vWF expressing cells significantly decreased in the Nes-iDTA group as compared with the Nes-RFP control group (Fig 4.6.3-A). The total blood vessel covered area significantly declined in the Nes-iDTA group as compared with the Nes-RFP group (7.67% ± 1.88 versus 11.69% ± 3.20; p < 0.0001, Fig. 4.6.3-B). When we ablated the RFP+ PPCs, the vessel area was reduced by 50% as compared to the Nes-RFP group. In addition, a significant reduction in vessel density (p = 0.0002) and vessel network complexity (p = 0.0096) was observed in the Nes-iDTA group as compared with the Nes-RFP group.
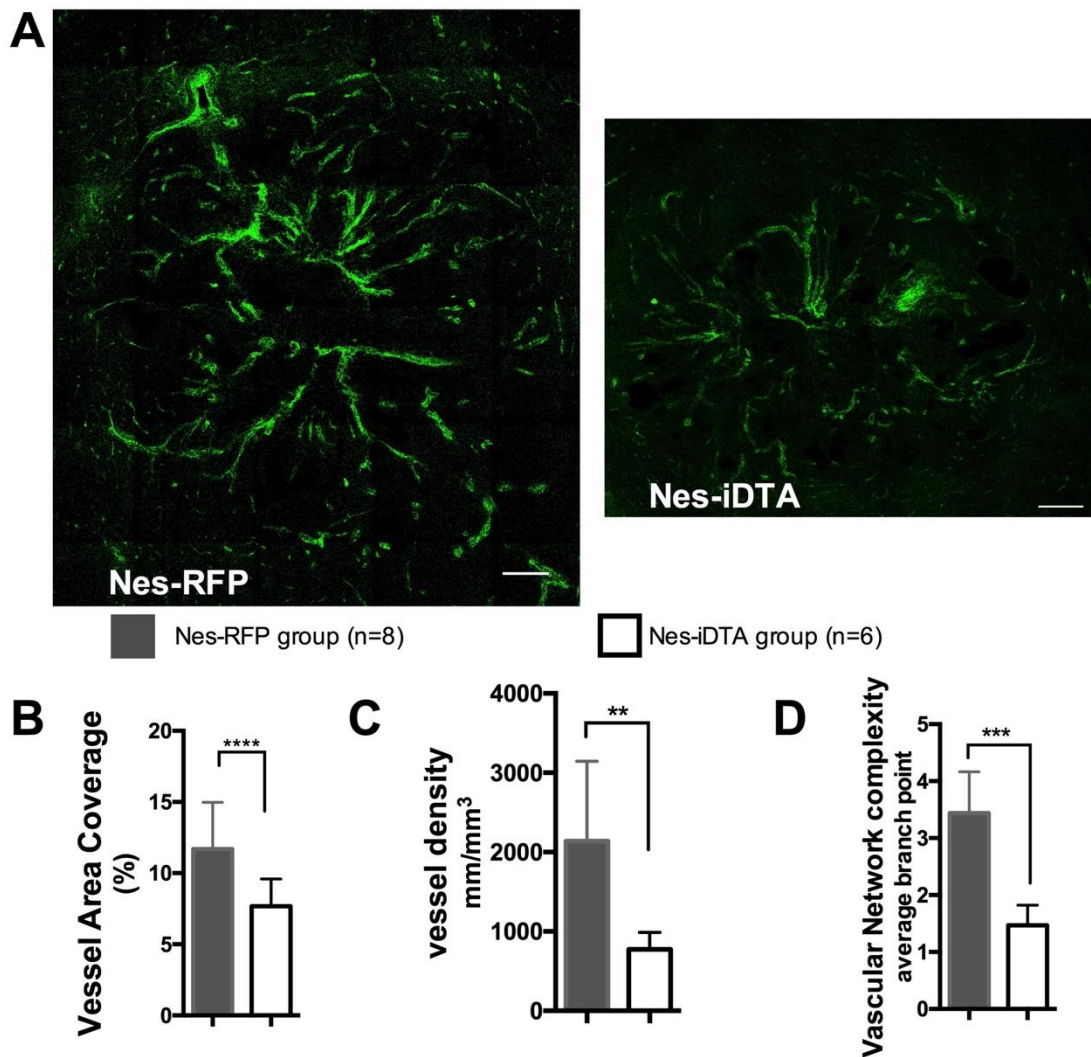
Figure 4.6.3. Ablation of pericyte progenitors is anti-angiogenic. A) Immunofluorescence detection of vWF in the entire tumor are (of representative horizontal cross-section); note that Vascular density and complexity are largely reduced in Nes-iDTA mice as compared to the Nes-RFP model. Quantification of vessel covered area (B), vessel density (C), and vessel network complexity (D) in both experimental groups. Data are represented as mean ± SEM (**$p < 0.01$, ***$p < 0.005$, **** $p < 0.0001$, [ns]no significant). Scale bars are 200 μm.

We further investigated PDGFR-β expression after RFP+ cell ablation. In Fig 4.6.4-A, in the tumor area, the number of RFP+, PDGFR-β+, and double positive cells significantly decreased in the Nes-iDTA group as compared with the Nes-RFP group. The quantification showed a significant reduction in the Nes-iDTA group as compared with the Nes-RFP group, in terms of the number of PDGFR-β+ (41.17 ± 8.99 versus 57.42 ± 7.44, $p < 0.05$) and PDGFR-β/RFP double positive cells (3.75 ± 1.56 versus 9.35 ± 3.08, $p < 0.05$), as shown in Fig. 4.6.4-B. The percentage of

PDGFR-β/RFP double positive cells accounting for all RFP+ cells showed a sharp reduction in the Nes-iDTA group (37.88% ± 4.31) as compared with the Nes-RFP group (54.69% ± 12.86, p < 0.05) (Fig. 4.6.4-C). A significant reduction was observed in the percentage of PDGFR-β/RFP double positive cells accounting for all PDGFR-β+ cells between two experimental groups (9.18% ± 5.58 versus 18.47% ± 5.63, p < 0.05) (Fig. 4.6.4-D).
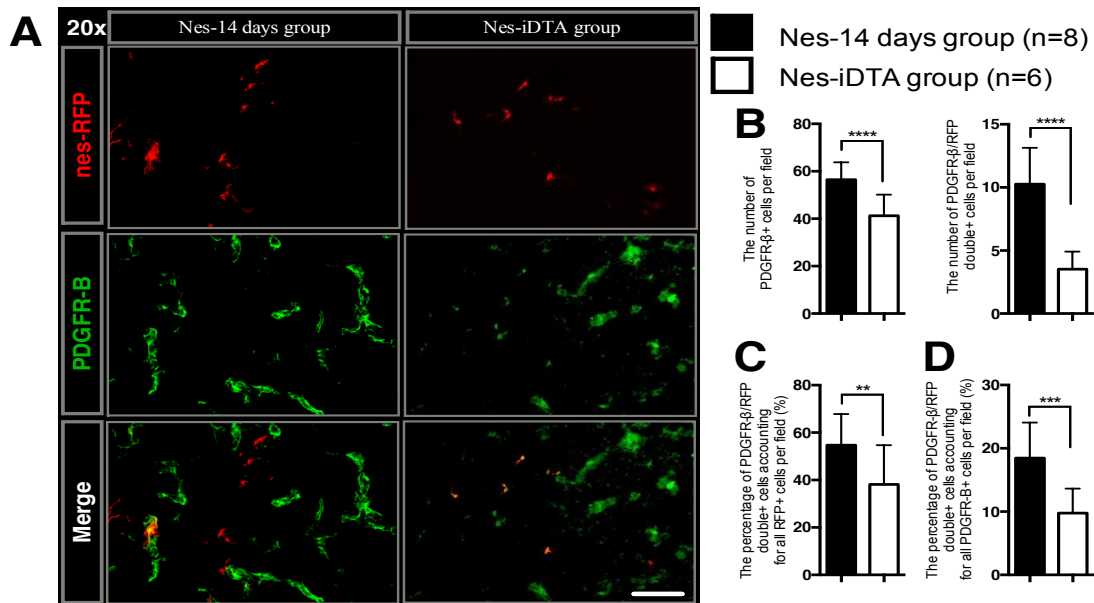
Figure 4.6.4 Immunofluorescence detection and quantification of PDGFR-β expressing cells in the tumor area between the Nes-iDTA group and the Nes-RFP group. A) Representative fluorescence images showed the expression of RFP (red) and PDGFR-β (green) between the Nes-iDTA group and the Nes-RFP group. The quantification of (B) PDGFR-β+, and RFP/PDGFR-β double+ cells (n = 12 random fields per mouse), (C) the percentage of RFP/PDGFR-β double+ accounting for all RFP+ cells and (D) for all PDGFR-β+ cells in both experimental groups. Data are represented as mean ± SEM (**p < 0.01, ***p < 0.005, ****p < 0.0001). Scale bar is 200 μm.

5 DISCUSSION

Pericytes are mural cells that contribute to vessel function and formation in both healthy (Garmy-Susini and Varner, 2005, Crisan et al., 2008, Armulik et al., 2010) and pathological tissues (Enge et al., 2002, Xian et al., 2006, Nishimura et al., 2016, Paez-Ribes et al., 2009, Paquet-Fifield et al., 2009). In the CNS, pericytes play an important role in establishing and maintaining the BBB and angiogenesis, together with endothelial cells, astrocytes, and neurons (Halliday et al., 2016, Caporali et al., 2016, Dumpich and Theiss, 2015). Moreover, using pericyte deficient mouse model, it has been proven previously that pericytes are involved in brain tumor progression and expansion (Youn et al., 2015, Yotsumoto et al., 2015). Several markers were applied to identify mature pericytes, including PDGFR-β, Desmin, NG2, CD146, Rgs5, etc (Armulik et al., 2011, Mitchell et al., 2008). However, none of these markers alone is fully sufficient to unequivocally identify pericytes. The current definition of a pericyte is based on a combination of morphological patterns and the expression of at least two pericyte markers (Armulik et al., 2011, Trost et al., 2016). It is the currant view in the field of vascular research that pericytes in the brain are derived from the neuronal crest and that developmentally generated mature pericytes can proliferate to provide more pericytes during neoangiogenesis in the postnatal brain (Viski et al., 2016, Simonavicius et al., 2012).

In the present study, applying transgenic lineage-racing and bone marrow chimeric glioma mouse models, we investigate the cell linage, origination, and abolition of pericyte progenitor cells within tumor progression. The principle findings of this study are as follows, 1) we found that a group of RFP positive cells does not express any pericyte markers in the early stages after tumor inoculation. While, in later stages

of tumorigenesis, most of the RFP+ cells differentiated into mature pericytes express pericyte markers. It is concluded from this study that the RFP+ and pericyte-marker negative cells are a pericyte progenitor (PPC), which is dormant without a demand for new vessels and become activated during angiogenesis; 2) In the tumor area, most of the newly generated pericytes (63.14%) are derived from PPCs; while RFP positive PPCs do not differentiate in the peritumoral and the contralateral tumor-free brain hemisphere; 3) The bone marrow chimeric experiment confirmed that PPCs are not derived from the bone marrow; Moreover, 4) Results from lineage ablation experiments showed that the ablation of RFP positive PPCs could reduce the tumor size, tumor angiogenesis, and the number of pericytes. Consequently, these findings suggested that RFP positive PPCs contribute a potential new therapeutic target to suppress the tumor progression.

5.1 Identification of the RFP+ pericyte progenitor-like cells

To delineate the cell linage of RFP+ cells, we performed *in vivo* experiments with the $NesCre_{ER}^{T2+/+}$;Td-Tomato mouse model. With tumor progression, the number of RFP expressing cells significantly increased in the tumor, the peritumoral, and the contralateral tumor-free hemisphere. At 21 days after tumor cell-inoculation, I found that most RFP+ cells present a vessel-like morphology and located nearby to the vessels. In addition, RFP positive cells have a somewhat reduced capacity to generate new progenies with advanced age.

Based on the localization and characterization of RFP expressing cells, we further performed immunofluorescence staining for VWF, Desmin, and PDGFR-β to characterize RFP+ PPCs. According to the confocal imaging, RFP+ cells were located close to VWF+ cells, and co-localized with Desmin+ or PDGFR-β+ cells at 21 days

after tumor inoculation. The quantification showed a significant increase in the number of pericytes in the tumor area of the Nes-21 days group as compared with the Nes-7 days group.

Considering that in blood vessels Desmin and PDGFR-β are only expressed in the mature pericyte, our findings indicated that the RFP/Desmin or RFP/PDGFR-β double positive cells are pericytes. The quantitative analysis showed that the number of RFP/Desmin or RFP/PDGFR-β double positive cells significantly increased during tumor progression. The proportion of these double positive cells was initially approximately 23.23% in RFP/Desmin double + cells and 27.01% in RFP/PDGFR-β double + cells of all RFP+ cells at 7 days after the tumor inoculation, then increased to 71.98% and 79.13% at 21 days. In the Nes-21 days group, RFP+ pericytes accounted for approximately one third of all mature pericytes in the tumor area. In addition, using multiple pericyte markers staining, we identified most of intratumoral RFP+ cells (75.04%) were negative for mature pericytes markers (Desmin, PDGFR-β, CD146, and NG2) at 7 days after the tumor inoculation. Then, approximately 88.10% of RFP+ cells expressed the pericyte markers at 21 days after tumor cell-inoculation. Present study suggests that pericytes marker negative RFP+ cells could be previously unrecognized PPCs, which mature into pericytes during glioma progression. In the tumor area, we found most of newly generated pericytes (63.14%) are RFP expressing cells.

This study demonstrated that the number of RFP+ cell significantly increased in the peritumoral and the contralateral area during glioma progression. However, we also found that no significant difference was observed in the number of RFP/Desmin or PDGFR-β double positive cells in the peritumoral and contralateral areas. Therefore,

we suggested that RFP+ PPCs only differentiated in the tumor area, rather than in the peritumoral area and the contralateral tumor-free hemisphere.

5.2 RFP positive pericyte progenitor like cells are not derived from bone marrow

Despite an increasing interest in the role of pericytes in brain tumor growth, the precise origination of brain pericyte remains poorly understood. Previous studies have identified several sources of pericytes in different tissues and organs. In heart tissue, several studies have shown that PDGFR-β positive mural progenitor cells are derived from the embryonic epicardium cells and differentiate into pericytes (Avolio and Madeddu, 2016, Chen et al., 2016). Chen et al. indicated that the endocardial endothelial cells in the murine embryonic heart are progenitors of coronary pericytes, which are relevant to heart function and diseases (Chen et al., 2016). In 2016, a new experiment demonstrated that the Procr+ (protein c receptor-expressing) endothelial cells are an additional local source of pericytes (Yu et al., 2016).

In the healthy and diseased brain, previous studies have proven that pericytes could originate from the glioma stem cells, mesenchymal stem cells, or bone marrow derived cells (Ricci-Vitiani et al., 2010, Lamagna and Bergers, 2006, Song et al., 2005, Bababeygy et al., 2008, Bexell et al., 2009). In the present research, the bone marrow chimeric mouse model was applied to further investigate the origination of the RFP+ pericyte progenitor cells. In the BM/PU1-GFP group, PU1-GFP+ cells were observed in the tumor area, indicating that bone marrow derived myeloid cells could migrate to the tumor area through the BBB. If RFP+ PPCs were derived from the bone marrow, I have been able to detect RFP+ cells in the tumor area of the BM/Nes-Td-Tomato group. However, I found no RFP+ cells infiltrating into the brain tumor area in this

model. Therefore, this study concluded that RFP+ PPCs are not generated from bone marrow derived cells.

In addition, we found that most intratumoral PU1-GFP+ cells are co-localized with the immunofluorescence labeling for Iba1+ cells in the BM/PU1-GFP group. The results demonstrated that most of infiltrated bone marrow derived PU1-GFP+ cells are microglia or macrophages.

5.3 The RFP+ pericyte progenitor like cells as a new therapeutic target for glioma

Malignant gliomas are characterized by microvascular proliferation and typically over-expresses vascular endothelial growth factor (VEGF), which promotes tumor angiogenesis, proliferation, and progression (Kargiotis et al., 2006, Jain et al., 2007, Fischer et al., 2005). In the past two decades, the endothelial cells were widely considered to be the main therapeutic target for anti-angiogenesis (Dumpich and Theiss, 2015, Beal et al., 2011). Bevacizumab (BV), a humanized monoclonal antibody for VEGF, has been approved by The U.S. Food and Drug Administration (FDA) for second-line treatment of recurrent GBM (Kreisl et al., 2009, Friedman et al., 2009). Several clinical trials have reported that treatment with combinations of BV and other therapeutic agents (temozolomide, sunitinib, carboplatin, ect.) results in stable responses and a prolonged 6-month progression-free survival (PFS) rate in patients with recurrent high-grade glioma, but do not significantly prolong overall survival (OS) (Gil et al., 2012, Moller et al., 2012, Paldino et al., 2012, Jakobsen et al., 2011, Duda et al., 2007, Bennett et al., 2017). Furthermore, most of the complications caused by the toxicity of the combined chemotherapy led to discontinuation of treatment for patients with glioma (Ballman et al., 2007). Recently, we performed a

meta-analysis to investigate the effect of bevacizumab for newly diagnosed glioma (Li et al., 2016). The results showed that bevacizumab did not improve the median overall survival but resulted in longer median PFS. Additionally, the long-term use of BV is associated with a higher incidence of adverse events and mortality. Some studies indicated that the long-term bevacizumab application could lead to drug resistance. Although anti-VEGF therapy could inhibit the VEGF–VEGFR signal pathway to suppress tumor growth and reduce cerebral oxygen delivery, the expression of hypoxia-inducible factor 1alpha (HIF-1 α) was up-regulated to further promote the expression of VEGF genes (Hormigo et al., 2011, Mizukami et al., 2005). Placental growth factor (PGF), a member of the VEGF sub-family, could also promote the proliferation and migration of endothelial cells. After inhibiting VEGF, endothelial cells could up-regulate the expression of PGF to maintain tumor-associated vascular growth (Fischer et al., 2007), which may represent on reason why the anti-VEGF therapies did not show benefits for patients with glioma.

Recently, more research has been focused on pericytes, another type of cell in the perivascular area. The aims of pericyte-targeted therapy are to maintain the normalization of tumor vascularization to increase tumor oxygenation and intracerebral blood flow. Several studies investigated the effect of different kinds of anti-pericyte therapies for tumorigenesis, including targeting pericyte overexpressed markers (Xian et al., 2006), signal pathway inhibitor 3 (Bergers et al., 2003), blocking PDGFR-β (Cooke et al., 2012, Song et al., 2005), and PDGF-B–PDGFR-β binding oligonucleotide aptamers (Sennino et al., 2007). The application of the anti-PDGFR-β antibody could deplete pericytes in the pancreatic cancer mouse model leading to enlargement of the tumor vessels and promotion of the apoptosis of endothelial cells (Song et al., 2005). These studies suggested that the anti-pericyte therapies could

reduce the pericyte coverage, vascular stabilization, and tumor volume. However, low pericyte coverage and vascular destabilization could promote tumor hypoxia, necrosis, and metastasis (Bergers et al., 2003, Xian et al., 2006). A study conducted by Sinha et al. indicated that low pericyte coverage was relevant to rapid progress and mortality of patients with ovarian cancer (Sinha et al., 2016). Some clinical trials also indicated that low pericyte coverage is associated with poor prognosis in patients with glioblastoma (Yonenaga et al., 2005, O'Keeffe et al., 2008). Considering that the co-targeting of endothelia and pericytes might be much more effective for glioblastoma, two phase-II clinical studies investigated the effect of nintedanib (a triple tyrosine kinase receptor inhibitor of PDGFR-α/β, FGFR 1/3, and VEGFR 1-3) for patients with recurrent high-grade gliomas (Norden et al., 2015, Muhic et al., 2013). However, these two clinical trials suggested that nintedanib does not show benefit for patients with glioma, and the reason for the poor outcomes in nintedanib group is still unclear.

In our study, we used the cell-lineage ablation glioma mouse model to investigate the role of PPCs during glioma progression. The ablation of recombined RFP positive cells was applied at the early stage of tumor development where most RFP+ cells are PPCs (negative for pericytes markers). We ablated approximately half of the lineage traced cells in the Nes-iDTA group, as compared to the Nes-14 days group. Ablation of RFP positive PPCs significantly reduced the tumor volume by 46%, vessel area coverage by 50%, vessel density 64%, and vessel network complexity by 56% in the Nes-iDTA group as compared with the WT-iDTA control group. Hence, we suggested that the RFP+ PPCs may support the glioma progression and tumor angiogenesis.

Birbrair et al. reported that type-2 pericytes (nestin+/NG2+) promoted tumor angiogenesis, which may provide a potential target for inhibiting malignant tumors. (Birbrair et al., 2014). In this study, I used cell lineage transgenic mouse model to trace PPCs during tumor growth, my results showed that PPCs are nestin positive but NG2 negative immature pericytes that promote tumor angiogenesis. During glioma progression, PPCs could differentiate into mature pericytes (expressing NG2) becoming type-2 pericytes. Therefore, the role of different type of pericytes during tumor angiogenesis remains to be clarified.

Unlike targeting PDGFR-β or NG2 to ablate pericytes or other cell types, we ablated RFP+ PPCs in the glioma-bearing mouse brain. Our study demonstrated that the RFP+ PPCs are only differentiated in the tumor area, rather than in the peritumoral area and the tumor-free hemisphere. In addition, I confirmed that PPCs are not derived from the bone marrow. Therefore, ablation of PPCs could avoid complications associated with excluding mature pericytes in the brain or other organs. Altogether our data indicate that the RFP+ PPCs contribute important roles in glioma progression and angiogenesis. Therefore, these newly-identified PPCs could be considered as a new therapeutic target for glioma.

6 SUMMARY

Pericytes are vascular mural cell, which can regulate vessel-tone and -remodeling. In the brain pericytes are maintained in a 1:1 ratio with endothelial cells, they are essential for the function of the blood-brain barrier and control vessel-architecture. Previous studies suggested that pericytes are generated in embryonic development and that mature pericytes would proliferate and expand during neo-angiogenesis. Furthermore, it was proposed that pathological angiogenesis in glioblastomas (GBM) is supported by bone marrow-derived pericytes. In the present study, applying newly established transgenic lineage-tracing glioma mouse models (Nes-CreER^{T2}; Td-Tomato), I newly observed that pericytes origin from a previously unknown pericyte progenitor cells (PPCs). These nesting-RFP positive PPCs are negative for mature pericyte markers, including Desmin, PDGFR-β, NG2, CD146 at 7 days after tumor inoculation. However, most PPCs (88.10%) developed into mature pericytes and expressed pericyte markers like Desmin, PGGFR-ß, NG2, or CD146 at 21 days after tumor injection. I suggested that pericytes marker negative RFP+ cells are a previously unrecognized PPCs. Interestingly, in the tumor area, more than 30% of all pericytes express RFP. Since we used cell lineage tracing mouse models, we indicated that these intratumoral newly generated mature pericytes are derived from PPCs. The RFP positive cells do not differentiate into mature pericyte in the peritumoral and the contralateral tumor-free brain hemisphere.

The bone marrow chimeric glioma mouse model was applied to investigate if RFP expressing cells derived from the brain or from bone marrow. In the BM/PU1-GFP mice, we confirm that bone marrow derived PU1-GFP+ myeloid cells could migrate to the tumor area through the BBB. However, in the BM/Nes-Td-Tomato group, no RFP expressing cells are detected in glioma. These findings indicated that PPCs are not generated from bone marrow derived cells.

In the final experiments of my thesis, a cell lineage ablation glioma mouse model was used to investigate the role of PPCs during glioma growth. The ablation of Cre recombined RFP + cells was applied at 4 days after tumor inoculation, due to most RFP positive cells are PPCs during this stage. The results showed that we ablate approximately half of the RFP+ cells in the Nes-iDTA group compared to the Nes-RFP group. After ablation of RFP+ cells in the Nes-iDTA group, we observed significant reductions in the tumor volume, tumor angiogenesis, and the number of pericytes as compared with the Nes-RFP group. This study suggests that the RFP+ PPCs contribute important roles in glioma progression and angiogenesis. Altogether our data hypothesize that pericyte progenitor cells are a new target for anti-angiogenesis in GBM, which will allow a specific and efficient therapeutic treatment.

APPENDIX

ABBREVIATIONS

Ang/Tie2	Angiopoietin-1/2 and Tie2
αSMA	α-smooth muscle actin
BBB	Blood brain barrier
bFGF	Basic fibroblasts growth factor
BM	Basement membrane
CNS	Central nervous system
CldU	Chlorodeoxyuridine
CSC	Cancer stem cell
d	Day
DAPI	4,6-diamidino-2-phenylindole
EC	Endothelial cells
FFPE	Formalin-fixed, paraffin-embedded
Fig.	Figure
GAPDH	Glyceraldehyde-3- phosphate dehydrogenase
GBM	Glioblastoma multiforme
GFP	Green fluorescent protein
GL261	Murine high-grade astrocytoma cell line
iDTA	Cre-inducible diphtheria toxin a
IdU	Iododeoxyuridine
IDH	isocitrate dehydrogenase
i.p.	Intraperitoneal
MGMT	O^6-methylguanin-DNA-methyltransferase

MSC	Mesenchymal stem cell
NG2	Nerve/glial antigen 2 proteoglycan
NVU	Neurovascular unit
o/n	Over night
PBS	Phosphate buffered saline
PDGF-B	Platelet-derived growth factor subunit B
PDGFR-β	Platelet-derived growth factor receptor β
PFA	Paraformaldehyde
PPC	Pericyte progenitor like cells
RFP	Red fluorescent protein
RT	Rome temperature
TAM	Tumor associated macrophage
TBS	Tris-buffered saline
TGF-β	Transforming growth factor-β
TMZ	Temozolomide
VEGF	Vascular endothelial growth factor
WHO	World Health Organization
WT	Wildtype

PERMISSION FOR REPRODUCTION OF PUBLISHED FIGURES

Permission for reproduction of published figures

Permission for reproduction of Table 1.1

ID: 215265 Permission authorization for WHO copyrighted material

by permissions@who.int

Dear Mr Li

Thank you for your request for permission to reprint and reproduce certain WHO copyrighted material.

On behalf of the World Health Organization, we are pleased to authorize your request to reproduce the WHO materials as detailed in the form below, subject to the terms and conditions of the non-exclusive licence below.

If you have questions regarding this authorization, please contact permissions@who.int.

We thank you for your interest in WHO published materials.

Kind regards,
WHO Permissions team

WORLD HEALTH ORGANIZATION (WHO)

Non-exclusive licence to use selected WHO published materials

You submitted a request, through WHO's online platform, for permission to reprint and reproduce certain WHO copyrighted material (the "Licensed Materials"). This is a legal agreement (the "Agreement") between you and WHO, granting you a licence to use the Licensed Materials subject to the terms and conditions herein.

Read this Agreement in its entirety before using the Licensed Materials.

By using the Licensed Materials, you enter into, and agree to be bound by, this Agreement.

This licence is granted only for original materials belonging to WHO. If any part of the WHO published materials you wish to reproduce are credited by WHO to a source other than WHO, those materials are not covered by this Agreement and are not part of the Licensed Materials. You are responsible for determining if this is the case, and if so, you are responsible for obtaining any necessary permission from the source of those third-party materials prior to their use.

If you enter into this Agreement on behalf of an organization, by using the Licensed Materials you confirm (represent and warrant) that you are authorized by your organization to enter into this Agreement on the organization's behalf. In such a case, the terms "you" and "your" in this Agreement refer to, and this Agreement applies to, the organization.

WHO grants this licence to you based on the representations and warranties you made in the licence request you submitted through WHO's online platform. If any of those representations and/or warranties are or become false or inaccurate, this licence agreement shall automatically terminate with immediate effect, without prejudice to any other remedies which WHO may have.

PERMISSION FOR REPRODUCTION OF PUBLISHED FIGURES

Permission for reproduction of Figure 1.1

NATURE PUBLISHING GROUP LICENSE
TERMS AND CONDITIONS

This Agreement between Yuping Li ("You") and Nature Publishing Group ("Nature Publishing Group") consists of your license details and the terms and conditions provided by Nature Publishing Group and Copyright Clearance Center.

License Number	4006150128070
License date	Dec 11, 2016
Licensed Content Publisher	Nature Publishing Group
Licensed Content Publication	Nature Neuroscience
Licensed Content Title	Pericytes of the neurovascular unit: key functions and signaling pathways
Licensed Content Author	Melanie D Sweeney, Shiva Ayyadurai, Berislav V Zlokovic
Licensed Content Date	May 26, 2016
Licensed Content Volume Number	19
Licensed Content Issue Number	6
Type of Use	reuse in a dissertation / thesis
Requestor type	academic/educational
Format	print and electronic
Portion	figures/tables/illustrations
Number of figures/tables/illustrations	1
High-res required	no
Figures	Figure 1 (b)
Author of this NPG article	no
Your reference number	
Title of your thesis / dissertation	The role of a previously unrecognized pericytes progenitor-like cell and their progeny in glioma expansion and progression
Expected completion date	Jan 2017
Estimated size (number of pages)	92
Requestor Location	Yuping Li No.98 nantong westroad Yangzhou, 225001 China Attn: Yuping Li
Billing Type	Invoice
Billing Address	Yuping Li No.98 nantong westroad

PERMISSION FOR REPRODUCTION OF PUBLISHED FIGURES

Permission for reproduction of Figure 1.2

JOHN WILEY AND SONS LICENSE
TERMS AND CONDITIONS

Dec 13, 2016

This Agreement between Yuping Li ("You") and John Wiley and Sons ("John Wiley and Sons") consists of your license details and the terms and conditions provided by John Wiley and Sons and Copyright Clearance Center.

License Number	4006170842672
License date	Dec 11, 2016
Licensed Content Publisher	John Wiley and Sons
Licensed Content Publication	American Journal of Hematology
Licensed Content Title	Pericytes and vessel maturation during tumor angiogenesis and metastasis
Licensed Content Author	Ahmad Raza,Michael J. Franklin,Arkadiusz Z. Dudek
Licensed Content Date	Apr 27, 2010
Licensed Content Pages	6
Type of Use	Dissertation/Thesis
Requestor type	University/Academic
Format	Print and electronic
Portion	Figure/table
Number of figures/tables	1
Original Wiley figure/table number(s)	Figure 1
Will you be translating?	No
Title of your thesis / dissertation	The role of a previously unrecognized pericytes progenitor-like cell and their progeny in glioma expansion and progression
Expected completion date	Jan 2017
Expected size (number of pages)	92
Requestor Location	Yuping Li No.98 nantong westroad
	Yangzhou, 225001 China Attn: Yuping Li
Publisher Tax ID	EU826007151
Billing Type	Invoice
Billing Address	Yuping Li No.98 nantong westroad
	Yangzhou, China 225001 Attn: Yuping Li
Total	**0.00 EUR**
Terms and Conditions	

REFERENCES

Albanese, C., Hulit, J., Sakamaki, T. & Pestell, R. G. 2002. Recent advances in inducible expression in transgenic mice. *Semin Cell Dev Biol*, 13**,** 129-41.

Armulik, A., Abramsson, A. & Betsholtz, C. 2005. Endothelial/pericyte interactions. *Circ Res*, 97**,** 512-23.

Armulik, A., Genove, G. & Betsholtz, C. 2011. Pericytes: developmental, physiological, and pathological perspectives, problems, and promises. *Dev Cell*, 21**,** 193-215.

Armulik, A., Genove, G., Mae, M., Nisancioglu, M. H., Wallgard, E., Niaudet, C., He, L., Norlin, J., Lindblom, P., Strittmatter, K., Johansson, B. R. & Betsholtz, C. 2010. Pericytes regulate the blood-brain barrier. *Nature*, 468**,** 557-61.

Avolio, E. & Madeddu, P. 2016. Discovering cardiac pericyte biology: From physiopathological mechanisms to potential therapeutic applications in ischemic heart disease. *Vascul Pharmacol*, 86**,** 53-63.

Bababeygy, S. R., Cheshier, S. H., Hou, L. C., Higgins, D. M., Weissman, I. L. & Tse, V. C. 2008. Hematopoietic stem cell-derived pericytic cells in brain tumor angio-architecture. *Stem Cells Dev*, 17**,** 11-8.

Back, J., Dierich, A., Bronn, C., Kastner, P. & Chan, S. 2004. PU.1 determines the self-renewal capacity of erythroid progenitor cells. *Blood*, 103**,** 3615-23.

Ballman, K. V., Buckner, J. C., Brown, P. D., Giannini, C., Flynn, P. J., LaPlant, B. R. & Jaeckle, K. A. 2007. The relationship between six-month progression-free survival and 12-month overall survival end points for phase II trials in patients with glioblastoma multiforme. *Neuro Oncol*, 9**,** 29-38.

Baluk, P., Morikawa, S., Haskell, A., Mancuso, M. & McDonald, D. M. 2003. Abnormalities of basement membrane on blood vessels and endothelial sprouts in tumors. *Am J Pathol*, 163**,** 1801-15.

Beal, K., Abrey, L. E. & Gutin, P. H. 2011. Antiangiogenic agents in the treatment of recurrent or newly diagnosed glioblastoma: analysis of single-agent and combined modality approaches. *Radiat Oncol*, 6**,** 2.

Bennett, I. E., Field, K. M., Hovens, C. M., Moffat, B. A., Rosenthal, M. A., Drummond, K., Kaye, A. H. & Morokoff, A. P. 2017. Early perfusion MRI predicts survival outcome in patients with recurrent glioblastoma treated with bevacizumab and carboplatin. *J Neurooncol*, 131**,** 321-329.

Bergers, G. & Song, S. 2005. The role of pericytes in blood-vessel formation and maintenance. *Neuro Oncol*, 7**,** 452-64.

Bergers, G., Song, S., Meyer-Morse, N., Bergsland, E. & Hanahan, D. 2003. Benefits of targeting both pericytes and endothelial cells in the tumor vasculature with kinase inhibitors. *J Clin Invest*, 111**,** 1287-95.

REFERENCES

Bergwerff, M., Verberne, M. E., DeRuiter, M. C., Poelmann, R. E. & Gittenberger-de Groot, A. C. 1998. Neural crest cell contribution to the developing circulatory system: implications for vascular morphology? *Circ Res*, 82**,** 221-31.

Bexell, D., Gunnarsson, S., Tormin, A., Darabi, A., Gisselsson, D., Roybon, L., Scheding, S. & Bengzon, J. 2009. Bone marrow multipotent mesenchymal stroma cells act as pericyte-like migratory vehicles in experimental gliomas. *Mol Ther*, 17**,** 183-90.

Birbrair, A., Zhang, T., Wang, Z. M., Messi, M. L., Olson, J. D., Mintz, A. & Delbono, O. 2014. Type-2 pericytes participate in normal and tumoral angiogenesis. *Am J Physiol Cell Physiol*, 307**,** C25-38.

Birnbaum, T., Hildebrandt, J., Nuebling, G., Sostak, P. & Straube, A. 2011. Glioblastoma-dependent differentiation and angiogenic potential of human mesenchymal stem cells in vitro. *J Neurooncol*, 105**,** 57-65.

Blocki, A., Wang, Y., Koch, M., Peh, P., Beyer, S., Law, P., Hui, J. & Raghunath, M. 2013. Not all MSCs can act as pericytes: functional in vitro assays to distinguish pericytes from other mesenchymal stem cells in angiogenesis. *Stem Cells Dev*, 22**,** 2347-55.

Bodnar, R. J., Rodgers, M. E., Chen, W. C. & Wells, A. 2013. Pericyte regulation of vascular remodeling through the CXC receptor 3. *Arterioscler Thromb Vasc Biol*, 33**,** 2818-29.

Brighton, C. T., Lorich, D. G., Kupcha, R., Reilly, T. M., Jones, A. R. & Woodbury, R. A., 2nd 1992. The pericyte as a possible osteoblast progenitor cell. *Clin Orthop Relat Res***,** 287-99.

Brockschnieder, D., Pechmann, Y., Sonnenberg-Riethmacher, E. & Riethmacher, D. 2006. An improved mouse line for Cre-induced cell ablation due to diphtheria toxin A, expressed from the Rosa26 locus. *Genesis*, 44**,** 322-7.

C, R. 1873. Memoire sur le developpement, la structure et les proprietes physiologiques des capillaires sanguins et lymphatiques. *Arch Physiol Normale Pathol*, 05**,** 603-611.

Calabrese, C., Poppleton, H., Kocak, M., Hogg, T. L., Fuller, C., Hamner, B., Oh, E. Y., Gaber, M. W., Finklestein, D., Allen, M., Frank, A., Bayazitov, I. T., Zakharenko, S. S., Gajjar, A., Davidoff, A. & Gilbertson, R. J. 2007. A perivascular niche for brain tumor stem cells. *Cancer Cell*, 11**,** 69-82.

Cancer Genome Atlas Research, N., Brat, D. J., Verhaak, R. G., et al. 2015. Comprehensive, Integrative Genomic Analysis of Diffuse Lower-Grade Gliomas. *N Engl J Med*, 372**,** 2481-98.

Caplan, A. I. 2008. All MSCs are pericytes? *Cell Stem Cell*, 3**,** 229-30.

Caporali, A., Martello, A., Miscianinov, V., Maselli, D., Vono, R. & Spinetti, G. 2016. Contribution of pericyte paracrine regulation of the endothelium to angiogenesis. *Pharmacol Ther*.

Caspani, E. M., Crossley, P. H., Redondo-Garcia, C. & Martinez, S. 2014. Glioblastoma: a pathogenic crosstalk between tumor cells and pericytes. *PLoS One*, 9**,** e101402.

Chao, H. & Hirschi, K. K. 2010. Hemato-vascular origins of endothelial progenitor cells? *Microvasc Res,* 79**,** 169-73.

Charles, N., Ozawa, T., Squatrito, M., Bleau, A. M., Brennan, C. W., Hambardzumyan, D. & Holland, E. C. 2010. Perivascular nitric oxide activates notch signaling and promotes stem-like character in PDGF-induced glioma cells. *Cell Stem Cell*, 6**,** 141-52.

Chen, H. M., Zhang, P., Voso, M. T., Hohaus, S., Gonzalez, D. A., Glass, C. K., Zhang, D. E. & Tenen, D. G. 1995. Neutrophils and monocytes express high levels of PU.1 (Spi-1) but not Spi-B. *Blood,* 85**,** 2918-28.

Chen, K., Mehta, J. L., Li, D., Joseph, L. & Joseph, J. 2004. Transforming growth factor beta receptor endoglin is expressed in cardiac fibroblasts and modulates profibrogenic actions of angiotensin II. *Circ Res,* 95**,** 1167-73.

Chen, Q., Zhang, H., Liu, Y., Adams, S., Eilken, H., Stehling, M., Corada, M., Dejana, E., Zhou, B. & Adams, R. H. 2016. Endothelial cells are progenitors of cardiac pericytes and vascular smooth muscle cells. *Nat Commun*, 7**,** 12422.

Chen, X., Cho, D. B. & Yang, P. C. 2010. Double staining immunohistochemistry. *N Am J Med Sci*, 2**,** 241-5.

Cheng, L., Huang, Z., Zhou, W., Wu, Q., Donnola, S., Liu, J. K., Fang, X., Sloan, A. E., Mao, Y., Lathia, J. D., Min, W., McLendon, R. E., Rich, J. N. & Bao, S. 2013. Glioblastoma stem cells generate vascular pericytes to support vessel function and tumor growth. *Cell*, 153**,** 139-52.

Chinot, O. L., Wick, W., Mason, W., Henriksson, R., Saran, F., Nishikawa, R., Carpentier, A. F., Hoang-Xuan, K., Kavan, P., Cernea, D., Brandes, A. A., Hilton, M., Abrey, L. & Cloughesy, T. 2014. Bevacizumab plus radiotherapy-temozolomide for newly diagnosed glioblastoma. *N Engl J Med*, 370**,** 709-22.

Cooke, V. G., LeBleu, V. S., Keskin, D., Khan, Z., O'Connell, J. T., Teng, Y., Duncan, M. B., Xie, L., Maeda, G., Vong, S., Sugimoto, H., Rocha, R. M., Damascena, A., Brentani, R. R. & Kalluri, R. 2012. Pericyte depletion results in hypoxia-associated epithelial-to-mesenchymal transition and metastasis mediated by met signaling pathway. *Cancer Cell*, 21**,** 66-81.

Crisan, M., Yap, S., Casteilla, L., Chen, C. W., Corselli, M., Park, T. S., Andriolo, G., Sun, B., Zheng, B., Zhang, L., Norotte, C., Teng, P. N., Traas, J., Schugar, R., Deasy, B. M., Badylak, S., Buhring, H. J., Giacobino, J. P., Lazzari, L., Huard, J. & Peault, B. 2008. A perivascular origin for mesenchymal stem cells in multiple human organs. *Cell Stem Cell*, 3**,** 301-13.

da Silva Meirelles, L., Chagastelles, P. C. & Nardi, N. B. 2006. Mesenchymal stem cells reside in virtually all post-natal organs and tissues. *J Cell Sci*, 119**,** 2204-13.

Daneman, R., Zhou, L., Kebede, A. A. & Barres, B. A. 2010. Pericytes are required for blood-brain barrier integrity during embryogenesis. *Nature*, 468**,** 562-6.

Darland, D. C. & D'Amore, P. A. 2001. TGF beta is required for the formation of capillary-like structures in three-dimensional cocultures of 10T1/2 and endothelial cells. *Angiogenesis*, 4**,** 11-20.

de Groot, J. F., Fuller, G., Kumar, A. J., Piao, Y., Eterovic, K., Ji, Y. & Conrad, C. A. 2010. Tumor invasion after treatment of glioblastoma with bevacizumab: radiographic and pathologic correlation in humans and mice. *Neuro Oncol*, 12**,** 233-42.

De Palma, M., Venneri, M. A., Galli, R., Sergi Sergi, L., Politi, L. S., Sampaolesi, M. & Naldini, L. 2005. Tie2 identifies a hematopoietic lineage of proangiogenic monocytes required for tumor vessel formation and a mesenchymal population of pericyte progenitors. *Cancer Cell*, 8**,** 211-26.

DeKoter, R. P. & Singh, H. 2000. Regulation of B lymphocyte and macrophage development by graded expression of PU.1. *Science*, 288**,** 1439-41.

Dellavalle, A., Sampaolesi, M., Tonlorenzi, R., Tagliafico, E., Sacchetti, B., Perani, L., Innocenzi, A., Galvez, B. G., Messina, G., Morosetti, R., Li, S., Belicchi, M., Peretti, G., Chamberlain, J. S., Wright, W. E., Torrente, Y., Ferrari, S., Bianco, P. & Cossu, G. 2007. Pericytes of human skeletal muscle are myogenic precursors distinct from satellite cells. *Nat Cell Biol*, 9**,** 255-67.

Diaz-Flores, L., Gutierrez, R., Madrid, J. F., Varela, H., Valladares, F., Acosta, E., Martin-Vasallo, P. & Diaz-Flores, L., Jr. 2009. Pericytes. Morphofunction, interactions and pathology in a quiescent and activated mesenchymal cell niche. *Histol Histopathol*, 24**,** 909-69.

Dome, B., Dobos, J., Tovari, J., Paku, S., Kovacs, G., Ostoros, G. & Timar, J. 2008. Circulating bone marrow-derived endothelial progenitor cells: characterization, mobilization, and therapeutic considerations in malignant disease. *Cytometry A*, 73**,** 186-93.

Du, R., Lu, K. V., Petritsch, C., Liu, P., Ganss, R., Passegue, E., Song, H., Vandenberg, S., Johnson, R. S., Werb, Z. & Bergers, G. 2008. HIF1alpha induces the recruitment of bone marrow-derived vascular modulatory cells to regulate tumor angiogenesis and invasion. *Cancer Cell*, 13**,** 206-20.

Duda, D. G., Batchelor, T. T., Willett, C. G. & Jain, R. K. 2007. VEGF-targeted cancer therapy strategies: current progress, hurdles and future prospects. *Trends Mol Med*, 13**,** 223-30.

Dumpich, M. & Theiss, C. 2015. VEGF in the nervous system: an important target for research in neurodevelopmental and regenerative medicine. *Neural Regen Res*, 10**,** 1725-6.

Eckel-Passow, J. E., Lachance, D. H., Molinaro, A. M., Walsh, K. M., Decker, P. A., Sicotte, H., Pekmezci, M., Rice, T., Kosel, M. L., Smirnov, I. V., Sarkar, G., Caron, A. A., Kollmeyer, T. M., Praska, C. E., Chada, A. R., Halder, C., Hansen, H. M., McCoy, L. S., Bracci, P. M., Marshall, R., Zheng, S., Reis, G. F., Pico, A. R., O'Neill, B. P., Buckner, J. C., Giannini, C., Huse, J. T., Perry,

A., Tihan, T., Berger, M. S., Chang, S. M., Prados, M. D., Wiemels, J., Wiencke, J. K., Wrensch, M. R. & Jenkins, R. B. 2015. Glioma Groups Based on 1p/19q, IDH, and TERT Promoter Mutations in Tumors. *N Engl J Med*, 372, 2499-508.

ElAli, A., Theriault, P. & Rivest, S. 2014. The role of pericytes in neurovascular unit remodeling in brain disorders. *Int J Mol Sci*, 15, 6453-74.

Enge, M., Bjarnegard, M., Gerhardt, H., Gustafsson, E., Kalen, M., Asker, N., Hammes, H. P., Shani, M., Fassler, R. & Betsholtz, C. 2002. Endothelium-specific platelet-derived growth factor-B ablation mimics diabetic retinopathy. *EMBO J*, 21, 4307-16.

Etchevers, H. C., Couly, G. & Le Douarin, N. M. 2002. Morphogenesis of the branchial vascular sector. *Trends Cardiovasc Med*, 12, 299-304.

Farin, A., Suzuki, S. O., Weiker, M., Goldman, J. E., Bruce, J. N. & Canoll, P. 2006. Transplanted glioma cells migrate and proliferate on host brain vasculature: a dynamic analysis. *Glia*, 53, 799-808.

Farrington-Rock, C., Crofts, N. J., Doherty, M. J., Ashton, B. A., Griffin-Jones, C. & Canfield, A. E. 2004. Chondrogenic and adipogenic potential of microvascular pericytes. *Circulation*, 110, 2226-32.

Feil, R., Wagner, J., Metzger, D. & Chambon, P. 1997. Regulation of Cre recombinase activity by mutated estrogen receptor ligand-binding domains. *Biochem Biophys Res Commun*, 237, 752-7.

Feldman, A. T. & Wolfe, D. 2014. Tissue processing and hematoxylin and eosin staining. *Methods Mol Biol*, 1180, 31-43.

Fine, H. A. 2014. Bevacizumab in glioblastoma--still much to learn. *N Engl J Med*, 370, 764-5.

Fischer, C., Jonckx, B., Mazzone, M., Zacchigna, S., Loges, S., Pattarini, L., Chorianopoulos, E., Liesenborghs, L., Koch, M., De Mol, M., Autiero, M., Wyns, S., Plaisance, S., Moons, L., van Rooijen, N., Giacca, M., Stassen, J. M., Dewerchin, M., Collen, D. & Carmeliet, P. 2007. Anti-PlGF inhibits growth of VEGF(R)-inhibitor-resistant tumors without affecting healthy vessels. *Cell*, 131, 463-75.

Fischer, I., Gagner, J. P., Law, M., Newcomb, E. W. & Zagzag, D. 2005. Angiogenesis in gliomas: biology and molecular pathophysiology. *Brain Pathol*, 15, 297-310.

Friedman, H. S., Prados, M. D., Wen, P. Y., Mikkelsen, T., Schiff, D., Abrey, L. E., Yung, W. K., Paleologos, N., Nicholas, M. K., Jensen, R., Vredenburgh, J., Huang, J., Zheng, M. & Cloughesy, T. 2009. Bevacizumab alone and in combination with irinotecan in recurrent glioblastoma. *J Clin Oncol*, 27, 4733-40.

Fuller, G. N. 2008. The WHO Classification of Tumours of the Central Nervous System, 4th edition. *Arch Pathol Lab Med*, 132, 906.

Furukawa, S., Nagaike, M. & Ozaki, K. 2017. Databases for technical aspects of immunohistochemistry. *J Toxicol Pathol*, 30**,** 79-107.

Gage, G. J., Kipke, D. R. & Shain, W. 2012. Whole animal perfusion fixation for rodents. *J Vis Exp*.

Garmy-Susini, B. & Varner, J. A. 2005. Circulating endothelial progenitor cells. *Br J Cancer*, 93**,** 855-8.

Gerhardt, H. & Betsholtz, C. 2003. Endothelial-pericyte interactions in angiogenesis. *Cell Tissue Res*, 314**,** 15-23.

Gil, M. J., de Las Penas, R., Reynes, G., Balana, C., Perez-Segura, P., Garcia-Velasco, A., Mesia, C., Gallego, O., Fernandez-Chacon, C., Martinez-Garcia, M., Herrero, A., Andres, R., Benavides, M., Quintanar, T. & Perez-Martin, X. 2012. Bevacizumab plus irinotecan in recurrent malignant glioma shows high overall survival in a multicenter retrospective pooled series of the Spanish Neuro-Oncology Research Group (GEINO). *Anticancer Drugs*, 23**,** 659-65.

Gilbert, M. R., Dignam, J. J., Armstrong, T. S., Wefel, J. S., Blumenthal, D. T., Vogelbaum, M. A., Colman, H., Chakravarti, A., Pugh, S., Won, M., Jeraj, R., Brown, P. D., Jaeckle, K. A., Schiff, D., Stieber, V. W., Brachman, D. G., Werner-Wasik, M., Tremont-Lukats, I. W., Sulman, E. P., Aldape, K. D., Curran, W. J., Jr. & Mehta, M. P. 2014. A randomized trial of bevacizumab for newly diagnosed glioblastoma. *N Engl J Med*, 370**,** 699-708.

Gilkes, D. M., Semenza, G. L. & Wirtz, D. 2014. Hypoxia and the extracellular matrix: drivers of tumour metastasis. *Nat Rev Cancer*, 14**,** 430-9.

Goodpaster, T. & Randolph-Habecker, J. 2014. A flexible mouse-on-mouse immunohistochemical staining technique adaptable to biotin-free reagents, immunofluorescence, and multiple antibody staining. *J Histochem Cytochem*, 62**,** 197-204.

Guimaraes-Camboa, N., Cattaneo, P., Sun, Y., Moore-Morris, T., Gu, Y., Dalton, N. D., Rockenstein, E., Masliah, E., Peterson, K. L., Stallcup, W. B., Chen, J. & Evans, S. M. 2017. Pericytes of Multiple Organs Do Not Behave as Mesenchymal Stem Cells In Vivo. *Cell Stem Cell*, 20**,** 345-359 e5.

Halliday, M. R., Rege, S. V., Ma, Q., Zhao, Z., Miller, C. A., Winkler, E. A. & Zlokovic, B. V. 2016. Accelerated pericyte degeneration and blood-brain barrier breakdown in apolipoprotein E4 carriers with Alzheimer's disease. *J Cereb Blood Flow Metab*, 36**,** 216-27.

Harrison-Brown, M., Liu, G. J. & Banati, R. 2016. Checkpoints to the Brain: Directing Myeloid Cell Migration to the Central Nervous System. *Int J Mol Sci*, 17.

Hashizume, H., Baluk, P., Morikawa, S., McLean, J. W., Thurston, G., Roberge, S., Jain, R. K. & McDonald, D. M. 2000. Openings between defective endothelial cells explain tumor vessel leakiness. *Am J Pathol*, 156**,** 1363-80.

Hellstrom, M., Gerhardt, H., Kalen, M., Li, X., Eriksson, U., Wolburg, H. & Betsholtz, C. 2001. Lack of pericytes leads to endothelial hyperplasia and abnormal vascular morphogenesis. *J Cell Biol*, 153**,** 543-53.

Hellstrom, M., Kalen, M., Lindahl, P., Abramsson, A. & Betsholtz, C. 1999. Role of PDGF-B and PDGFR-beta in recruitment of vascular smooth muscle cells and pericytes during embryonic blood vessel formation in the mouse. *Development*, 126**,** 3047-55.

Holl, E. K. 2013. Generation of bone marrow and fetal liver chimeric mice. *Methods Mol Biol*, 1032**,** 315-21.

Hormigo, A., Ding, B. S. & Rafii, S. 2011. A target for antiangiogenic therapy: vascular endothelium derived from glioblastoma. *Proc Natl Acad Sci U S A*, 108**,** 4271-2.

Huang, F. J., You, W. K., Bonaldo, P., Seyfried, T. N., Pasquale, E. B. & Stallcup, W. B. 2010. Pericyte deficiencies lead to aberrant tumor vascularizaton in the brain of the NG2 null mouse. *Dev Biol*, 344**,** 1035-46.

Hughes, S. & Chan-Ling, T. 2004. Characterization of smooth muscle cell and pericyte differentiation in the rat retina in vivo. *Invest Ophthalmol Vis Sci*, 45**,** 2795-806.

Jain, R. K., di Tomaso, E., Duda, D. G., Loeffler, J. S., Sorensen, A. G. & Batchelor, T. T. 2007. Angiogenesis in brain tumours. *Nat Rev Neurosci*, 8**,** 610-22.

Jakobsen, J. N., Hasselbalch, B., Stockhausen, M. T., Lassen, U. & Poulsen, H. S. 2011. Irinotecan and bevacizumab in recurrent glioblastoma multiforme. *Expert Opin Pharmacother*, 12**,** 825-33.

Kargiotis, O., Rao, J. S. & Kyritsis, A. P. 2006. Mechanisms of angiogenesis in gliomas. *J Neurooncol*, 78**,** 281-93.

Keunen, O., Johansson, M., Oudin, A., Sanzey, M., Rahim, S. A., Fack, F., Thorsen, F., Taxt, T., Bartos, M., Jirik, R., Miletic, H., Wang, J., Stieber, D., Stuhr, L., Moen, I., Rygh, C. B., Bjerkvig, R. & Niclou, S. P. 2011. Anti-VEGF treatment reduces blood supply and increases tumor cell invasion in glioblastoma. *Proc Natl Acad Sci U S A*, 108**,** 3749-54.

Kreisl, T. N., Kim, L., Moore, K., Duic, P., Royce, C., Stroud, I., Garren, N., Mackey, M., Butman, J. A., Camphausen, K., Park, J., Albert, P. S. & Fine, H. A. 2009. Phase II trial of single-agent bevacizumab followed by bevacizumab plus irinotecan at tumor progression in recurrent glioblastoma. *J Clin Oncol*, 27**,** 740-5.

Lakso, M., Sauer, B., Mosinger, B., Jr., Lee, E. J., Manning, R. W., Yu, S. H., Mulder, K. L. & Westphal, H. 1992. Targeted oncogene activation by site-specific recombination in transgenic mice. *Proc Natl Acad Sci U S A*, 89**,** 6232-6.

Lamagna, C. & Bergers, G. 2006. The bone marrow constitutes a reservoir of pericyte progenitors. *J Leukoc Biol*, 80**,** 677-81.

Leveen, P., Pekny, M., Gebre-Medhin, S., Swolin, B., Larsson, E. & Betsholtz, C. 1994. Mice deficient for PDGF B show renal, cardiovascular, and hematological abnormalities. *Genes Dev,* 8**,** 1875-87.

Li, Y., Hou, M., Lu, G., Ciccone, N., Wang, X. & Zhang, H. 2016. The Prognosis of Anti-Angiogenesis Treatments Combined with Standard Therapy for Newly Diagnosed Glioblastoma: A Meta-Analysis of Randomized Controlled Trials. *PLoS One,* 11**,** e0168264.

Louis DN, O. H., Wiestler OD, Cavenee WK 2016. *World Health Organization Histological Classification of Tumours of the Central Nervous System*, France, International Agency for Research on Cancer.

Louis, D. N., Perry, A., Reifenberger, G., von Deimling, A., Figarella-Branger, D., Cavenee, W. K., Ohgaki, H., Wiestler, O. D., Kleihues, P. & Ellison, D. W. 2016. The 2016 World Health Organization Classification of Tumors of the Central Nervous System: a summary. *Acta Neuropathol,* 131**,** 803-20.

Mignone, J. L., Kukekov, V., Chiang, A. S., Steindler, D. & Enikolopov, G. 2004. Neural stem and progenitor cells in nestin-GFP transgenic mice. *J Comp Neurol,* 469**,** 311-24.

Missirlis, P. I., Smailus, D. E. & Holt, R. A. 2006. A high-throughput screen identifying sequence and promiscuity characteristics of the loxP spacer region in Cre-mediated recombination. *BMC Genomics,* 7**,** 73.

Mitchell, T. S., Bradley, J., Robinson, G. S., Shima, D. T. & Ng, Y. S. 2008. RGS5 expression is a quantitative measure of pericyte coverage of blood vessels. *Angiogenesis,* 11**,** 141-51.

Mizukami, Y., Jo, W. S., Duerr, E. M., Gala, M., Li, J., Zhang, X., Zimmer, M. A., Iliopoulos, O., Zukerberg, L. R., Kohgo, Y., Lynch, M. P., Rueda, B. R. & Chung, D. C. 2005. Induction of interleukin-8 preserves the angiogenic response in HIF-1alpha-deficient colon cancer cells. *Nat Med,* 11**,** 992-7.

Moller, S., Grunnet, K., Hansen, S., Schultz, H., Holmberg, M., Sorensen, M., Poulsen, H. S. & Lassen, U. 2012. A phase II trial with bevacizumab and irinotecan for patients with primary brain tumors and progression after standard therapy. *Acta Oncol,* 51**,** 797-804.

Muhic, A., Poulsen, H. S., Sorensen, M., Grunnet, K. & Lassen, U. 2013. Phase II open-label study of nintedanib in patients with recurrent glioblastoma multiforme. *J Neurooncol,* 111**,** 205-12.

Muramatsu, R. & Yamashita, T. 2014. Pericyte function in the physiological central nervous system. *Neurosci Res,* 81-82**,** 38-41.

Nagy, J. A., Chang, S. H., Dvorak, A. M. & Dvorak, H. F. 2009. Why are tumour blood vessels abnormal and why is it important to know? *Br J Cancer,* 100**,** 865-9.

Nishimura, A., Ago, T., Kuroda, J., Arimura, K., Tachibana, M., Nakamura, K., Wakisaka, Y., Sadoshima, J., Iihara, K. & Kitazono, T. 2016. Detrimental role

of pericyte Nox4 in the acute phase of brain ischemia. *J Cereb Blood Flow Metab*, 36**,** 1143-54.

Norden, A. D., Drappatz, J. & Wen, P. Y. 2008. Novel anti-angiogenic therapies for malignant gliomas. *Lancet Neurol*, 7**,** 1152-60.

Norden, A. D., Schiff, D., Ahluwalia, M. S., Lesser, G. J., Nayak, L., Lee, E. Q., Rinne, M. L., Muzikansky, A., Dietrich, J., Purow, B., Doherty, L. M., LaFrankie, D. C., Pulverenti, J. R., Rifenburg, J. A., Ruland, S. F., Smith, K. H., Gaffey, S. C., McCluskey, C., Ligon, K. L., Reardon, D. A. & Wen, P. Y. 2015. Phase II trial of triple tyrosine kinase receptor inhibitor nintedanib in recurrent high-grade gliomas. *J Neurooncol*, 121**,** 297-302.

O'Keeffe, M. B., Devlin, A. H., Burns, A. J., Gardiner, T. A., Logan, I. D., Hirst, D. G. & McKeown, S. R. 2008. Investigation of pericytes, hypoxia, and vascularity in bladder tumors: association with clinical outcomes. *Oncol Res*, 17**,** 93-101.

Olar, A., Wani, K. M., Alfaro-Munoz, K. D., Heathcock, L. E., van Thuijl, H. F., Gilbert, M. R., Armstrong, T. S., Sulman, E. P., Cahill, D. P., Vera-Bolanos, E., Yuan, Y., Reijneveld, J. C., Ylstra, B., Wesseling, P. & Aldape, K. D. 2015. IDH mutation status and role of WHO grade and mitotic index in overall survival in grade II-III diffuse gliomas. *Acta Neuropathol*, 129**,** 585-96.

Ozerdem, U. & Stallcup, W. B. 2004. Pathological angiogenesis is reduced by targeting pericytes via the NG2 proteoglycan. *Angiogenesis*, 7**,** 269-76.

Paez-Ribes, M., Allen, E., Hudock, J., Takeda, T., Okuyama, H., Vinals, F., Inoue, M., Bergers, G., Hanahan, D. & Casanovas, O. 2009. Antiangiogenic therapy elicits malignant progression of tumors to increased local invasion and distant metastasis. *Cancer Cell*, 15**,** 220-31.

Paldino, M. J., Desjardins, A., Friedman, H. S., Vredenburgh, J. J. & Barboriak, D. P. 2012. A change in the apparent diffusion coefficient after treatment with bevacizumab is associated with decreased survival in patients with recurrent glioblastoma multiforme. *Br J Radiol*, 85**,** 382-9.

Paquet-Fifield, S., Schluter, H., Li, A., Aitken, T., Gangatirkar, P., Blashki, D., Koelmeyer, R., Pouliot, N., Palatsides, M., Ellis, S., Brouard, N., Zannettino, A., Saunders, N., Thompson, N., Li, J. & Kaur, P. 2009. A role for pericytes as microenvironmental regulators of human skin tissue regeneration. *J Clin Invest*, 119**,** 2795-806.

Park, T. I., Feisst, V., Brooks, A. E., Rustenhoven, J., Monzo, H. J., Feng, S. X., Mee, E. W., Bergin, P. S., Oldfield, R., Graham, E. S., Curtis, M. A., Faull, R. L., Dunbar, P. R. & Dragunow, M. 2016. Cultured pericytes from human brain show phenotypic and functional differences associated with differential CD90 expression. *Sci Rep*, 6**,** 26587.

Rajantie, I., Ilmonen, M., Alminaite, A., Ozerdem, U., Alitalo, K. & Salven, P. 2004. Adult bone marrow-derived cells recruited during angiogenesis comprise precursors for periendothelial vascular mural cells. *Blood*, 104**,** 2084-6.

Ramos-Vara, J. A. 2005. Technical aspects of immunohistochemistry. *Vet Pathol*, 42**,** 405-26.

Reuss, D. E., Mamatjan, Y., Schrimpf, D., Capper, D., Hovestadt, V., Kratz, A., Sahm, F., Koelsche, C., Korshunov, A., Olar, A., Hartmann, C., Reijneveld, J. C., Wesseling, P., Unterberg, A., Platten, M., Wick, W., Herold-Mende, C., Aldape, K. & von Deimling, A. 2015. IDH mutant diffuse and anaplastic astrocytomas have similar age at presentation and little difference in survival: a grading problem for WHO. *Acta Neuropathol*, 129**,** 867-73.

Ricci-Vitiani, L., Pallini, R., Biffoni, M., Todaro, M., Invernici, G., Cenci, T., Maira, G., Parati, E. A., Stassi, G., Larocca, L. M. & De Maria, R. 2010. Tumour vascularization via endothelial differentiation of glioblastoma stem-like cells. *Nature*, 468**,** 824-8.

Rice, T., Lachance, D. H., Molinaro, A. M., Eckel-Passow, J. E., Walsh, K. M., Barnholtz-Sloan, J., Ostrom, Q. T., Francis, S. S., Wiemels, J., Jenkins, R. B., Wiencke, J. K. & Wrensch, M. R. 2016. Understanding inherited genetic risk of adult glioma - a review. *Neurooncol Pract*, 3**,** 10-16.

Ruoslahti, E. 2002. Specialization of tumour vasculature. *Nat Rev Cancer*, 2**,** 83-90.

Saunders, W. B., Bohnsack, B. L., Faske, J. B., Anthis, N. J., Bayless, K. J., Hirschi, K. K. & Davis, G. E. 2006. Coregulation of vascular tube stabilization by endothelial cell TIMP-2 and pericyte TIMP-3. *J Cell Biol*, 175**,** 179-91.

Schlingemann, R. O., Rietveld, F. J., Kwaspen, F., van de Kerkhof, P. C., de Waal, R. M. & Ruiter, D. J. 1991. Differential expression of markers for endothelial cells, pericytes, and basal lamina in the microvasculature of tumors and granulation tissue. *Am J Pathol*, 138**,** 1335-47.

Sennino, B., Falcon, B. L., McCauley, D., Le, T., McCauley, T., Kurz, J. C., Haskell, A., Epstein, D. M. & McDonald, D. M. 2007. Sequential loss of tumor vessel pericytes and endothelial cells after inhibition of platelet-derived growth factor B by selective aptamer AX102. *Cancer Res*, 67**,** 7358-67.

Simonavicius, N., Ashenden, M., van Weverwijk, A., Lax, S., Huso, D. L., Buckley, C. D., Huijbers, I. J., Yarwood, H. & Isacke, C. M. 2012. Pericytes promote selective vessel regression to regulate vascular patterning. *Blood*, 120**,** 1516-27.

Sims, D. E. 1986. The pericyte--a review. *Tissue Cell*, 18**,** 153-74.

Sinha, D., Chong, L., George, J., Schluter, H., Monchgesang, S., Mills, S., Li, J., Parish, C., Bowtell, D., Kaur, P. & Australian Ovarian Cancer Study, G. 2016. Pericytes Promote Malignant Ovarian Cancer Progression in Mice and Predict Poor Prognosis in Serous Ovarian Cancer Patients. *Clin Cancer Res*, 22**,** 1813-24.

Song, S., Ewald, A. J., Stallcup, W., Werb, Z. & Bergers, G. 2005. PDGFRbeta+ perivascular progenitor cells in tumours regulate pericyte differentiation and vascular survival. *Nat Cell Biol*, 7**,** 870-9.

Soriano, P. 1994. Abnormal kidney development and hematological disorders in PDGF beta-receptor mutant mice. *Genes Dev*, 8**,** 1888-96.

Soriano, P. 1999. Generalized lacZ expression with the ROSA26 Cre reporter strain. *Nat Genet*, 21**,** 70-1.

Stapor, P. C., Sweat, R. S., Dashti, D. C., Betancourt, A. M. & Murfee, W. L. 2014. Pericyte dynamics during angiogenesis: new insights from new identities. *J Vasc Res*, 51**,** 163-74.

Stupp, R., Hegi, M. E., Mason, W. P., van den Bent, M. J., Taphoorn, M. J., Janzer, R. C., Ludwin, S. K., Allgeier, A., Fisher, B., Belanger, K., Hau, P., Brandes, A. A., Gijtenbeek, J., Marosi, C., Vecht, C. J., Mokhtari, K., Wesseling, P., Villa, S., Eisenhauer, E., Gorlia, T., Weller, M., Lacombe, D., Cairncross, J. G., Mirimanoff, R. O., European Organisation for, R., Treatment of Cancer Brain, T., Radiation Oncology, G. & National Cancer Institute of Canada Clinical Trials, G. 2009. Effects of radiotherapy with concomitant and adjuvant temozolomide versus radiotherapy alone on survival in glioblastoma in a randomised phase III study: 5-year analysis of the EORTC-NCIC trial. *Lancet Oncol*, 10**,** 459-66.

Stupp, R., Pavlidis, N., Jelic, S. & Force, E. G. T. 2005. ESMO Minimum Clinical Recommendations for diagnosis, treatment and follow-up of malignant glioma. *Ann Oncol*, 16 Suppl 1**,** i64-5.

Svensson, A., Ozen, I., Genove, G., Paul, G. & Bengzon, J. 2015. Endogenous brain pericytes are widely activated and contribute to mouse glioma microvasculature. *PLoS One*, 10**,** e0123553.

Sweeney, M. D., Ayyadurai, S. & Zlokovic, B. V. 2016. Pericytes of the neurovascular unit: key functions and signaling pathways. *Nat Neurosci*, 19**,** 771-83.

Tang, W., Zeve, D., Suh, J. M., Bosnakovski, D., Kyba, M., Hammer, R. E., Tallquist, M. D. & Graff, J. M. 2008. White fat progenitor cells reside in the adipose vasculature. *Science*, 322**,** 583-6.

Traktuev, D. O., Merfeld-Clauss, S., Li, J., Kolonin, M., Arap, W., Pasqualini, R., Johnstone, B. H. & March, K. L. 2008. A population of multipotent CD34-positive adipose stromal cells share pericyte and mesenchymal surface markers, reside in a periendothelial location, and stabilize endothelial networks. *Circ Res*, 102**,** 77-85.

Trost, A., Lange, S., Schroedl, F., Bruckner, D., Motloch, K. A., Bogner, B., Kaser-Eichberger, A., Strohmaier, C., Runge, C., Aigner, L., Rivera, F. J. & Reitsamer, H. A. 2016. Brain and Retinal Pericytes: Origin, Function and Role. *Front Cell Neurosci*, 10**,** 20.

Veeravagu, A., Bababeygy, S. R., Kalani, M. Y., Hou, L. C. & Tse, V. 2008. The cancer stem cell-vascular niche complex in brain tumor formation. *Stem Cells Dev*, 17**,** 859-67.

Viski, C., Konig, C., Kijewska, M., Mogler, C., Isacke, C. M. & Augustin, H. G. 2016. Endosialin-Expressing Pericytes Promote Metastatic Dissemination. *Cancer Res*, 76**,** 5313-25.

Wang, R., Chadalavada, K., Wilshire, J., Kowalik, U., Hovinga, K. E., Geber, A., Fligelman, B., Leversha, M., Brennan, C. & Tabar, V. 2010. Glioblastoma stem-like cells give rise to tumour endothelium. *Nature*, 468**,** 829-33.

Weller, M., Weber, R. G., Willscher, E., Riehmer, V., Hentschel, B., Kreuz, M., Felsberg, J., Beyer, U., Loffler-Wirth, H., Kaulich, K., Steinbach, J. P., Hartmann, C., Gramatzki, D., Schramm, J., Westphal, M., Schackert, G., Simon, M., Martens, T., Bostrom, J., Hagel, C., Sabel, M., Krex, D., Tonn, J. C., Wick, W., Noell, S., Schlegel, U., Radlwimmer, B., Pietsch, T., Loeffler, M., von Deimling, A., Binder, H. & Reifenberger, G. 2015. Molecular classification of diffuse cerebral WHO grade II/III gliomas using genome- and transcriptome-wide profiling improves stratification of prognostically distinct patient groups. *Acta Neuropathol*, 129**,** 679-93.

Winkler, E. A., Bell, R. D. & Zlokovic, B. V. 2010. Pericyte-specific expression of PDGF beta receptor in mouse models with normal and deficient PDGF beta receptor signaling. *Mol Neurodegener*, 5**,** 32.

Winkler, F., Kienast, Y., Fuhrmann, M., Von Baumgarten, L., Burgold, S., Mitteregger, G., Kretzschmar, H. & Herms, J. 2009. Imaging glioma cell invasion in vivo reveals mechanisms of dissemination and peritumoral angiogenesis. *Glia*, 57**,** 1306-15.

Xian, X., Hakansson, J., Stahlberg, A., Lindblom, P., Betsholtz, C., Gerhardt, H. & Semb, H. 2006. Pericytes limit tumor cell metastasis. *J Clin Invest*, 116**,** 642-51.

Yonenaga, Y., Mori, A., Onodera, H., Yasuda, S., Oe, H., Fujimoto, A., Tachibana, T. & Imamura, M. 2005. Absence of smooth muscle actin-positive pericyte coverage of tumor vessels correlates with hematogenous metastasis and prognosis of colorectal cancer patients. *Oncology,* 69**,** 159-66.

Yotsumoto, F., You, W. K., Cejudo-Martin, P., Kucharova, K., Sakimura, K. & Stallcup, W. B. 2015. NG2 proteoglycan-dependent recruitment of tumor macrophages promotes pericyte-endothelial cell interactions required for brain tumor vascularization. *Oncoimmunology,* 4**,** e1001204.

Youn, S. W., Jung, K. H., Chu, K., Lee, J. Y., Lee, S. T., Bahn, J. J., Park, D. K., Yu, J. S., Kim, S. Y., Kim, M., Lee, S. K., Han, M. H. & Roh, J. K. 2015. Feasibility and Safety of Intra-arterial Pericyte Progenitor Cell Delivery Following Mannitol-Induced Transient Blood-Brain Barrier Opening in a Canine Model. *Cell Transplant*, 24**,** 1469-79.

Yu, Q. C., Song, W., Wang, D. & Zeng, Y. A. 2016. Identification of blood vascular endothelial stem cells by the expression of protein C receptor. *Cell Res*, 26**,** 1079-1098.

Yung, W. K., Albright, R. E., Olson, J., Fredericks, R., Fink, K., Prados, M. D., Brada, M., Spence, A., Hohl, R. J., Shapiro, W., Glantz, M., Greenberg, H., Selker, R. G., Vick, N. A., Rampling, R., Friedman, H., Phillips, P., Bruner, J., Yue, N., Osoba, D., Zaknoen, S. & Levin, V. A. 2000. A phase II study of temozolomide vs. procarbazine in patients with glioblastoma multiforme at first relapse. *Br J Cancer*, 83**,** 588-93.

Zimmermann, K. W. 1923. Der feinere Bau der Blutcapillaren. *Z. ges. Anat*, 68**,** 20–109.

Zuniga, R. M., Torcuator, R., Jain, R., Anderson, J., Doyle, T., Ellika, S., Schultz, L. & Mikkelsen, T. 2009. Efficacy, safety and patterns of response and recurrence in patients with recurrent high-grade gliomas treated with bevacizumab plus irinotecan. *J Neurooncol*, 91**,** 329-36.

PUBLICATIONS

During my doctorate study, I was able to contribute the following publications.

1. **Li YP**, Hou MZ, Lu GY, et al. Decompressive craniectomy for severe middle cerebral artery infarction: a meta-analysis of randomised controlled trials. The Lancet. 2016; 31(388): S92.

2. **Li YP,** Hou MZ, Lu GY, et al. Neurological Functional Outcomes of Decompressive Hemicraniectomy versus Conventional Treatment for Malignant Middle Cerebral Artery Infarction: a Systematic Review and Mata-Analysis. World Neurosurg. 2017; 99(3): 709-725.

3. **Li YP,** Hou MZ, Lu GY, et al. The Prognosis of Anti-Angiogenesis Treatments Combined with Standard Therapy for Newly Diagnosed Glioblastoma: A Meta-Analysis of Randomized Controlled Trials. PLoS ONE. 2016; 11(12): e0168264.

4. Zhang HZ, **Li YP**, Yan ZC, et al. Endoscopic evacuation of basal ganglia hemorrhage via keyhole approach using an adjustable cannula in comparison with craniotomy. Biomed Res Int. 2014: 898762 (Correspondence author)

5. Dong L, **Li YP**, Han CX, et al. miRNA microarray reveals specific expression in the peripheral blood of glioblastoma patients. International Journal of Oncology, 2014, 45(2): 746-756.

ACKNOWLEDGEMENTS

depressions and culture shocks away, and well-adjusted myself into the new environment when I was just in the very beginning of my study in Germany.

I also want to thank all my friends I met in Germany, without you all I could not have my spare time such enjoyable and being fulfilled with pleasure. Especially I would like to thank my girlfriend, thanks for always supporting me on every decision I made and knowing me so well. Thanks for making me believe in having happiness life with you in the future.

Last but not the least, I want to thank my families. I want to give my deepest grateful to my parents, thanks for bringing me up into an optimistic and inner strong person. Thanks for always supporting me and encouraging me to study what I like. Thanks for the whole family that whenever I need any supports, I could get doubled or tripled supports what I expected from you. Thanks for supporting me going abroad to pursue a doctoral degree, thanks for trusting me that I could do it well, and thanks for letting me to being myself. I really feel so proud and grateful to owning my families.